Université Libre de Bruxelles

Faculty of Sciences

Department of Physics

A thesis presented for the degree of
Master of Physics

Study of the Proton Transverse Momentum Distributions

with the Parton Branching Method

Max Vanden Bemden

Promoter:
Prof. Laurent Favart

Co Promoter:
Dr. Anastasia Grebenyuk

23 August 2019
Belgium

Abstract

The topic of this thesis is to understand a new approach to solve the DGLAP evolution equations to obtain not only the collinear Parton Distribution Functions (PDFs) but also the Transverse Momentum Dependent PDFs (TMDs). The DGLAP evolution equations are solved with the Parton Branching (PB) method, which includes a determination of kinematic variables and which keeps the information of parton transverse momentum at every branching. PB method allows a construction of the TMDs in a large range in longitudinal momentum fraction x and evolution scale μ^2.
I performed the Parton Branching evolution from scratch to simulate the production of Z boson at LHC at 13 TeV. I studied the connection between the evolution scale and kinematic variables, and obtained the transverse momentum of Z boson for different ordering conditions. I also explored a tool called CASCADE which allows to use TMDs from the PB method to the LHC measurement, particularly the Drell Yan measurement by ATLAS experiment.
The PB TMD approach is a part of a broader program which aims to more precise predictions for observables at high energy collisions.

Key words : Parton Distribution Function, Parton Density, Drell Yan, Evolution Equation, DGLAP Equation, Transverse Momentum Dependence, Quantum Chromodynamics, Monte Carlo.

Résumé

Le but de ce mémoire est de comprendre une nouvelle approche pour résoudre les équations d'évolution DGLAP afin d'obtenir non seulement les fonctions de distributions de partons (PDFs) mais aussi une généralisation dépendante en l'impulsion transverse (TMD PDFs). La résolution des équations d'évolution DGLAP est réalisée par la méthode de branchement successif de parton (PB), qui inclut la détermination des variables cinématiques et qui garde en mémoire l'information sur l'impulsion transverse du parton pour chaque branchement. La méthode PB permet une construction des TMDs dans un grand intervalle de fraction d'impulsion longitudinale x et d'échelle d'évolution μ^2.
J'ai réalisé une évolution par branchement successif de parton à partir de zéro pour simuler la production du boson Z au LHC à 13 TeV. J'ai étudié le lien entre l'échelle d'évolution et les variables cinématiques, et j'ai obtenu l'impulsion transverse du boson Z pour différentes conditions d'ordonnancement. J'ai aussi exploré un outil appelé CASCADE qui permet l'utilisation des TMDs de la méthode PB sur les mesures du LHC, en particulier les analyses sur le processus Drell Yan de l'expérience ATLAS.
L'approche des TMDs par PB est une partie d'un projet plus large qui vise des prédictions plus précises pour les observables des collisions à haute énergie.

Mots clés : Fonction de Distribution de Parton, Densité de Parton, Drell Yan, Equation d'Evolution, Equation DGLAP, Dépendance en l'Impulsion Transverse, Chromodynamique quantique, Monte Carlo.

Acknowledgements

First of all I would like to express my profound gratitude to my supervisor Prof. Laurent Favart for his support, his explanations and his encouragement. I also want to thank Dr. Anastasia Grebenyuk, for all the help she has provided during this year. Thank you so much Nastja for your kind encouragements. I have also to warmly thank Louis Moureaux for his efforts to help me debugging my code and my calculations.
Among the other people I want to thank, Dr. Aleksandra Lelek for her work, which has been a great reference for this thesis, and her helpful explanations, and Radek Žlebcík for his help in the code.

I would like also to thank my readers, Prof. Riccardo Argurio and Prof. Pascal Vanlaer for the time they will be spending reading my thesis.

Now comes the place to cite a person who helped me a lot during my bachelor and master studies, a big thank you to Caroline Jonas.

I am also thankful to my family, my parents and my sisters and brother as well as my friends, for having given me the opportunity to be who I am and for all the love they have shown me up to now. Last but not least, I am so grateful for the permanent support of a wonderful little human being, Roxane.

Contents

Chapter 1

Introduction

1.1 Standard Model

All around us, the Nature is incredibly diversified. The variety of forms, structures, colours and properties that it offers to our senses seems infinite. But is this variety fundamental or induced? This question was already asked by Greek philosophers such as Leucippe, Democritus and Aristotle. Leucippe is reported to be the first to develop a theory in which our whole universe is made of atoms (from the Greek $\alpha\tau o\mu o\varsigma$: atomos, meaning indivisible). Even though our current usage of the word atom refers to the smallest unit that defines the chemical elements. We now know that they are made of electrons orbiting around a nucleus composed of protons and neutrons themselves built up of even smaller constituents called quarks.
Today we know that the variety is induced: if the Nature is plethoric in forms and properties, it is extremely thrifty in basic elements and fundamental interactions. At any scale of the matter, from the microscopic particles produced in our accelerators to the furthest galaxy clusters, and at every degree of complexity, from the hydrogen atom to the most complicated biological macromolecules, every one owe their structure to four fundamental interactions. They are presented here by order of increasing intensity:

(i) Gravitational interactions
They are known from our everyday life. They are responsible for the fall of apples on Earth and for the structure of the universe. Nevertheless, at a microscopical scale, their intensity is usually completely negligible.

(ii) Weak interactions
Responsible for the radioactive decay, they are at the origin of the processes of fusion producing the energy of the stars.

(iii) Electromagnetic interactions
Already known from the macroscopic physics, they are also responsible for the structure of the atoms and molecules as well as most of the properties of the condensed matter.

(iv) Strong interactions
They are responsible for the cohesion in the nuclear material. They are attractive between the constituents of the nuclei, protons and neutrons. It is much

stronger than the electrostatic repulsion between the protons.

The theory of elementary particles has been studied since the discovery of the atom, it is the essence of the Standard Model (SM). The SM is the theory that provides the best description of the interactions between elementary particles constituting our universe. It is a quantum field theory based on both special relativity and quantum mechanics. This model arose in the latter half of the 20^{th} century with the current formulation being finalised in the mid-1970s upon experimental confirmation of the existence of quarks. It is successful in describing three of the four known fundamental forces, namely the electromagnetic force, the weak force (these two forces are actually unified and described by the electroweak interaction in which they are seen as two different aspects of the same force) and the strong force.

The remaining force is gravity. In the 1910s, Albert Einstein has generalised special relativity and Newton's law of universal gravitation to achieve a proper description of the gravitation. The SM does not include general relativity and therefore can not describe gravitation effects. However, such effects are orders of magnitude smaller than the weakest effects of the weak interactions and ignorance of gravitation in high energy physics is a perfectly valid approximation.

Elementary particles are divided into fermions and bosons. The quarks and leptons are spin-$\frac{1}{2}$ fermions, we can differentiate them into three generations as illustrated in Fig (1.1). Each generation is a heavier copy of the first one.

The six quarks are grouped in three pairs, one for each generation, and each quark comes with three colours states. Quarks are electrically charged and colour charged. They also have a weak charge and being massive, quarks participate also to gravitational interactions. From the six leptons, three are charged and are subject to both weak and electromagnetic forces, whilst the three electrically neutral leptons are solely interacting through weak force. They are called neutrinos and are very difficult to observe. Note that each fermion comes with its corresponding antiparticle which has same mass but opposite charges. They are not represented in Fig (1.1).

Since the SM is a gauge theory, the interactions between elementary particles are described by the exchange of gauge bosons that mediate the forces. The gauge bosons are, for the electromagnetic interactions the photon, for the weak interactions the $W^{\pm}$ and the Z, and the gluons (there are eight of them) for the strong interactions. Last but not least, the Higgs boson, predicted by Brout-Englert-Higgs 50 years ago has been discovered in July 2012 and has given further credence to the SM. The Higgs particle, unstable boson with no spin, electric charge nor colour charge is the quantum manifestation of the Higgs field, responsible for elementary particle masses.

As the SM is based on the *Quantum Field Theory* (QFT), this allows one to write the *Lagrangian density* (often called *Lagrangian*) to describe the dynamics of the theory. The SM is a gauge invariant theory which means that its Lagrangian is invariant under the local $SU(3)_c \times SU(2)_L \times U(1)_Y$ symmetry. The group symmetry of colour is $SU(3)_c$, $SU(2)_L$ is the approximate isospin symmetry (exact if u and

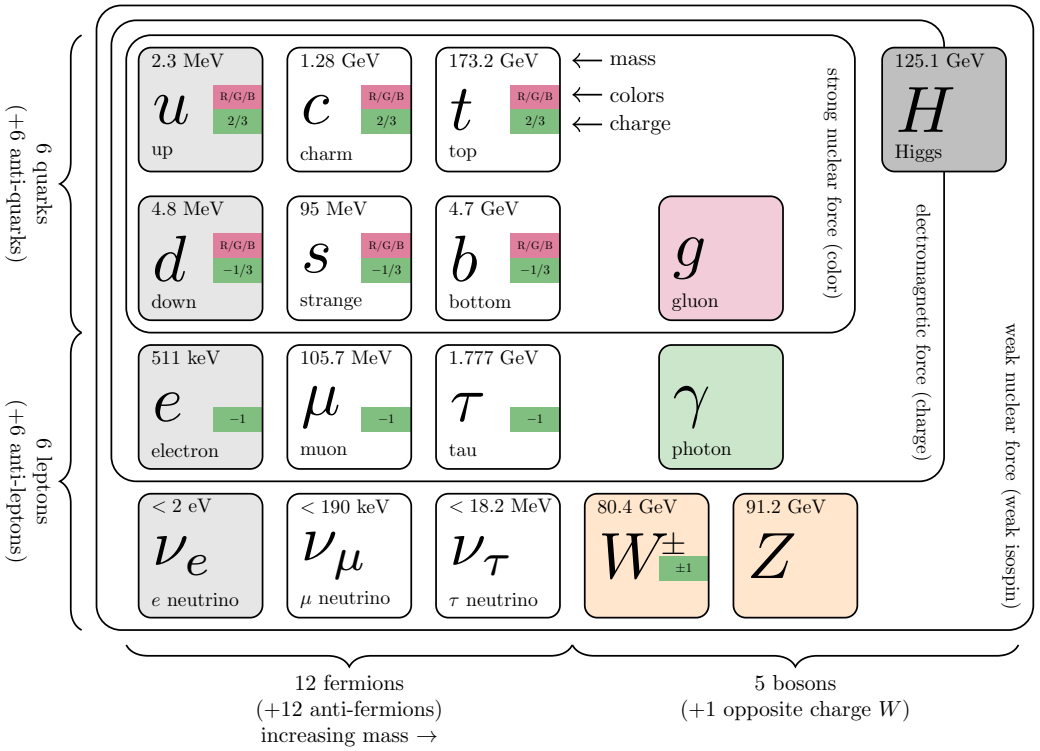

Figure 1.1: *Particle contents of the Standard Model* (adapted from [1]).

d quarks had the same mass) and the symmetry $U(1)_Y$ corresponds to the weak hypercharge conservation.

This thesis is focused on the *Quantum Chromodynamics* (QCD) part of the SM. This is the theory of the strong interaction between quarks and gluons, the fundamental particles that make up composite hadrons like the proton, the neutron and pions. QCD exhibits two main properties: colour confinement and asymptotic freedom. These are consequences of the running of the QCD coupling α_S which will be the subject of the next section.

The SM had unprecedented success in describing to very high level of accuracy a large variety of experimental observations. Nevertheless, it leaves some phenomena unexplained and falls short of being a complete theory of fundamental interactions. It can neither fully explain baryon asymmetry in the Universe, the neutrino oscillations and their non-zero masses, nor incorporate the full theory of gravitation as described by general relativity. This model does not contain any viable dark matter particle that possesses all of the required properties deduced from observational cosmology. For some physicists, SM is used up as a basis for building more exotic models, beyond the SM (BSM), that incorporate hypothetical particles, extra dimensions, and elaborate symmetries (such as supersymmetry) in an attempt to explain experimental results. To find hints of this theory, SM must be well understood, provide precise predictions and be confronted to precision measurements. Every inconsistency can be a clue of how to construct the BSM theory and which

of the existing ones can be preserved and which should be abandoned.

1.2 Colour confinement and asymptotic freedom in QCD

Before the actual introduction of the topic, this section introduces some basic features of QCD: the QCD running coupling, the asymptotic freedom and the quark confinement. This section follows the argumentation of [2].

In order to introduce the concept of the running coupling, let us assume a dimensionless physical observable R dependent on a single energy scale Q^2. This scale is much bigger than all other scale in the process. In a renormalizable quantum field theory, one calculates R as a perturbation series of the coupling α_S. The perturbation series requires renormalization to remove the ultraviolet divergence. Consequently, this procedure introduces a second mass scale μ, at which the subtractions are performed. The physical observable R will therefore depend on the ratio Q^2/μ^2 and be dimensionless. Thus the renormalized coupling depends on the arbitrary choice made for the subtraction point μ. But physical quantities such as R should not depend on this choice. Mathematically, this condition may be guaranteed by the following equation

$$\mu^2 \frac{\mathrm{d}}{\mathrm{d}\mu^2} R(Q^2/\mu^2, \alpha_S) \equiv \left[\mu^2 \frac{\partial}{\partial \mu^2} + \mu^2 \frac{\partial \alpha_S}{\partial \mu^2} \frac{\partial}{\partial \alpha_S} \right] R = 0 \, . \tag{1.1}$$

To rewrite this equation one can define the notations

$$t = \ln\left(\frac{Q^2}{\mu^2}\right) \, , \qquad \beta(\alpha_S) = \mu^2 \frac{\partial \alpha_S}{\partial \mu^2} \, . \tag{1.2}$$

Substituting these variable in Eq (1.1) one gets

$$\left[-\frac{\partial}{\partial t} + \beta(\alpha_S) \frac{\partial}{\partial \alpha_S} \right] R(e^t, \alpha_S) = 0 \, . \tag{1.3}$$

To solve this first order partial differential equation, a new function is needed, the *running coupling* $\alpha_S(Q^2)$

$$t = \int_{\alpha_S}^{\alpha_S(Q^2)} \frac{dx}{\beta(x)} \, , \quad \alpha_S(\mu^2) \equiv \alpha_S \, . \tag{1.4}$$

From that one can deduce that $R(1, \alpha_S(Q^2))$ is a solution of Eq (1.3). This whole analysis shows that all the of the scale dependence in R comes from the running of the coupling α_S, which is determined by the renormalization group equation

$$Q^2 \frac{\partial \alpha_S(Q^2)}{\partial Q^2} = \beta(\alpha_S(Q^2)) \, . \tag{1.5}$$

The function β has a perturbative expression

$$\beta(\alpha_S) = -b_1 \alpha_S^2 (1 + b_2 \alpha_S + b_3 \alpha_S^2 + O(\alpha_S^3)) \, . \tag{1.6}$$

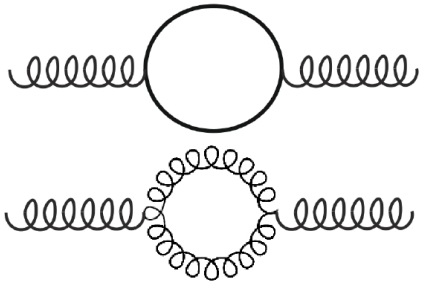

Figure 1.2: *Graphs which contribute to the β function in the one loop approximation.*

The coefficients were obtained at 1-loop level in [3, 4], at 2-loop in [5] and at 3-loop in [6] by calculating the higher-order corrections to the bare QCD vertices. The 1-loop coefficient is given by

$$b_1 = \frac{33 - 2n_f}{12\pi} \,, \tag{1.7}$$

with n_f the number of active light flavours. Fig (1.2) shows the diagrams contributing to the β function of QCD in the 1-loop approximation.

If both $\alpha_S(Q^2)$ and $\alpha_S(\mu^2)$ are in the perturbative regime, one can truncate the series of Eq (1.6), neglecting the b_2 and higher coefficients, then solve for $\alpha_S(Q^2)$ using Eq (1.5)

$$\alpha_S(Q^2) = \frac{\alpha_S(\mu^2)}{1 + \alpha_S(\mu^2) b_1 t} \,, \quad t = \ln\left(\frac{Q^2}{\mu^2}\right) \,. \tag{1.8}$$

As t becomes very large $t \to \infty$, the strong coupling decreases to zero $\alpha_S(Q^2) \to 0$ which is true only if $n_f < 16$. This property is called *asymptotic freedom*. This means that at higher scales (at small distances), the strong coupling is small and partons can be treated as free particles. The approach to this regime is rather slow because $\alpha_S(Q^2)$ decreases only as an inverse power of $\ln Q^2$. On the contrary, at smaller scales (large distances), the strong coupling is very strong and partons are said to be *confined* inside the hadrons. This explains why we cannot see free quarks or free gluons. This behaviour is opposite to the QED coupling α which increases with scale.

We can also rewrite Eq (1.3) as a series expansion

$$R(1, \alpha_S(Q^2)) = R_1 \alpha_S(\mu^2) \left[1 - \alpha_S(\mu^2) bt + \alpha_S(\mu^2)^2 (bt)^2 + ...\right] \,. \tag{1.9}$$

Thus one can see that order by order in perturbation theory there are $\ln(Q^2/\mu^2)$ which are automatically resummed by using the running coupling. By cutting the series at terms of pieces proportional to α_S, one obtains the *leading order* approximation (LO), by cutting at α_S^2 one obtains the *next-to-leading order* approximation (NLO), etc.

We can also adopt the approach which was used historically, and is still very appropriate for many purposes. One introduces a dimensionful parameter directly into the definition of $\alpha_S(Q^2)$. This parameter is called Λ and is defined by the relation

$$\ln \frac{Q^2}{\Lambda^2} = - \int_{\alpha_S(Q^2)}^{\infty} dx \frac{1}{\beta(x)} \,. \tag{1.10}$$

Λ corresponds to the scale at which the running coupling α_S diverges. It indicates the order of magnitude of the scale at which $\alpha_S(Q^2)$ becomes strong. Λ can be defined to leading or next-to-leading order and its value is in the neighbourhood of 200 MeV. Thus at this scale α_S becomes large and perturbation theory breaks down. This happens for scales comparable to the mass of light hadrons, $Q \simeq 1\text{GeV}$. This could be a sign that the *confinement* of quarks and gluons inside the hadrons is actually a consequence of the growth of the coupling at low scales, which follows directly from the decrease at high scales that leads to asymptotic freedom.
At leading order, Λ allows us to write an asymptotic solution for α_S

$$\alpha_S(Q^2) = \frac{1}{b \ln\left(Q^2/\Lambda^2\right)} \,. \tag{1.11}$$

Λ depends also on the number of active flavours. One only needs to impose continuity conditions for α_S at the scale $\mu = m$, where m is the mass of the heavy quark.

Perturbative QCD tells us how the coupling constant varies with the scale, not its absolute value. Only experiments can provide this one. What we can do is to choose our fundamental parameter of the theory to be the parameter at a convenient reference scale. This scale must be large enough to be in the perturbative domain, such as M_Z^2. Measured at another scale Q, it can then be evolved to the mass of the Z boson using the renormalization group equation truncated at a given order.

A compilation of some measurements of α_S performed at electron-proton and proton-proton colliders are shown in Fig (1.3) [7]. The 2018 world average value [8] of the strong coupling at the squared mass of the Z is

$$\alpha_S(M_Z^2) = 0.1181 \pm 0.0011 \,. \tag{1.12}$$

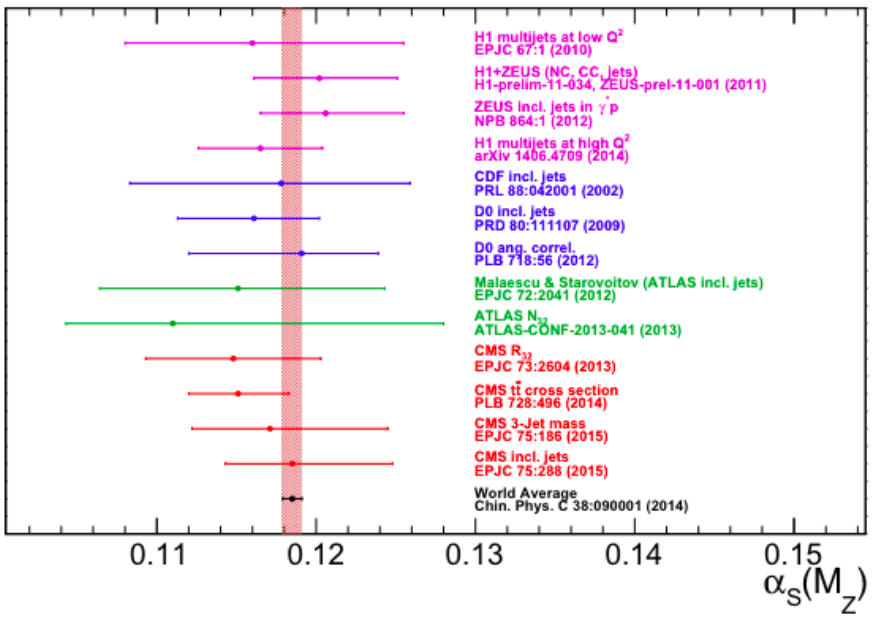

Figure 1.3: *An overview of some of the α_S measurements* [7].

1.3 Preface

The thesis is organised as follows:

In Chapter 1 we introduce the Standard Model and the basic concepts of QCD: asymptotic freedom and colour confinement.

Chapter 2 explains the origin of DGLAP evolution equation, the central equation of this thesis. We begin with the Parton Model to explain the Deep Inelastic Scattering and we show how, by including the QCD corrections, one can explain the Bjorken scaling violation. We introduce the concept of Parton Distribution Functions (PDFs) and factorization theorem.

In Chapter 3 the Drell-Yan process is discussed. We give the DY cross section, first in the parton model and then including perturbative corrections, illustrating the factorization property. We also discuss the Z boson transverse momentum and the relative calculations.

In Chapter 4 we start to talk about beyond fixed order calculations and we motivate the TMDs. We move forward to the Parton Branching method and discuss the aspects of DGLAP necessary to interpret the equation in terms of a parton branching process. We show how the association of the kinematic variables with the evolution scale leads to a certain ordering conditions. We present the idea of the Sudakov form factor which allows for a probabilistic interpretation of the evolution equation and enables the solution using Monte Carlo methods.

In Chapter 5 the analysis of the thesis is introduced. The Monte Carlo technique and the probability theory are discussed. We present the analysis strategy and the results.

In Chapter 6 we summarize the results presented in this thesis and give conclusions and prospects.

Chapter 2

Proton Structure and QCD Evolution Equations

This chapter gives a short overview on the structure of the proton and of the evolution of its constituents. To do so, we review briefly the Deep Inelastic Scattering (DIS), the Parton Model, the Parton Distribution Functions and QCD evolution equations - the basics of this thesis. We discuss how the Parton Model can explain the Björken scaling and how the QCD corrections justify the Björken scaling violation and lead to the DGLAP evolution equation. Finally we describe how the PDFs can be obtained at any scale. This chapter is inspired by many textbooks that treat these subjects much more extensively (e.g. [2, 9]), here only the most important results are summarized.

2.1 Deep Inelastic scattering

This section follows the argumentation from [10]. The non-elementary structure of hadrons, and of the proton in particular, has been revealed in 1967 at the Standford Linear Accelerator (SLAC). They made collisions of 21 GeV electrons off liquid hydrogen and later a deuterium fixed target. While dominated by elastic scattering ($e^- p \to e^- p$), the total cross section exhibits a large contribution of *deep inelastic scattering* (DIS) event ($e^- p \to \gamma \to e^- X$)[1] where the hadronic final state X is made of a large number of hadrons. The definition of the four-momentum vectors is given in Fig (2.1). We consider:

$$e^-(k^\mu) + p(p^\mu) \to \gamma^*(q^\mu) \to e^-(k'^\mu) + X \ . \tag{2.1}$$

SLAC experiment only measured the scattered electron (energy and angles), which is sufficient to determine completely the kinematics. The invariant mass of the hadronic final state W can be computed by:

$$W^2 = (q+p)^2 = X^2 = q^2 + 2p \cdot q + m_P^2 \ . \tag{2.2}$$

[1] If the beam had more energy, the exchanged boson could also be a Z. In this section, the electroweak effects are neglected.

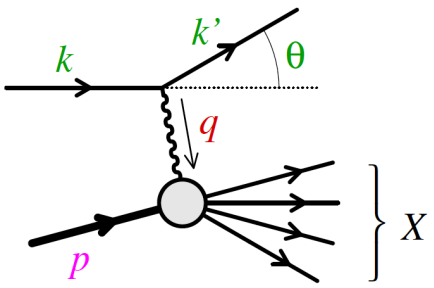

Figure 2.1: *DIS diagram defining the 4-vectors.*

The standard deep inelastic variables are defined by:

$$\begin{aligned} Q^2 &= -q^2 \,, \\ x &= \frac{Q^2}{2p\cdot q} \,, \\ y &= \frac{p\cdot q}{p\cdot k} \,. \end{aligned} \tag{2.3}$$

The variables x and y are the relativist invariants of Björken having values between 0 and 1. Neglecting the electron and the proton masses in front of their momenta, these invariants are related by:

$$Q^2 = xys \,, \tag{2.4}$$

from which one can deduce that $Q^2 \leq s$, with s the square of the center of mass available energy: $s = (k+p)^2$.

To write down the DIS cross section we need to introduce the unknown functions $F_1(x, Q^2)$ and $F_2(x, Q^2)$ called *structure functions* which parametrize the structure of the target as 'seen' by the virtual photon. In the asymptotic regime of Björken, defined by:

$$\begin{aligned} Q^2 &\to \infty \,, \\ s, \nu &\to \infty \,, \\ x &\text{ fixed} \,, \end{aligned} \tag{2.5}$$

one can write the inclusive cross-section of the $e + p \to e + X$ scattering as:

$$\begin{aligned} \frac{\mathrm{d}^2\sigma}{\mathrm{d}x\mathrm{d}Q^2} &= \frac{4\pi\alpha^2}{xQ^4}\left[xy^2 F_1(x,Q^2) + (1-y)F_2(x,Q^2)\right] \\ &= \frac{4\pi\alpha^2}{Q^4}\left[\left[1+(1-y)^2\right]F_1 + \frac{(1-y)}{x}(F_2 - 2xF_1)\right] \,. \end{aligned} \tag{2.6}$$

Applying this formalism on the measurements performed at SLAC in the 1960s, it has been observed that despite the large domain covered in Q^2, the structure function F_2 seems to be independent of Q^2 as we can see in Fig (2.2).

$$F_2(x, Q^2) \to F_2(x) \,. \tag{2.7}$$

This independence is called *Björken scaling*. We will come back on it at the end of the next section.

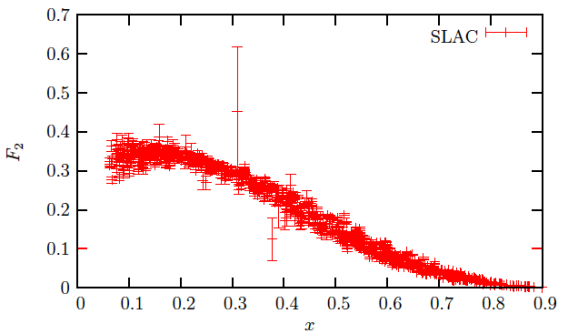

Figure 2.2: *Measurement of the structure function F_2 of the proton at SLAC. This figure compiles the measurement of F_2 for a large amount of data with different values of Q^2.* [11, 12]

2.2 Parton Model

The *parton model* has been introduced by Robert Feynman in the late 1960s in an attempt to explain the Björken scaling as a consequence of the point-like nature of nucleon's constituents incoherently scattered by the incident electron. He named the point-like constituents partons, which have a electrical charge and are classified as spin-1/2 particles. A few years later physicists identified the partons with quarks. As QCD did not exist yet, the gluons did not enter the picture at first. A nucleon consists of three *valence* quarks which build up the nucleon's quantum numbers and a *sea* of quarks and antiquarks. In this naive Parton Model, partons inside one hadron do not interact with each other.

In the following we will make the ultra-relativistic approximation, such that the electron and proton masses are negligeable. As it is an ahead collision, the four-momentum of the proton is $p^\mu = (p, 0, 0, p)$ and the one of the electron is $k^\mu = (k, 0, 0, -k)$. According to the parton model, the inclusive DIS cross section is given by the sum of the cross section on the individual quarks times their density of probability. At the Leading Order (LO) the electron-quark scattering cross section can be calculated within pQCD. As can be seen from Fig (2.3), the electron, carrying a four-momentum k^μ scatters on a quark q with four-momentum l. In the collinear approximation, the quark carries a fraction ξ of the proton momentum $l = \xi p^\mu$. The electron and the quark interacts through the exchange of a virtual photon γ^* with a four-momentum q^μ. The outgoing particles are the scattered electron carrying the four-momentum k'^μ and the scattered quark of the same flavour as the incoming one carrying the four-momentum l'.

The LO differential cross section for electron-quark scattering is given by the formula (see for e.g. [2]):

$$\frac{\mathrm{d}\hat{\sigma}}{d\hat{t}}(e^- q \to e^- q) = \frac{2\pi\alpha^2 e_q^2}{\hat{s}^2}\left(\frac{\hat{s}^2 + \hat{u}^2}{\hat{t}^2}\right) , \tag{2.8}$$

with α the fine-structure constant, e_q the fractional charge of the quark, and $\hat{s}$, $\hat{u}$, $\hat{t}$ the Mandelstam variables of the subprocess.

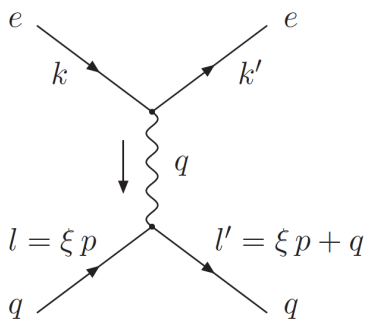

Figure 2.3: *LO Feynman diagram contributing to DIS process.*

Substituting for the kinematic variables gives:

$$\frac{\mathrm{d}\hat{\sigma}}{\mathrm{d}Q^2} = \frac{2\pi\alpha^2 e_q^2}{Q^4}[1 + (1-y)^2] \; . \tag{2.9}$$

The mass-shell constraint for the outgoing quark, assumed to be massless

$$(l')^2 = (l+q)^2 = q^2 + 2l \cdot q = -2l \cdot q(x - \xi) = 0 \; , \tag{2.10}$$

implies $x = \xi$. Thus Björken x has a clear physical interpretation, it is the longitudinal fraction of the proton's momentum carried by the parton.

By writing $\int_0^1 \mathrm{d}x \; \delta(x - \xi) = 1$, one obtains the double differential cross section for the quark scattering process:

$$\frac{\mathrm{d}^2\hat{\sigma}}{\mathrm{d}x\mathrm{d}Q^2} = \frac{4\pi\alpha^2}{Q^4}[1 + (1-y)^2]\frac{1}{2}e_q^2\delta(x - \xi) \; . \tag{2.11}$$

The inclusive cross section of DIS $ep \to eX$ is given by the cross section of the electron-quark scattering, multiplied by a probability of density $f_q(\xi)d\xi$ to find in the proton a certain flavoured quark q carrying a momentum fraction between ξ and $\xi + d\xi$. It has to be summed over all possible quark flavours.

$$\begin{aligned} \frac{\mathrm{d}^2\sigma}{\mathrm{d}x\mathrm{d}Q^2} &= \int_0^1 \mathrm{d}\xi \sum_q f_q(\xi) \frac{\mathrm{d}^2\hat{\sigma}}{\mathrm{d}x\mathrm{d}Q^2}(\xi) \\ &= \int_0^1 \mathrm{d}\xi \sum_q f_q(\xi) \frac{4\pi\alpha^2}{Q^4}[1 + (1-y)^2]\frac{1}{2}e_q^2 \; \delta(x - \xi) \; . \end{aligned} \tag{2.12}$$

The functions $f_q(\xi)$ are called *parton distribution functions* (PDFs) or *collinear* PDFs. In the approach of pQCD they cannot be computed because they contain non-perturbative information on hadron structure and thus they must be extracted from measurements.

By comparing Eq (2.6) and Eq (2.12) we see that the structure functions in this simple model are equivalent to:

$$F_2(x, Q^2) = 2xF_1(x, Q^2) = \sum_{q,\bar{q}} e_q^2 \; x f_q(x) \; , \tag{2.13}$$

where the sum is made over all the quarks and antiquarks.

In this naive free parton model, the only Q^2 dependence in this partonic cross section comes from the photon propagator. The absence of Q^2 dependence in the right-hand-side term in Eq (2.13) justifies the absence of scaling giving structure functions independent of Q^2. F_2 represents the sum on all flavours of the density of probability of quarks carrying a momentum fraction x of the proton.

In particular, for the scattering of a charged electron off a proton target by virtual photon exchange, $e^- p \to e^- X$, with enough energy for four quark flavours, in the approximation of a single γ exchange, the F_2 structure function is given by:

$$F_2(x) = x\left[\frac{4}{9}(u(x) + \bar{u}(x) + c(x) + \bar{c}(x)) + \frac{1}{9}(d(x) + \bar{d}(x) + s(x) + \bar{s}(x))\right] . \tag{2.14}$$

The result $2xF_1 = F_2$ in Eq (2.13) is called *Callan-Gross* relation, it is a direct consequence of the spin-$\frac{1}{2}$ property of the quarks [13]. This relation is only true for quarks that are massless and without intrinsic transverse momenta. When QCD corrections are taken into account, this property does not hold anymore.

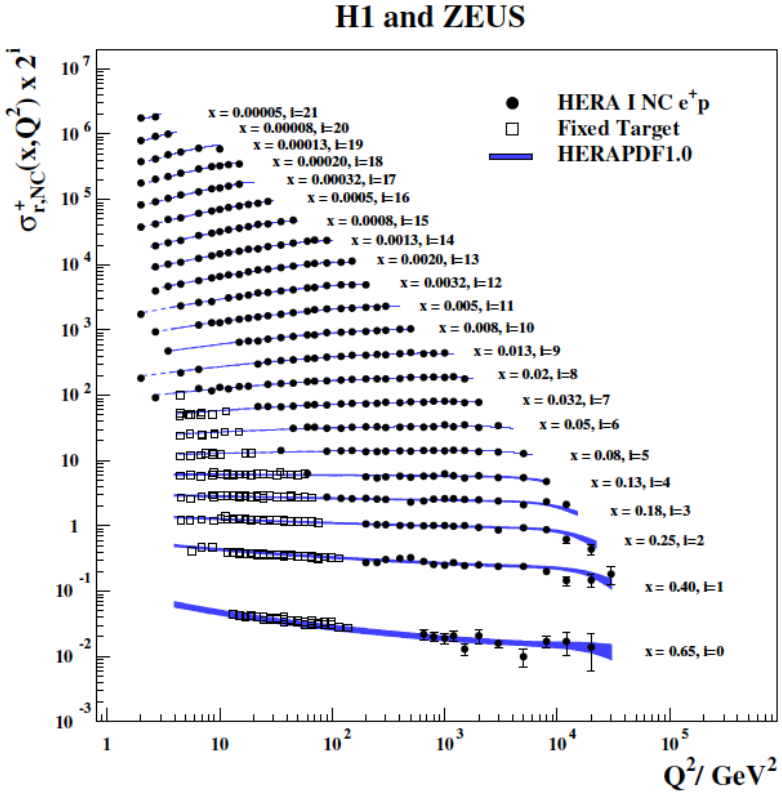

Figure 2.4: *HERA combined e^+p reduced cross section and fixed-target data as a function of Q^2* [14].

In Fig (2.4), the reduced cross section σ_r is shown as a function of Q^2 for different

values of x. The *reduced cross section* os obtained by dividing Eq (2.12) by a factor $\frac{2\pi\alpha^2}{xQ^4}(1+(1-y)^2)$. It is equal to F_2 at low Q^2 and not very large y [14]. These cross sections were computed from H1 and Zeus measurements which are two particle detectors that operated at HERA, the Hadron-Electron Ring Accelerator in Hamburg. At HERA, electrons (or positrons) were collided with protons at a center of mass energy of $\sqrt{s} = 318$ GeV. These measurements correspond to the black points in the plot. The squares on Fig (2.4) are the fixed-target measurements from the BCDMS (Bologna-CERN-Dubna-Munich-Saclay) collaboration [15, 16]. The blue lines correspond to a fit which includes NLO corrections, called HERAPDF1.0. The combined data set on neutral current (NC) and charged current (CC) DIS inclusive cross sections is used as the sole input for the HERAPDF1.0 fit.

The figure shows that the Björken scaling expected in the naive parton model is a very good approximation for $0.13 < x < 0.18$, i.e. the quark valence region. For smaller or very large x one can clearly see the violation of Björken scaling. This violation comes from higher order QCD contributions to DIS that will be discussed in the next section.

2.3 DGLAP evolution equation

2.3.1 Scale violation

The limited validity of the naive parton model comes from the fact that it neglects gluon radiations from quarks as expected by QCD. These radiated gluons may emit other gluons, be reabsorbed, or even emit a quark-antiquark pair. Inside a proton, all these quantum fluctuations occur but will be undetectable if no interaction (e.g. with a photon) takes place during their lifetime. Furthermore in the naive model, partons have only a momentum strictly parallel to the momentum of the proton. In case of parton emission there will be an additional *transverse* component. The probability to emit a quark or a gluon is of order $\mathrm{O}(\alpha_S)$, here below we consider first order QCD corrections.

Note that the α_S scale dependence in α_S has a $1/(\ln Q^2)$ term (see Eq (1.8)). For increasing Q^2 one accesses the domain where α_S is small (asymptotic freedom property). It allows us to apply perturbation theory for interactions on quarks whose distributions have non-perturbative origins.

2.3.2 QCD corrections

In order to describe the parton density evolution, we need to study the contribution of the gluon emission to the DIS cross section, i.e.

$$\gamma^* q \to qg \tag{2.15}$$

This section follows the argumentation from [9].

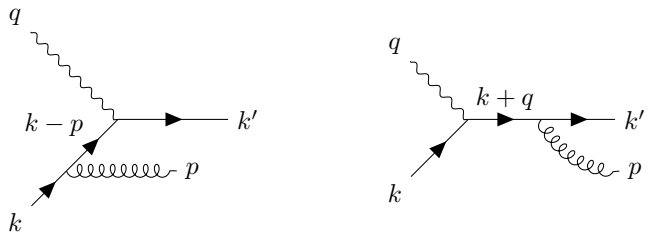

Figure 2.5: *DIS diagram with a gluon emission.*

The contribution coming from the two diagrams in Fig (2.5) can be expressed as:

$$\overline{|\mathcal{M}|^2} = 32\pi^2(e_q^2\alpha\alpha_S)\frac{4}{3}\left[-\frac{\hat{t}}{\hat{s}} - \frac{\hat{s}}{\hat{t}} + \frac{2\hat{u}Q^2}{\hat{s}\hat{t}}\right] . \tag{2.16}$$

where e_q is the fractional charge of the quark and where the color factor 4/3 takes into account the summation over final colours and the averaging over the initial ones. The hat ($\hat{}$) Mandelstam variables, $\hat{s}, \hat{t}, \hat{u}$ indicates that the parton subprocess is considered. In our notation we get:

$$\hat{s} = (k+q)^2 = (k'+p)^2 , \tag{2.17}$$

$$\hat{t} = (k-p)^2 = (k'-q)^2 , \tag{2.18}$$

$$\hat{u} = (q-p)^2 = (k-k')^2 . \tag{2.19}$$

In the limit of high energies, $-\hat{t} \ll \hat{s}$, one can express the cross section differentiated with respect to the transverse momentum of the scattered quark ($p_T = k' \sin\theta$), as in [9], where θ is the angle between the gluon and the scattered quark:

$$\begin{aligned}\frac{\mathrm{d}\hat{\sigma}}{\mathrm{d}p_T^2} &= \frac{4\pi^2\alpha e_q^2}{\hat{s}}\frac{1}{p_T^2}\frac{\alpha_S}{2\pi}P_{qq}^R(z) \\ &= e_q^2\hat{\sigma}_0\frac{1}{p_T^2}\frac{\alpha_S}{2\pi}P_{qq}^R(z) .\end{aligned} \tag{2.20}$$

where $\hat{\sigma}_0 = 4\pi^2\alpha/\hat{s}$ and the $P_{qq}^R(z)$ function is called the *splitting function*, where the (R) stands for real emissions. It may be written as:

$$P_{qq}^R(z) = \frac{4}{3}\left[\frac{1+z^2}{1-z}\right] , \tag{2.21}$$

which is a function of the longitudinal momentum fraction z of the incident quark "seen" by the incoming photon:

$$z \equiv \frac{Q^2}{2k\cdot q} = \frac{Q^2}{(k+q)^2 - q^2} = \frac{Q^2}{\hat{s}+Q^2} . \tag{2.22}$$

The function $P_{qq}^R(z)$ represents the probability of a quark emitting a gluon and becoming a quark with momentum reduced by a fraction z. In our massless approximation, this function is the same for quarks and antiquarks $P_{\bar{q}\bar{q}}^R(z) = P_{qq}^R(z)$.

The $z \to 1$ singularity is associated with the emission of a "soft" massless gluon which corresponds to an infrared divergence. There is another infrared divergence

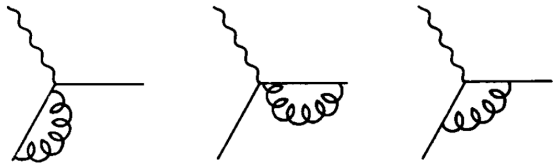

Figure 2.6: *Virtual contributions to the LO P_{qq} splitting function.*

when the transverse momentum of the radiated gluon is very small, $p_T^2 \to 0$. One needs to find a way to regularize this singularity. Finally, there are also virtual corrections, shown in Fig (2.6), which must be included. These virtual corrections can be computed from the diagrams or from unitarity arguments and it can be shown that they cancel exactly the real emission $z \to 1$ singularity (for more details see [9]). The full expression for the P_{qq} splitting function is then given by:

$$P_{qq}(z) = \frac{4}{3}\left[\frac{1+z^2}{(1-z)_+} + \frac{3}{2}\delta(1-z)\right] , \tag{2.23}$$

where the "+ prescription" was used for regularization, it is defined such that for any test function f:

$$\int_0^1 \mathrm{d}z \frac{f(z)}{(1-z)_+} = \int_0^1 \mathrm{d}z \frac{f(z)-f(1)}{(1-z)} , \tag{2.24}$$

where $(1-z)_+ = (1-z)$ for $z < 1$ but is infinite at $z = 1$.

2.3.3 Factorisation and Evolution

The contribution of the gluon emission Eq (2.20) has to be considered as a contribution to the structure function F_2 which enters in the DIS cross section. Integrating the gluon emission cross section over p_T^2 yields:

$$\sigma(\gamma^* \mathrm{q} \to \mathrm{qg}) = \int_{\kappa^2}^{\hat{s}/4} \mathrm{d}p_T^2 \frac{\mathrm{d}\hat{\sigma}}{\mathrm{d}p_T^2} \tag{2.25}$$

$$= e_q^2 \hat{\sigma}_0 \int_{\kappa^2}^{\hat{s}/4} \frac{\mathrm{d}p_T^2}{p_T^2} \frac{\alpha_S}{2\pi} P_{qq}(z) \tag{2.26}$$

$$= e_q^2 \hat{\sigma}_0 \left(\frac{\alpha_S}{2\pi} P_{qq}(z) \ln \frac{Q^2}{\kappa^2}\right) , \tag{2.27}$$

where one had to introduce a small cut-off κ^2 to cancel the divergence for $p_T^2 \to 0$. Before explaining the treatment of this singularity, let us write the gluon emission contribution to F_2 in the parton model and modify the Eq (2.13) to:

$$F_2(x,Q^2) = x \sum_{q,\bar{q}} e_q^2 \int_x^1 \frac{\mathrm{d}x'}{x'} q(x') \left(\delta\left(1-\frac{x}{x'}\right) + \frac{\alpha_S}{2\pi} P_{qq}\left(\frac{x}{x'}\right) \ln \frac{Q^2}{\kappa^2} + ...\right) , \tag{2.28}$$

where x' is the momentum fraction of the "mother" quark and x of the "daughter" one. We have introduced the notation that the quark structure function $f_q(x) \equiv q(x)$. One can see that the Björken scaling prediction for the structure function is violated. In other words beyond leading order, F_2 is not only a function of x, but

also of Q^2, even if the variation with Q^2 is only logarithmic.

So far the singularity when $p_T^2 \to 0$ remains through the κ^2 parameter. To begin with, this limit corresponds to a "long-range" part of the strong interaction, so we cannot compute it in pQCD. Eq (2.28) may be understood as the first two terms of a power series in α_S. One can regard the quark distribution $q(x)$ as an unmeasurable, *bare* distribution. The collinear singularities can be absorbed into this bare distribution at a *factorization scale* μ^2, which plays a similar role to the renormalization scale for α_S (see e.g. [2]). In other terms, one defines a *renormalized* or *dressed* distribution at a given scale μ^2:

$$q(x,\mu^2) = q(x) + \frac{\alpha_S}{2\pi}\int_x^1 \frac{\mathrm{d}x'}{x'} q(x') P_{qq}\left(\frac{x}{x'}\right) \ln\frac{\mu^2}{\kappa^2} + \dots \,, \tag{2.29}$$

where the κ^2 parameter has been absorbed into the definition of the quark distribution $q(x,\mu^2)$. Therefore one has an expression of F_2 independent of κ^2:

$$F_2(x,Q^2) = x\sum_{q,\bar{q}} e_q^2 \int_x^1 \frac{\mathrm{d}x'}{x'} q(x',\mu^2)\left[\delta\left(1-\frac{x}{x'}\right) + \frac{\alpha_S}{2\pi} P_{qq}\left(\frac{x}{x'}\right)\ln\frac{Q^2}{\mu^2} + \dots\right] . \tag{2.30}$$

The quark distributions $q(x,\mu^2)$ cannot be calculated in pQCD but they can be determined from structure functions data at any particular scale, since $F_2(x,Q^2) = x\sum_{q,\bar{q}} e_q^2 q(x,Q^2)$ and their Q^2 evolution are predicted by pQCD.

How can we understand that the proton structure exhibits an evolution between different scales? Fig (2.7) represents the proton and its evolution with the scale. The left part of the illustration presents a proton with partons as seen by a virtual photon of virtuality Q_0 which corresponds to a resolution scale $\sim 1/Q_0$. On the right, the same proton is probed by a photon with higher virtuality $Q > Q_0$. The latter is able to resolve shorter transverse distances $\sim 1/Q$, which is why DIS is often compared to a microscope.

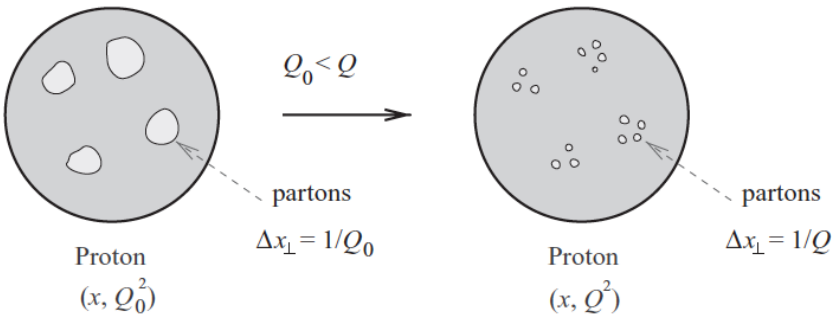

Figure 2.7: *Illustration of the evolution equations. The blobs indicate partons* [17].

If there were only valence quarks, no further structure would be resolved as Q increases, and the parton model would be fully satisfactory. However, QCD predicts that for larger resolution ($Q_0 \ll Q$), one should "see" that each quark is itself

surrounded by a cloud of partons. The number of resolved partons which share the proton's momentum increases with Q as shows the right term of Eq (2.30) where the probability of gluon radiation is enhanced by a factor $\ln Q^2$. These gluons can then emit quark-antiquark pairs so the probability to find quarks (or antiquarks) at small x increases.

The evolution of the quark density with the scale μ^2 can be rewritten as an integro-differential equation for $q(x, \mu^2)$:

$$\frac{\mathrm{d}q(x,\mu^2)}{\mathrm{d}\ln\mu^2} = \frac{\alpha_S}{2\pi}\int_x^1 \frac{\mathrm{d}x'}{x'} q(x',\mu^2) P_{qq}\left(\frac{x}{x'}\right) \ . \tag{2.31}$$

This equation is still incomplete because quarks can also come from the splitting of a gluon into a quark-antiquark pair. This is discussed in the next subsection.

2.3.4 LO splitting functions and DGLAP evolution equations

Up to know, only the splitting of a quark into another quark has been considered. Indeed, the only contributions to DIS incorporated are $\gamma^* q \to q$ and $\gamma^* q \to qg$. To order α_S, we should also include the contributions where a gluon in the initial proton produces a quark-antiquark pair to which the virtual photon then couples ($\gamma^* g \to q\bar{q}$). This is the process illustrated in Fig (2.8).

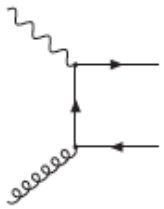

Figure 2.8: *DIS diagram with a gluon in the initial state.*

Its contribution to the structure function F_2 is then given by:

$$F_2(x,Q^2)\big|_{\gamma^* g\to q\bar{q}} = x\sum_{q,\bar{q}} e_q^2 \int_x^1 \frac{\mathrm{d}x'}{x'} g(x',\mu^2)\frac{\alpha_S}{2\pi} P_{qg}\left(\frac{x}{x'}\right)\ln\frac{Q^2}{\mu^2} \ , \tag{2.32}$$

where $g(x)$ is the gluon density in the proton and where

$$P_{qg}^R(z) = \frac{1}{2}\left[z^2 + (1-z)^2\right] \tag{2.33}$$

is the LO part of the splitting function of a gluon into a real quark-antiquark pair. It represents the probability that a gluon materialises into a quark-antiquark pair, such that the quark has a fraction $z = x/x'$ of its momentum. This expression is not divergent and there are no virtual contributions at LO so $P_{qg}^R(z) = P_{qg}(z)$. Note also that in our massless approximation the splitting function is the same for all quark flavours so $P_{q_f g} = P_{\bar{q}_f g} \equiv P_{qg}$.

Including the quark-antiquark pair production to the evolution of the quark density, Eq (2.31) becomes:

$$\frac{\mathrm{d}q(x,\mu^2)}{\mathrm{d}\mu^2} = \frac{\alpha_S}{2\pi}\int_x^1 \frac{\mathrm{d}x'}{x'}\left(q(x',\mu^2)P_{qq}\left(\frac{x}{x'}\right) + g(x',\mu^2)P_{qg}\left(\frac{x}{x'}\right)\right) , \tag{2.34}$$

for each flavour q. This equation mathematically expresses that a quark with momentum fraction x ($q(x,\mu^2)$) at the left-hand-side could have come from a "parent" quark or gluon with larger momentum fraction x' at the right-hand-side. The parent parton ($q(x',\mu^2)$ or $g(x',\mu^2)$) has lost momentum radiating a gluon or giving a $q\bar{q}$ pair respectively. The probability that it happens is proportional to $\alpha_S P_{qq}$ or $\alpha_S P_{qg}$ and the integral is taken over all possible momentum fractions $x'(> x)$ of the parent parton.

One requires also an evolution equation for the gluon density in the proton. Following the same path, it can be found (see e.g. [2, 9]) that the gluon distribution function can be written as:

$$\frac{\mathrm{d}g(x,\mu^2)}{\mathrm{d}\ln\mu^2} = \frac{\alpha_S}{2\pi}\int_x^1 \frac{\mathrm{d}x'}{x'}\left(\sum_{q,\bar{q}} q(x',\mu^2)P_{gq}\left(\frac{x}{x'}\right) + g(x',\mu^2)P_{gg}\left(\frac{x}{x'}\right)\right) , \tag{2.35}$$

where the LO splitting functions P_{gq} and P_{gg} are given by (see [18]):

$$P_{gq}(z) = \frac{4}{3}\left[\frac{1+(1-z)^2}{z}\right] , \tag{2.36}$$

$$P_{gg}(z) = 6\left[\frac{z}{(1-z)_+} + \frac{1-z}{z} + z(1-z)\right] + \frac{33-2n_f}{6}\,\delta(1-z) . \tag{2.37}$$

The divergence in P_{gg} when $z \to 1$ corresponds again to the emission of a soft gluon. The P_{gg} splitting function above is already corrected for the virtual emissions and this divergence is canceled, as in the P_{qq} case. In addition, there is a divergence when $z \to 0$ in both P_{gq} and P_{gg}. It corresponds to the situation when the gluon is entering the hard scattering with an energy $\to 0$. To be able to use pQCD in the calculation, one needs some minimum scale of the hard process $\hat{s}$. Study such a process with a gluon at very low x requires considerable energy of the incoming beams. The formalism used in this section is not a good description in the limit $s \to \infty$ needed to reached $x \to 0$. We will introduce a small cut-off on the value of z to protect against these situations. However there are other formalisms better suited to the region of small x, such as BFKL equation (see e.g. [19]).

Eq (2.34) and Eq (2.35) can be put together in a more compact form

$$\begin{aligned}\frac{\mathrm{d}}{\mathrm{d}\ln\mu^2}\begin{pmatrix} q_i(x,\mu^2) \\ g(x,\mu^2)\end{pmatrix} = \frac{\alpha_S}{2\pi}\sum_{q_j}\int_x^1 \frac{\mathrm{d}x'}{x'} \\ \times \begin{pmatrix} Pqq(z)\ \delta_{ij} & Pqg(z) \\ Pgq(z) & Pgg(z)\end{pmatrix}\begin{pmatrix} q_j(x',\mu^2) \\ g(x',\mu^2)\end{pmatrix} .\end{aligned} \tag{2.38}$$

These are the well known *Dokshitzer-Gribov-Lipatov-Altarelli-Parisi* (DGLAP) equations which are ones of the most important equations of QCD. They describe the evolution of the parton distribution functions with the scale μ^2.

For a given PDF (e.g. extracted from DIS cross section measurements), the DGLAP equations allow us to compute its evolution. This evolution is illustrated in Fig (2.9) by the MRST PDF library (valence u and d, sea $\bar{u}$ and gluon). When the value of Q^2 increases, the space phase to radiate a gluon grows. The emitted gluon will carry a fraction of the proton's momentum, leaving a lower momentum fraction to the quark. The quark density of the sea should thus increase at small values of x when Q^2 increases. It means that the variation of Q^2 affects the partons densities: i.e. the *violation of Björken scaling*. While the valence peak stays for any Q^2 scale: i.e. the *Björken scaling*.

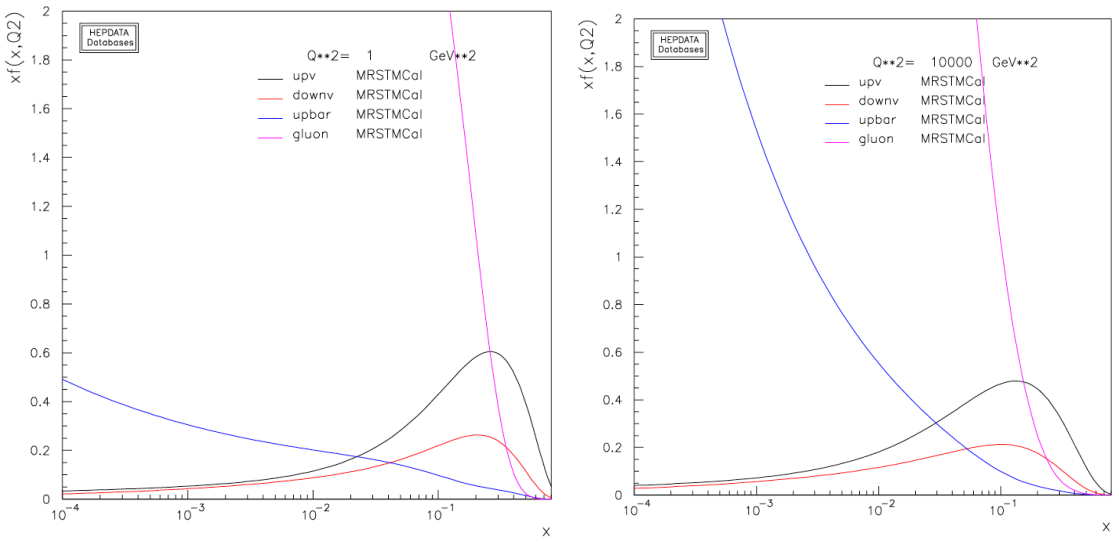

Figure 2.9: *Valence u and d quarks, upbar quark and gluons distributions in the proton estimated by MSRT Group at two different Q^2 values. Left: $Q^2 = 1 GeV^2$. Right: $Q^2 = 10000 GeV^2$. Distributions generated with the online tool* [20].

Chapter 3

The Drell-Yan process

The study of DIS has brought a detailed understanding of how the proton momentum is shared in the longitudinal direction between its different constituents, the partons. Their evolution as a function of the longitudinal momentum fraction x with the scale of the interaction is given by the DGLAP equation. The DIS cross section can be written as the convolution of the evolved PDF and the hard cross section where only longitudinal momentum dependence is considered. These PDFs are universal quantities, i.e. they can be used in other type of interactions like in hadron-hadron collisions. Possible transverse momentum, not accessible in DIS, are not considered up to here. The Drell-Yan process in hadron-hadron collisions can bring, as we will see, additional information on the transverse momentum dependence of the PDF.

The *Drell-Yan process* (DY) corresponds to a quark-antiquark annihilation into a pair of oppositely-charged leptons, l^+l^-, with invariant mass $M^2 = (p_{l^+} + p_{l^-})^2 \gg 1\text{GeV}^2$. It has been first presented in 1970 by Sydney Drell and Tung-Mow Yan [21]. The DY takes place in hadron-hadron collision, the quark and antiquark being constituents of the two incoming hadrons. They can create an off-shell virtual boson (γ^* or Z) and this boson then decays into a pair of charged leptons which have a clear signature into the detectors. From now on, we will take the hadrons to be protons, as illustrated in Fig (3.1).

At high energies, in presence of a hard scale, the partons are assumed to be quasi-free due to the property of asymptotic freedom. The interactions between the partons inside a proton can then be neglected. In a high energy proton-proton collision, the hard scattering process (hard indicates a large momentum transfer Q^2) is initiated by two partons of the two protons. The square center-of-mass energy of the proton-proton collision is defined as:

$$s = (P_1 + P_2)^2 \ , \tag{3.1}$$

with P_i the four-momentum of the proton i. In the collinear approximation, the transverse momentum of the partons is neglected, the four-momenta of the two partons can thus be written as:

$$\begin{aligned} p_1 &= \frac{\sqrt{s}}{2}(x_1, 0, 0, x_1) \ , \\ p_2 &= \frac{\sqrt{s}}{2}(x_2, 0, 0, -x_2) \ , \end{aligned} \tag{3.2}$$

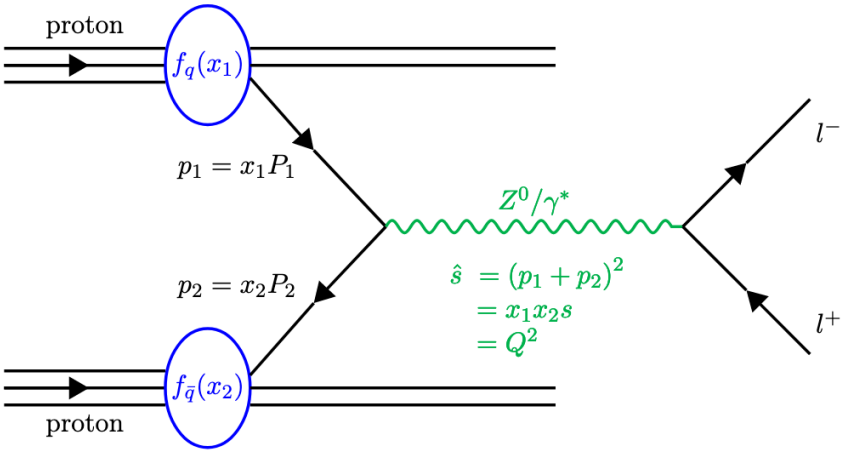

Figure 3.1: *LO Drell-Yan process in the parton model* [22].

with the momentum fraction x_i of the parton i. The square center-of-mass energy of the parton-parton scattering yields

$$\hat{s} = (p_1 + p_2)^2 = x_1 x_2 s = Q^2 = M^2 \, . \tag{3.3}$$

3.1 Factorisation

In order to calculate the cross section of a hard process, the collinear factorization theorem can be used. The factorization theorem separates the short-distance terms like the partonic cross section including QCD radiation, which can be computed perturbatively, and long-distance contributions, such as hadronisation, PDFs and collinear singularities. In section (2.2), we used the theorem to write the DIS cross section as a convolution of the partonic hard cross section and the PDFs of the incoming partons. This formalism can be generalised to the DY process. The formalism for the partons is nearly the same in the DY process than in the DIS scattering, although there are of course two partons evolutions involved in the DY process. In the perturbative expansion of the partonic cross section at NLO (or higher-orders), the real and virtual gluon emissions have to be included. Due to the collinear and soft emissions in the perturbative expansion of the cross section, the perturbative series breaks down. In order to cancel the divergent behaviour at small scales the factorization scale μ_F is introduced, as in the DIS case, see section (2.3.3). The collinear singularities are then absorbed in the PDFs by introducing renormalized scale-dependent PDFs $f_i(x, \mu_F^2)$.

In practice, the factorisation theorem claims that the cross section $\sigma(P_1, P_2)$ for a hard scattering process between two protons with four-momentum P_1 and P_2 can be obtained by weighting the partonic cross section $\hat{\sigma}_{q\bar{q}}$ with the PDF $f_q(x_i, \mu_F^2)$ defined as the probability density of finding a quark q with a certain longitudinal momentum fraction x_i at the factorization scale μ_F^2 inside the incoming proton. This expression is then integrated over all possible momentum fractions carried by the partons and summed over all possible quark flavours q to give the differential DY

cross section:

$$\frac{\mathrm{d}\sigma_{pp\to l^+l^-}}{\mathrm{d}M^2} = \sum_{q\bar{q}} \int_0^1 \mathrm{d}x_1 \int_0^1 \mathrm{d}x_2 \left\{ f_q(x_1,\mu_F^2) f_{\bar{q}}(x_2,\mu_F^2)\ \hat{\sigma}_{q\bar{q}\to l^+l^-} + (q \leftrightarrow \bar{q}) \right\} \delta(\hat{s} - M^2) \tag{3.4}$$

where M is the lepton pair invariant mass and where the sum runs over all quark antiquark combinations. The hard subprocess can be expanded as:

$$\hat{\sigma}_{q\bar{q}\to l^+l^-} = \{\hat{\sigma}_{LO}(\mu_F^2) + \alpha_S(\mu_R^2)\hat{\sigma}_{NLO}(\mu_F^2,\mu_R^2) + \ ... \}_{q\bar{q}\to l^+l^-} \tag{3.5}$$

Typically, the renormalization and factorisation scales are taken to be the same order of magnitude as well as the momentum scale of the hard process $Q^2 = M^2$.

3.2 Cross sections

In the following we discuss the DY cross section, first in the parton model and then including perturbative corrections, illustrating the factorization property described above. The DY process has been calculated up to NNLO but this accuracy won't be discussed here.

3.2.1 Parton Model and Leading Order

The cross section in the parton model follows Eq (3.4). At lowest order in pQCD, the subprocess cross section $\hat{\sigma}_{q\bar{q}\to l^+l^-}$ via an intermediate off-mass-shell photon can be obtained from the $e^+e^- \to q\bar{q}$ cross section (see e.g. [2]). One needs to correct this cross section by a colour factor of $1/N_c = 1/3$ due to the average of the colours of the initial state quarks.

$$\hat{\sigma}(q(p_1)\bar{q}(p_2) \to l^+l^-) = \frac{4\pi\alpha^2}{3\hat{s}} \frac{1}{N_c} Q_q^2 \,, \tag{3.6}$$

with $\hat{s}$ given by Eq (3.3) and Q_q the quark electric charge. The incoming quark and antiquark reveal different collision energies $\sqrt{\hat{s}}$, hence different invariant masses of the lepton pair can be produced. The differential cross section in the lepton pair mass, M, is given by:

$$\frac{\mathrm{d}\hat{\sigma}}{\mathrm{d}M^2} = \frac{4\pi\alpha^2}{3M^2} \frac{1}{N_c} Q_q^2 \delta(\hat{s} - M^2) \,. \tag{3.7}$$

The proton-proton cross section for this process yields

$$\begin{aligned} \frac{\mathrm{d}\sigma}{\mathrm{d}M^2} &= \int_0^1 \mathrm{d}x_1 \mathrm{d}x_2 \sum_q^{N_f} \{f_q(x_1) f_{\bar{q}}(x_2) + f_{\bar{q}}(x_1) f_q(x_2)\} \times \frac{\mathrm{d}\hat{\sigma}}{\mathrm{d}M^2} \\ &= \frac{4\pi\alpha^2}{3M^2} \int_0^1 \mathrm{d}x_1 \mathrm{d}x_2 \delta(x_1 x_2 s - M^2) \left[\sum_q^{N_f} Q_q^2 \{f_q(x_1) f_{\bar{q}}(x_2) + f_{\bar{q}}(x_1) f_q(x_2)\} \right] \end{aligned} \tag{3.8}$$

where we have used Eq (3.3) to replace $\hat{s}$.

In the naive parton model, the DY cross section should observe an analogous Björken scaling as in DIS structure function $F_i(x, Q^2)$ of section (2.2). Indeed in this approximation, the PDFs $f_i(x)$ are independent of the scale of the process $Q^2 = M^2$ and multiplying Eq (3.8) by M^4 one finds a scaling in the dimensionless variable $\tau = M^2/s$:

$$\begin{aligned} M^4 \frac{\mathrm{d}\sigma}{\mathrm{d}M^2} &= \frac{4\pi\alpha^2}{3N_c}\tau \int_0^1 \mathrm{d}x_1 \mathrm{d}x_2 \delta(x_1 x_2 - \tau) \left[\sum_q^{N_f} Q_q^2 \{ f_q(x_1) f_{\bar{q}}(x_2) + f_{\bar{q}}(x_1) f_q(x_2) \} \right] \\ &= \frac{4\pi\alpha^2}{3N_c}\tau \mathcal{F}(\tau) \, . \end{aligned} \tag{3.9}$$

In general, the differential cross section should be a function of the center-of-mass energy s and of the mass of the system M. This equation shows clearly a dependence on the scaling $\tau = M^2/s$. The measured DY cross section do exhibit a scaling behaviour to a good approximation, which confirms the parton model picture, see for example the review in [23].

3.2.2 Z boson production

By increasing the center of mass energies, the $q\bar{q} \to \gamma^* \to l^+ l^-$ contribution must be supplemented by the additional contribution of the Z boson in the s-channel. Eq (3.6) is thus completed by the Z contribution σ_Z and the γ/Z interference contribution σ_{int}:

$$\begin{aligned} \hat{\sigma}\Big(q(p_1)\bar{q}(p_2) \to l^+ l^-\Big)_{LO} &= \hat{\sigma}_{\gamma^*} + \hat{\sigma}_{int} + \hat{\sigma}_Z \\ &= \frac{4\pi\alpha^2}{3\hat{s}} \frac{1}{N_c} \Big[Q_q^2 + 2Q_q \, V_l \, V_q \, \chi_1(\hat{s}) \\ &+ \, (A_l^2 + V_l^2)(A_q^2 + V_q^2) \, \chi_2(\hat{s}) \Big] \end{aligned} \tag{3.10}$$

with

$$\chi_1 = \kappa \frac{\hat{s}(\hat{s} - M_Z^2)}{(\hat{s} - M_Z^2)^2 + M_Z^2 \Gamma_Z^2} \, , \quad \chi_2 = \kappa^2 \frac{\hat{s}^2}{(\hat{s} - M_Z^2)^2 + M_Z^2 \Gamma_Z^2} \, , \quad \kappa = \frac{1}{\sin^2 2\theta_W}$$

where M_Z and Γ_Z are the mass and total decay width of the Z boson respectively. The vector and axial couplings of the fermions to the Z are:

$$V_f = T_F^3 - 2Q_f \sin^2 \theta_W \, , \qquad A_f = T_F^3 \tag{3.11}$$

with $T_f^3 = +\frac{1}{2}$ for $f = \nu, u, ...$ and $T_f^3 = -\frac{1}{2}$ for $f = e, d, ...$. Note that the fermion masses have been neglected in the computation of this cross section.

The χ_2 term comes from the square amplitude of the Z-exchange and the χ_1 term from the γ/Z interference. The behaviour of the cross section depends of the center of mass scattering energies. On the one hand, far below the Z peak, the ratio $\hat{s}/M_Z^2$ is small so $1 \gg \chi_1 \gg \chi_2$, i.e. the weak effects which appear in the terms involving the vector and axial couplings, are small and can be neglected. On the

other hand, close to the Z pole, $\sqrt{\hat{s}} \sim M_Z$, the χ_2 term dominates.

These results represents the first term of Eq (3.5): $\hat{\sigma}_{LO}$. Again, as different invariant masses of the lepton pair can be produced, it is more appropriate to use the differential cross section as a function of the lepton pair invariant mass M^2, as in Eq (3.7). It gives:

$$\begin{aligned}\frac{\mathrm{d}\hat{\sigma}_{LO}}{\mathrm{d}M^2} = \frac{4\pi\alpha^2}{3M^2N_c}\delta(\hat{s}-M^2) \times \Big[Q_q^2 + 2Q_q\ V_l\ V_q\ \chi_1(M^2) \\ +\ (A_l^2+V_l^2)(A_q^2+V_q^2)\ \chi_2(M^2)\Big]\,.\end{aligned} \tag{3.12}$$

We can finally insert the partonic cross section result into the expression based on QCD factorization theorem (Eq (3.8)), to obtain the proton-proton cross section for the DY process at leading order:

$$\frac{\mathrm{d}\sigma_{LO}}{\mathrm{d}M^2} = \int_0^1 \mathrm{d}x_1\mathrm{d}x_2 \sum_{q=1}^{N_f}\{f_q(x_1)f_{\bar{q}}(x_2) + f_{\bar{q}}(x_1)f_q(x_2)\} \times \frac{\mathrm{d}\hat{\sigma}_{LO}}{\mathrm{d}M^2} \tag{3.13}$$

3.2.3 Perturbative QCD corrections

In this section we calculate the NLO partonic cross section of Eq (3.5). Only the photon exchange channel is considered for simplicity but the NLO corrections are similar for the Z boson and the interference. The calculation is analogous to that of the corresponding correction to the DIS structure function F_2, described in section 2.3.2. The $O(\alpha_S)$ QCD corrections to the partonic cross section correspond to loop and real corrections, where the latter is correlated with an additional parton emission. We begin by considering the LO parton model cross section of Eq (3.9) and its scaling behaviour:

$$M^4\frac{\mathrm{d}\hat{\sigma}}{\mathrm{d}M^2} = \frac{4\pi\alpha^2}{3N_c}\tau\hat{\mathcal{F}}(\tau)\,, \tag{3.14}$$

with

$$\hat{\mathcal{F}}(\tau) = Q_q^2\delta(1-\tau)\,. \tag{3.15}$$

In pQCD, the function $\hat{\mathcal{F}}$ can be expanded in powers of α_S:

$$\hat{\mathcal{F}}(\tau) = \hat{\mathcal{F}}_0(\tau) + \hat{\mathcal{F}}_1(\tau) + \ldots\,. \tag{3.16}$$

The only Feynman diagram present at LO for the DY process was the radiation-less quark-antiquark annihilation which does not contain any QCD vertex. The diagrams which contribute at $O(\alpha_S)$ are depicted in Fig (3.2). There are three types of diagrams, one where the incoming quark or antiquark emits a real gluon, the second where a virtual gluon is radiated and reabsorbed. The proton containing also gluons, a new type of diagram has to be considered, with gluon in the initial state. In short, the three types of contribution at $O(\alpha_S)$ are: real gluon corrections ($\hat{\mathcal{F}}_1^{q\bar{q},R}$), virtual gluon correction to the LO contribution ($\hat{\mathcal{F}}_1^{q\bar{q},V}$) and quark(antiquark)-gluon scattering ($\hat{\mathcal{F}}_1^{qg}$).

The corrections in the cross section computation introduce divergences. The three classes of divergences that can be encountered are:

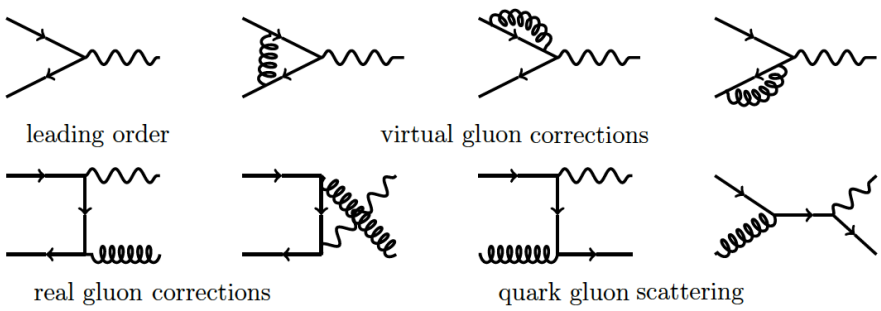

Figure 3.2: *LO and NLO Feynman diagrams dor the Drell Yan process.*

1. *Ultraviolet* (UV) divergences from the loop diagrams, if the energy of the radiated parton tends to infinity ($k^\mu \to \infty$).

2. *Infra-red* (IR) divergences due to *soft* ($k^\mu \to 0$) gluon emission from both real and virtual contributions.

3. *Collinear* divergences when the transverse momentum of the emitted parton goes to zero $p_T \to 0$.

The UV divergences are treated with renormalization, where different types of regularisation schemes can be used. The results showed below follow the approach of dimensional regularisation, which is discussed in [24]. This scheme allows us to simultaneously regularise both infrared and ultraviolet divergences. In the dimensional regularisation, the integration variables in space-time dimension are set to $4-2\epsilon$ instead of 4, with a regulator $\epsilon < 0$, and a scale μ^2 is introduced to preserve the dimensions of physical quantities. The contributions yield:

$$\begin{aligned}
\hat{\mathcal{F}}_1^{q\bar{q}} &= \hat{\mathcal{F}}_1^{q\bar{q},R} + \hat{\mathcal{F}}_1^{q\bar{q},V} \\
&= Q_q^2 \frac{\alpha_S(\mu^2)}{2\pi}\left[2\Big(-\frac{1}{\epsilon} - \ln(4\pi) + \gamma_E + \ln\frac{M^2}{\mu^2}\Big)P_{qq}^{(0)}(\tau) + D_q(\tau)\right] \\
\hat{\mathcal{F}}_1^{qg} &= Q_q^2 \frac{\alpha_S(\mu^2)}{2\pi}\left[\Big(-\frac{1}{\epsilon} - \ln(4\pi) + \gamma_E + \ln\frac{M^2}{\mu^2}\Big)P_{qg}^{(0)}(\tau) + D_g(\tau)\right]
\end{aligned} \tag{3.17}$$

where we ignored terms $O(\epsilon)$ or higher and with $\gamma_E = 0.5772...$ is the Euler constant. D_q and D_g are defined as [25, 26]:

$$\begin{aligned}
D_q(z) &= \frac{4}{3}\left[4(1+z^2)\left(\frac{\ln(1-z)}{1-z}\right)_+ - 2\frac{1+z^2}{1-z}\ln z + \delta(1-z)\left(\frac{2\pi^2}{3} - 8\right)\right], \\
D_g(z) &= \frac{1}{2}\left[(z^2+(1-z)^2)\ln\frac{(1-z)^2}{z} + \frac{1}{2} + 3z - \frac{7}{2}z^2\right].
\end{aligned} \tag{3.18}$$

One can see that only the collinear divergences fail to cancel when we take into account all the diagrams. The coefficient of $1/\epsilon$ singularity are the LO splitting functions defined in Eqs (2.23, 2.33). Thus convoluting the bare parton distributions with the $\hat{\mathcal{F}}_1^{q\bar{q}}$ and $\hat{\mathcal{F}}_1^{qg}$ functions, and replacing them by scale dependent "renormalized" distributions as in Eq (2.29), the singularities exactly cancel. This

annulment is achieved by the replacement $q_0(x) \to q(x, \mu^2)$:

$$\begin{aligned} q(x,\mu^2) = & q_0(x) + \frac{\alpha_S(\mu^2)}{2\pi}\left(-\frac{1}{\epsilon} - \ln(4\pi) + \gamma(E)\right) \\ & \times \int_x^1 \frac{\mathrm{d}\xi}{\xi}\Big[P_{qq}(x/\xi)\, q_0(\xi) + P_{qg}(x/\xi)\, g_0(\xi)\Big] + O(\alpha_S^2)\,. \end{aligned} \tag{3.19}$$

This calculation follows the factorisation theorem stating that for the DY process, all collinear singularities at every order in perturbation theory can be absorbed into universal parton distributions. The scale dependence of these PDF is determined by the DGLAP evolution equations. The remaining finite perturbative corrections modify the LO parton-model cross section.

The full cross section to $O(\alpha_S)$, with $\mu^2 = M^2$, is then

$$\begin{aligned} M^4 \frac{\mathrm{d}\sigma}{\mathrm{d}M^2} = & \frac{4\pi\alpha^2}{3N_c}\tau \int_0^1 \mathrm{d}x_1\, \mathrm{d}x_2\, \mathrm{d}z\, \delta(x_1 x_2 z - \tau) \\ & \times \Bigg[\sum_q Q_q^2 \left\{f_q(x_1, M^2) f_{\bar{q}}(x_2, M^2) + (q \leftrightarrow \bar{q})\right\} \times \left(\delta(1-z) + \frac{\alpha_S(M^2)}{2\pi} D_q(z)\right) \\ & + \sum_q Q_q^2 \{f_g(x_1, M^2)[f_q(x_2, M^2) + f_{\bar{q}}(x_2, M^2)] + (q, \bar{q} \leftrightarrow g)\} \times \frac{\alpha_S(M^2)}{2\pi} D_g(z)\Bigg]\,. \end{aligned} \tag{3.20}$$

3.3 Transverse momentum distributions

The Drell-Yan transverse momentum is a crucial observable to test perturbative as well as non-perturbative QCD. The particles produced by the DY at LO are two opposite charged leptons, here taken to be muons. These particles are referred as the dimuon system. Note that the following discussion would also be applicable if the leptons were electrons. The vectorial transverse momentum of the dimuon system $\vec{p}_T^{\,\mu\mu}$ is simply defined as the sum of the momenta of the two muons:

$$\vec{p}_T^{\,\mu\mu} = |\vec{p}_T^{\,\mu^+} + \vec{p}_T^{\,\mu^-}|\,. \tag{3.21}$$

This transverse momentum can be interpreted as the p_T of the γ/Z. At LO in the parton model using PDF, it should be zero because of momentum conservation in the transverse plane. At NLO the radiation of a hard gluon carrying some p_T will be balanced by the dimuon $p_T^{\mu\mu}$. The expected contributions of LO and NLO events to the transverse momentum are sketched in Fig (3.3).

Nevertheless, at very small $p_T^{\mu\mu}$, the intrinsic transverse motion of the partons inside the colliding protons cannot be neglected. There is a non-perturbative contribution due to the Fermi motion of the partons. It comes from the Heisenberg's uncertainty principle which asserts a fundamental limit to the precision with which the position x and the momentum p of a particle can be known: $\Delta x \cdot \Delta p \geq \hbar/2$. Taking the charge radius of the proton, $\Delta x = 0.87$ fm, it yields:

$$\Delta p \geq \frac{\hbar}{2\Delta x} = 113.41\,\mathrm{MeV}\,. \tag{3.22}$$

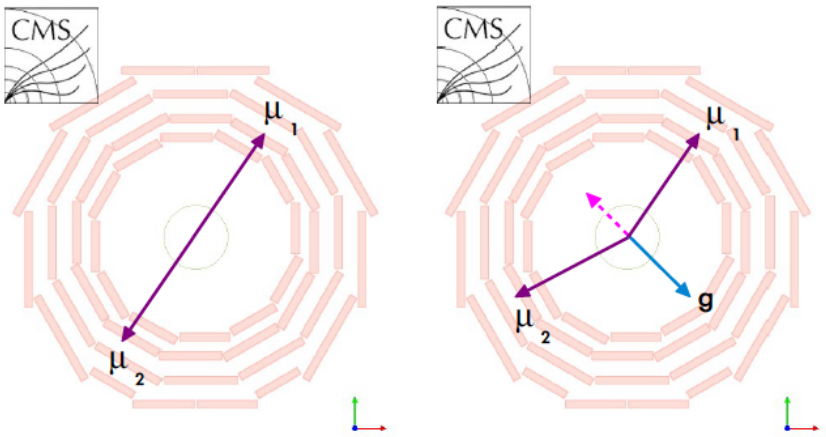

Figure 3.3: *Drell-Yan production decaying in two muons (left) and with an additional gluon (right), shown in the transverse plane of the CMS detector. For a LO event (left), the dimuon system has "zero" transverse momentum, the muons are thus emitted back-to-back. For some NLO event (right), one additional gluon (shown in blue) may be radiated, providing non-zero p_T to the dimuon system. The purple dashed arrow indicates the transverse momentum of the dimuon system, which can be computed from the measurement of the two individual muons* [22].

Such a contribution is to be expected in both x and y distribution, and for each parton interacting in the DY. Combining both transverse momentum directions: k_x, k_y; and taking into account the two partons, the Fermi motion contribution p_T^{Fermi} yields:

$$\begin{aligned} p_T^{Fermi} &= \sqrt{k_{x_1}^2 + k_{y_1}^2 + k_{x_2}^2 + k_{y_2}^2} \\ &\geq \sqrt{4 \cdot (113.41)^2} = 226.82\,\text{MeV}\,. \end{aligned} \tag{3.23}$$

It has been shown that the Fermi motion takes a Gaussian form. It follows that the differential $p_T^{\mu\mu}$ cross section also obeys the Gaussian distribution in very small $p_T^{\mu\mu}$ regions [2, 27]. The differential cross section as a function of p_T measured by the CFS collaboration [28] (from fixed-target pN collisions with $p_{lab} = 400$GeV, $\sqrt{s} = 27.4$ GeV) is shown in Fig (3.4) for a mass between 6 and 7 GeV. The parton can only have a limited transverse momentum k_T relative to the direction of the parent hadron. The curve fitting the low-p_T data corresponds to a Gaussian k_T distribution:

$$h(\vec{k}_T) = \frac{b}{\pi} \exp(-b k_T^2)\,. \tag{3.24}$$

The result obtained is $\langle k_T \rangle = 760$ MeV which is a value clearly larger that we expected from Fermi motion.

To investigate further, one can look at higher center-of-mass energy data and in particular the Z boson production. The differential cross section in p_T is shown in Fig (3.5), from the ATLAS collaboration [29] for $Z \to ee$, $66 < M_{ll} < 116$ GeV, $|y_{ll}| < 2.4$. Note that the leptons in these analysis are electrons and not muons, but this has no influence to our discussion so we will continue to talk in terms of muons. Assuming both transverse momentum component p_x and p_y obeys a Gaussian distribution, one can combine them and fit the result to the data at low-p_T. We find

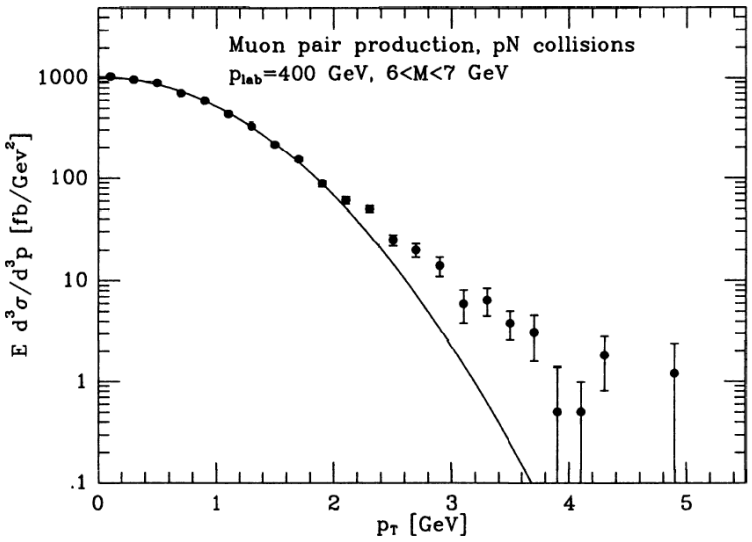

Figure 3.4: *The lepton pair transverse momentum from the CFS collaboration. The curve corresponds to a Gaussian intrinsic k_T distribution for tha annihilating partons* [28].

a mean of $\langle p_T \rangle = 3.6$ GeV, again not compatible with Fermi motion. It shows that the low-p_T peak position evolves with the scale and cannot just describe the Fermi motion, there must be another contribution in it.

The data of Fig (3.4) and Fig (3.5) also exhibits a large transverse momentum region. That leads us to consider new perturbative mechanisms, involving at least one QCD vertex. The relevant processes are the NLO $2 \to 2$ scattering: $q\bar{q} \to Zg$ and $qg \to Zq$. The diagrams are those of the second line of Fig (3.2).

The distribution at large $p_T^{\mu\mu}$ ($\geq M_{\mu\mu}$) follows perturbative QCD corrections that can be computed only to a certain fixed-order. The contributions have been calculated until next-to-next-to-leading order (NNLO), involving real emission processes like $q\bar{q} \to Zgg$ as well as virtual (loop) corrections to the NLO, see e.g. [30]. We will follow the argumentation of [2].

The prediction of the NLO cross section is in good agreement with the data at large-$p_T^{\mu\mu}$ but diverges as $p_T^{\mu\mu} \to 0$. The leading behaviour at small $p_T^{\mu\mu}$ comes from the emission of soft (four-momentum $k \to 0$) gluons. As we discussed in section 3.2.3, the total cross section is finite. Virtual corrections to the LO process $q\bar{q} \to Z$ only contribute at $p_T = 0$, i.e. $\mathrm{d}\sigma^V/\mathrm{d}p_T^2 \propto \delta(p_T^2)$, which essentially regularises the singular parts of the gluon emission cross section. Additionally, the perturbative and non-perturbative contributions from low-$p_T^{\mu\mu}$ must be combined with this perturbative large p_T tail given by the NLO cross section.

However a new problem arises in the region $\Lambda_{QCD} \ll p_T^{\mu\mu} \ll M^{\mu\mu}$: the higher-order terms in the perturbative series cannot be neglected. In particular, the soft gluon emissions become multiple and the leading contributions at each order in the perturbative series cannot be neglected. At each order, the differential cross section for these multiple soft gluon emissions obeys the following perturbative expansion

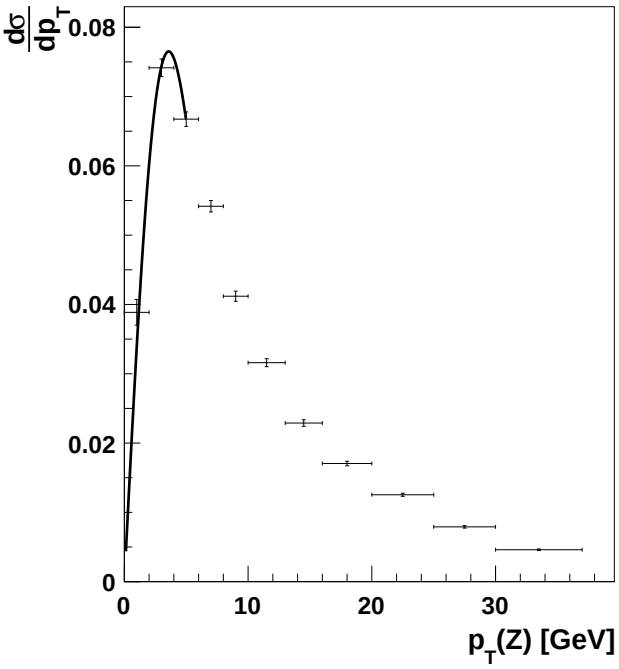

Figure 3.5: *The Z boson transverse momentum from ATLAS collaboration for $Z \to ee$, $66 < M_{ll} < 116$ GeV, $|y_{ll}| < 2.4$. The curve corresponds to our fit at low-p_T* [29].

in α_S:

$$\frac{1}{\sigma}\frac{\mathrm{d}\sigma}{\mathrm{p_T^2}} \simeq \frac{1}{p_T^2}\left[A_1\alpha_S \ln\frac{M^2}{p_T^2} + A_2\alpha_S^2 \ln^3\frac{M^2}{p_T^2} + ... + A_n\alpha_S^n \ln^{2n-1}\frac{M^2}{p_T^2} + ...\right], \quad (3.25)$$

with calculable coefficients A_i. The perturbative expansion in α_S is only reliable assuming that the scales are of the same order of magnitude. If $p_T \ll M$, the higher-order terms become non-negligible and we cannot keep the leading logarithms contributions anymore:

$$\alpha_S \ln^2\frac{M^2}{p_T^2} \gtrsim 1\,. \quad (3.26)$$

It follows that the fixed-order perturbative expansion is not appropriate to describe the behaviour of this p_T region. This corresponds to p_T values less than 10-15 GeV after taking into account the magnitude of the A_i coefficients. A solution to characterise the soft gluon emissions at low-p_T is given by the *resummation* approach. This method will be discussed in the next chapter among others techniques beyond pQCD at fixed order.

Chapter 4

TMDs from the Parton Branching solution of DGLAP

4.1 Beyond the Fixed Order Calculations

4.1.1 Parton Shower

In the 1970s Monte Carlo event generators were developed to simulate the fully exclusive final state of an interaction. They include different hadronization models to generate the hadrons of the final state.

Higher order corrections, beyond the order of the hard scattering process, are important and must be described properly. This was accomplished by introducing the concept of *parton showers*, which is an explicit simulation of higher order radiation according to the evolution equations. Parton shower formally works in the strongly-ordered limit. They start from a given leading order prediction and effectively multiply it by splitting probabilities for each additional emission. This allows in principle any observable to be predicted at leading logarithmic (LL) (and including some next-to leading logarithmic (NLL) effects).

In this formalism, standard Monte Carlo event generators for high-energy collisions, such as PYTHIA [31], have adjustable parameters to control the behaviour of its event modelling. The PYTHIA program comprises a coherent set of physics models for the evolution from a few-body hard process to a complex multi hadronic final state. It contains among other things a library of hard processes and models for initial- and final-state parton showers. A specific set of these parameters (called *tunes*) is adjusted to better fit some aspects of the data. It is worth mentioning that for precision calculations the accuracy of the parton shower has to be estimated. The control of soft gluon emission is the weakest aspect of the predictions.

Parton shower has long formed the basis for QCD applications at colliders. One of the limitations of the method described above is the requirement that the hard scattering and the parton evolution are collinear with the colliding hadrons, while parton radiations in the initial state (via parton showers) introduce transverse dimensions. Such a one dimensional (collinear) treatment is typically valid for single-scale observables, but encounters issues when a second scale appears, such as the

transverse momentum of the Z boson in a DY process.

4.1.2 Resummation

The *resummation* approach offers a solution to characterise the soft gluon emissions at low-p_T. For instance let us consider the Drell Yan process as in the previous chapter. The contributions of the leading logarithms in Eq (3.25) can be resummed to all orders in perturbation theory. It yields:

$$\begin{aligned}\frac{1}{\sigma}\frac{\mathrm{d}\sigma}{\mathrm{d}p_T^2} &\sim \frac{\mathrm{d}}{\mathrm{d}p_T^2}\exp\left(-\frac{\alpha_S}{2\pi}C_F\ln^2\frac{M^2}{p_T^2}\right)\\ &= \frac{\alpha_S}{2\pi}C_F\frac{\ln\frac{M^2}{p_T^2}}{p_T^2}\exp\left(-\frac{\alpha_S}{2\pi}C_F\ln^2\frac{M^2}{p_T^2}\right),\end{aligned} \tag{4.1}$$

vanishing at $p_T = 0$. $C_F = 4/3$ is the colour factor.

For a more complete analysis of this p_T region, one needs to properly treat the momentum conservation in multiple gluon emissions. The above approach assumes that only soft gluons are radiated when the $p_T^{\mu\mu}$ is close to zero. But actually only their vector transverse momentum sum should be small. Thus a more complete computation of multiple gluon emissions with small vector p_T sum is needed to describe the rise of the cross section at small p_T. This requires the introduction of the two-dimensional impact parameter vector $\vec{b}$ [32].

CSS formalism

In order to proceed properly to the resummation, the bi-dimensional impact parameter $\vec{b}$, the Fourier conjugate of $\vec{p}_T$, is used. The phase space of the impact parameter $\vec{b}$ has to be split into a perturbative part, that can be computed using perturbative QCD approach, and a non-perturbative part that has to be parametrised and extracted from the data. For the emission of n soft gluons, one writes

$$\delta^{(2)}\left(\sum_{i=1}^{n}\vec{k}_{T_i} - \vec{p}_T\right) = \frac{1}{(2\pi)^2}\int \mathrm{d}^2b\; e^{-i\vec{b}\cdot\vec{p}_T}\prod_{i=1}^{n} e^{-i\vec{b}\cdot\vec{k}_{T_i}}, \tag{4.2}$$

with $\vec{k}_{T_i}$ the transverse momentum of the gluon i.

In this context, the full calculation of the p_T resummation has been developed by Collins, Soper and Sterman (CSS) [33]. In the CSS formalism, contributions from all orders in α_S are resummed providing a finite result at small p_T. The cross section for the DY production in the collision of two hadrons (A and B) $AB \to Z/\gamma^* X$ where X represents any particle, is given by [27]:

$$\frac{\mathrm{d}\sigma_{AB}}{\mathrm{d}M^2\mathrm{d}p_T^2\mathrm{d}y} \approx \underbrace{\int \frac{\mathrm{d}^2b}{2\pi^2}e^{i\vec{p_T}\cdot\vec{b}}\,\widetilde{W}_{AB}(\vec{b},M,x_1,x_2)}_{\text{Resummed }\widetilde{W}\text{-term}} + Y(\vec{b},M,x_1,x_2), \tag{4.3}$$

with

$$Y = \left(\frac{\mathrm{d}\sigma_{AB}}{\mathrm{d}M^2\mathrm{d}p_T^2\mathrm{d}y}\right)_{fixed-order} - \left(\frac{\mathrm{d}\sigma_{AB}}{\mathrm{d}M^2\mathrm{d}p_T^2\mathrm{d}y}\right)_{asymptotic}, \tag{4.4}$$

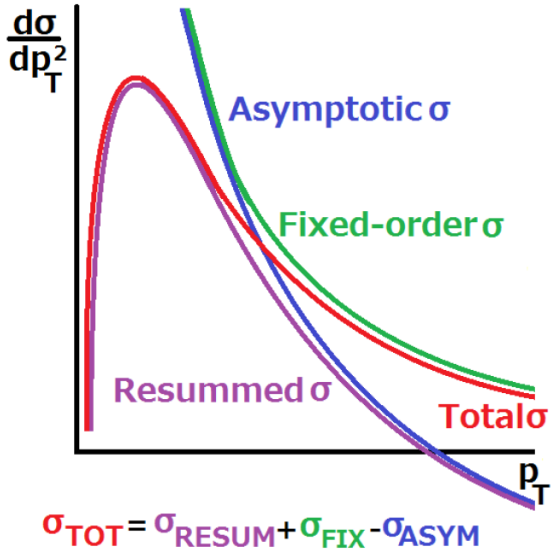

Figure 4.1: *Drell Yan $p_T^{\mu\mu}$ spectrum in the CSS resummation formalism approach* [27].

where M is the invariant mass, y the rapidity and $\vec{b}$ the two-dimensional impact parameter. The $\widetilde{W}_{AB}$-term is the resummed cross section in the small $p_T^{\mu\mu}$ region, and the Y term is obtained by subtracting the singular terms from the exact fixed-order result.

Fig (4.1) illustrates the full $p_T^{\mu\mu}$ distribution with the approach of the CSS resummation formalism. The total differential cross section is defined by Eq (4.3). The resummed cross section includes both the perturbative correction part and the non-perturbative one. The most singular part of the fixed-order cross section in the limit $p_T^{\mu\mu} \to 0$, is called the asymptotic cross section. The latter removes overlap between the resummed cross section and the fixed-order cross section. At small $p_T^{\mu\mu} \sim 0$, the fixed-order and the asymptotic cross section cancel and the Y term of Eq (4.4) goes to zero. The total differential cross section is then only determined by the resummed cross section in this region. The peak of the distribution comes from non-collinear parton collisions because, as we discussed, the colliding partons have gained transverse momenta through many soft gluon emissions. The number of such radiations increases for higher scale (higher dimuon masses) due to phase space expansion which explains the observed dependence of the peak position with the DY mass (see Fig (3.4) and (3.5) of previous chapter).

Such calculations are successful to describe the full p_T spectrum, for example at the LHC (see e.g. [34]), but only characterises the inclusive cross section.

4.1.3 Parton shower + Resummation

Only in very rare cases, a measurement can be compared directly with (semi-) analytic calculations. In a parton shower, at each parton branching, the transverse momentum of the emitted parton has to be balanced, resulting in a net transverse momentum entering the hard scattering. In Z-production, only the net effect of the multiple gluon radiation is important, and an analytic resummation can be

performed. In other measurements not only the net effect of multiple soft-gluon emission is important, but also the distribution of the partons in phase space plays a role, for example when jets in the final state are involved. In such cases, an explicit (exclusive) treatment of the partons is needed, and presently the parton shower is the only way to simulate those.

Clearly, to obtain the best possible predictions, it is desirable to combine the different theoretical descriptions in such a way that one benefits from the advantages of each. Fixed order predictions are necessary for a precise description of additional hard emissions. For observables sensitive to many soft and collinear emissions generating large logarithms, fixed order predictions are not suitable and resummation and parton showers are necessary. To obtain a prediction of the final state that is fully exclusive in all emissions, parton showers are required. In particular, parton shower predictions allow one to further attach a hadronization model to generate fully exclusive hadron-level events. These are an essential requirement for experiments to be able to simulate the data and study detector effects, and allow for the most direct comparison with experimental data.

Fig (4.2) shows the data of the $p_T^{\mu\mu} = p_T(Z)$ spectrum compared with their theoretical predictions [34]. The NNLO calculation (in green) describes quite well the high-p_T region, however it cannot describe the low-p_T. On the other hand, the resummation at NNLL (in blue) and parton shower based MC (in red) can describe the low-p_T.

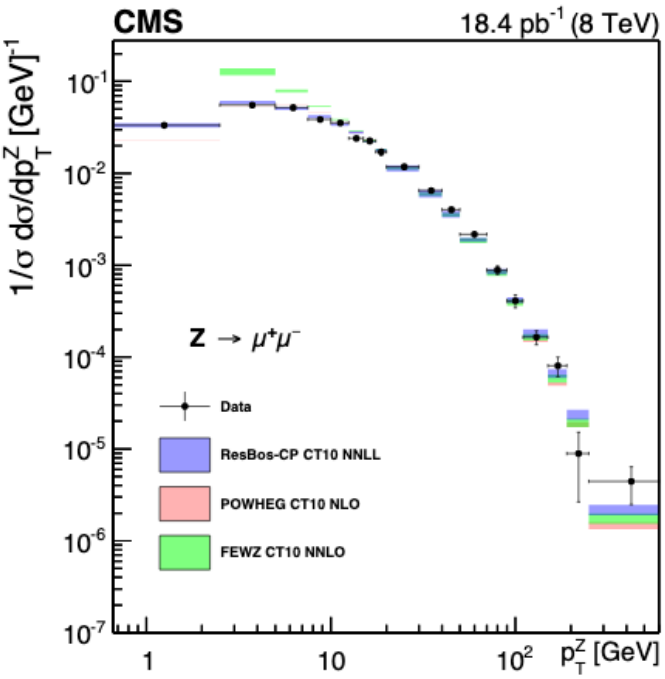

Figure 4.2: *Comparison of the normalized dimuon differential transverse momentum distributions from data with different theoretical predictions. The range of the dimuon mass is* $60 < M^{\mu\mu} < 120$ *GeV* [34].

4.1.4 Transverse Momentum Dependent PDFs

Above the Monte Carlo and the analytic resummation were discussed. In both cases, the transverse momentum from soft gluon resummation is added after the partonic cross section is calculated in collinear factorisation. The extension where the hard scattering is no longer collinear with the initial hadrons can be described by Transverse Momentum (k_T-) Dependent (TMD) Parton Distribution Functions (PDFs). Such a generalisation of the concept of PDF is the Transverse Momentum Dependent (TMD) PDF. TMD PDFs thus depend not only on x and μ^2 but also on k_T. Note that the PDFs and TMD PDFs describe the hadron structure in terms of momentum sharing, not of spatial structure.

The precision of predictions, and in particular the uncertainty coming from higher order radiation simulated by parton showers can be significantly improved when parton-distributions, which include information on the transverse momenta (TMD) [35], are used. Throughout this thesis we will refer to TMD PDFs as TMDs for reasons of brevity. TMDs encode non perturbative information on hadron structure, which is essential in the context of QCD factorisation theorems for multi-scale, non-inclusive collider observables, like the transverse momentum of the Z boson from Drell-Yan process.

TMD factorisation theorem is proven for small transverse momenta k_T in deep-inelastic and Drell Yan-type pp processes (see e.g; [36]). It is also demonstrated for small momentum fractions x high-energy factorisation [37, 38] following the BFKL (see e.g. [39] and CCFM [40] evolution equations.

The presence of a large variety of TMD factorisation and evolution frameworks complicates efforts to compare different TMDs. An example is the difference between the Collins-Soper-Sterman (CSS) style of TMD factorisation (see e.g. [36]) compared with the high-energy TMD factorisation style (see e.g. [41]). Moreover, within each category there are also competing subcategories of approaches.

TMDlib and TMDplotter are two useful tools available on internet [42, 43] to help study TMDs quantitatively [44]: the former is a C++ library that centralizes many TMD parametrisations in a common framework, similarly to the LHAPDF library [45] for collinear PDFs. The latter is an online tool making use of TMDlib to plot and compare TMDs among them, or to integrate and compare them with collinear PDFs.

The examples of TMDs motivations in the following come from [46] and from an overview of the subject [47].

For the DY $p_T(Z)$ spectrum discussed in the previous subsection TMDs combined with the resummation approach can describe low-p_T by resumming the logarithmically enhanced contributions in M/q_T up to all orders in α_S [36]. It is only after a generalized factorisation analysis, which goes beyond the collinear factorisation, that the physical behaviour of the Z boson spectrum can be predicted [47]. Also, it turned out that the non perturbative part of the impact parameter introduced in subsection 4.1.2 can be interpreted in terms of parton TMDs [36].

A second example concerns the extensive measurements of the Higgs boson at LHC. With the Higgs, new QCD processes become available in which the boson acts as a colour-singlet, a point-like source which couples to gluons. This allows precision QCD measurements in gluon fusion at high mass scales.

Theoretical predictions for the Higgs boson differential cross section as a function of q_T requires also generalized QCD factorisation that should be based on initial-state gluon distributions including polarization as well as transverse momentum. The main channel of Higgs boson production is gluon fusion which depends on gluon polarization and transverse momentum [41]. In the region of low-q_T ($q_T \ll m_H$), the contributions to the Higgs distributions have been studied both perturbatively (see e.g. [48]) and with non perturbative corrections (see e.g. [49]). The study of Higgs boson production at higher transverse momenta (but still $q_T < m_H$) can also be carried out with TMDs [50].

Besides the above examples, a famous problem of the collinear approach which can be solved by TMD factorisation is the rise of proton's structure functions at small longitudinal momentum fraction x. In proton-proton collisions, the product of the initial-state momentum fractions $x_1 \cdot x_2$ scales like $1/s$ at fixed momentum transfer, with s the squared centre-of-mass energy. Therefore, as the energy is increased $s \to \infty$, there are more events at small x which contribute to the probing of short-distance physics. This region is crucial for many hard-scattering cross sections measured at the LHC. At very low parton longitudinal momentum $x \to 0$, the fraction of momentum carried by the transverse components is expected to become a lot higher. The parton distributions have big uncertainties in this low-x regime and the higher order corrections can change a lot the distribution. The large corrections in this region come from multiple radiation of gluons not ordered in the gluon transverse momenta p_T. With the CSS TMD factorisation theorem [36], it is possible to resum logarithmically enhanced contributions coming from these unordered gluons, proportional to $\sqrt{s}/Q$, with Q the evolution mass scale [51].

Another exciting field where the TMDs have made huge progress is Double Parton Scattering (DPS). DPS occurs when two partons inside one hadrons collide with two partons in another hadron. These scatterings can generate particles with high invariant mass or high transverse momenta. These processes become important only at high-energy, like at the LHC energies. Usually, DPS are described in the framework of collinear factorisation with the Double Parton Distribution Functions (DPDFs), but there are ongoing attempts to describe DPS also in terms of TMDs [52].

To conclude, these fields (among others) where TMDs can be important should show how large the interest in TMDs is and how numerous the applications of TMDs are.
The method we follow in this thesis is an alternative method based on a Monte Carlo procedure, i.e. keeping the kinematic information at every gluon radiation steps and therefore a possible way to describe non inclusive cross sections in a fully differential way. This approach will be the subject of the next chapter.

4.2 DGLAP with Parton Branching method

The DGLAP evolution equations can be solved with a *Parton Branching* (PB) method [53, 54]. The PB method allows to generate the splitting variables z and scales μ^2, at which the branchings happen. All the evolution "chain" can be generated, with the information about all partons and their momenta. Moreover this method is attractive because it manages to treat exclusive processes while other semi analytical solutions of the evolution equations cannot. Indeed, with the PB method, the kinematics of every single splitting process can be treated exactly. The PB allows also to construct MC parton shower programs.

4.2.1 Why Parton Branching?

The collinear approach may give a high precision description of sufficiently inclusive processes where only one hard scale is involved, but when a second scale enters the picture, the collinear approach encounters some issues. This second scale can be for example the transverse momentum of the final state. Most of the predictions for the hard scattering cross sections in high energies collisions are calculated with pQCD, at NLO or NNLO. Monte Carlo (MC) event generators carry out *parton showers* to include the higher order radiations in the calculations (see subsection 4.1.1). The general procedure of a MC event generator in hadronic collisions within the collinear approximation is as follows: at first, the hard scattering process is generated with the initial momenta distributed according to collinear PDFs. Afterwards, a parton shower is applied on the interacting partons by going *backwards* (for efficiency reasons [2]). Backwards evolution means one starts from the hard scattering process parton and goes back to the beam particles.

As discussed previously in section 4.1, the spectrum of the Z boson transverse momentum q_T is an observable where the fixed order theory breaks out (see Fig (4.2)). There are at least four different ranges in this spectrum: the high-q_T, which is well described by perturbation theory; the low-q_T, dominated by multiple soft gluon emissions; the very low-q_T, controlled by non perturbative physics; and the intermediate-q_T. Difficulties are encountered in the treatment of this last region, the intermediate-q_T has to be treated carefully to match all these different prescriptions and avoid double counting. Finally, a good description is achievable but relies on many different tunes. Furthermore, this kind of problems must be treated process by process, there is no universal description.

The effects of parton shower on inclusive quantities have been studied (see e.g. [55]). It was showed that the transverse momentum was not the only observable impacted by the parton shower, in fact the longitudinal momentum x is also affected when it is defined in the light-cone coordinates. This is a consequence of the energy-momentum conservation: if transverse momentum is generated, the longitudinal momentum must decrease. In general, the MC event generators apply a rotation and a boost on the hard process to conserve energy-momentum. All the simulations of QCD processes are affected by these effects. As an example, the Fig (4.3) shows

the x distribution for inclusive jet events at $\sqrt{s} = 7$ TeV. One can see that including

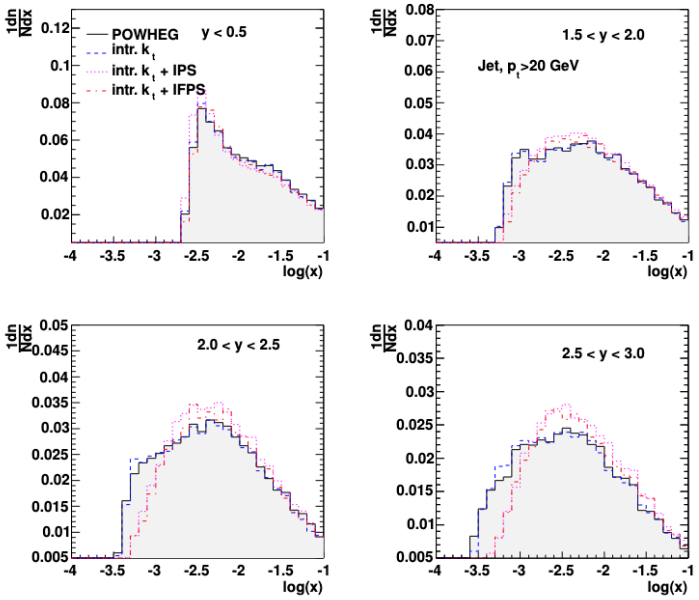

Figure 4.3: *The shift in parton longitudinal momentum fraction x distributions for inclusive jet production ($\sqrt{s} = 7$ TeV) at different rapidities. The effects shown are the inclusion of intrinsic k_T, initial (IPS) and initial+final state (IFPS) parton shower* [55].

the different prescriptions, one changes significantly the x distribution (POWHEG [56]) before showering.

An alternative idea arose [57]: to generate x, k_T of the matrix element at the given μ^2 according to a TMD, so no readjusting of the momenta is required. The TMD fixes the values of x, k_T, μ^2 and it is possible to construct a parton shower evolving exactly according to the kinematics contained in the TMD. This would bring a reconciliation between the parton shower and the matrix elements, as both would follow the same TMD. Of course, this is a ongoing project which requires several steps to be fulfilled. These steps can be divided in three sectors of research: first of all, procure the TMD PDF sets; then, the writing of a program generating the matrix elements. At the end, one needs to generate the parton shower which follows the kinematics according to TMDs. Of course, all these steps have to be properly combined to succeed.

A solution to obtain the TMD PDF sets for all flavours, which should be valid over the wide range of x and Q^2, is to use the DGLAP evolution equation. The idea was developed in [53, 54] and applied in [46]. It is important to mentioned that the PB TMD are fitted to the HERA data with *xFitter* [58].

In the method I am studying in my thesis a different approach is used. One applies and solves the DGLAP evolution equations with a particular method, the Parton Branching (PB) method [54, 59, 60], which allows to calculate the standard parton densities, $f(x, \mu^2)$, and at the same time parton densities $A(x, kt^2, \mu^2)$ including a transverse momentum. The transverse momenta which develops during

the parton cascade evolution is a consequence of energy momentum conservation (which is treated exactly in the simulation of the parton showers and in the PB method). The cross section in terms of TMDs is written as:

$$\sigma_{(A+B->X)} = A_i^A(x_1, k_{T_1}^2, \mu^2) \times \hat{\sigma}_{(i+j->X)} \times A_j^B(x_2, k_{T_2}^2, \mu^2)\,, \tag{4.5}$$

with the partons i, j and the hadrons A, B. The hard cross section is still calculated with collinear initial partons, while the transverse momenta of the initial partons are included in the kinematical calculations (in contrast to using kt dependent hard processes in BFKL and CCFM). The parton distribution functions have to be calculated including the full parton evolution.

With this Parton Branching (PB) approach one can, for the first time, calculate the complete evolution of the parton density which at the same time gives full information on the kinematics of the evolution process. Within this method, the parton shower is strictly tied to the parton density which includes soft-gluon resummation to all orders in α_S. The PB method has the further advantage, that parton showers can be included following exactly the evolution of the TMD parton density.

This thesis aimed to apply a simplified solution, based on [46], to the Drell Yan process. The rest of this chapter discusses the Parton Branching method to solve the DGLAP evolution equations.

4.2.2 Iterative solution with the Sudakov form factor

In this section we discuss a way to solve the evolution equation and to treat the soft limit. We follow the development of [61] (for a detailed discussion of the parton evolution see e.g. [2]). In the Parton Branching method one introduces a function, called the *Sudakov form factor*, which will allow us to rewrite DGLAP and to find an iterative solution. To begin with, recall the DGLAP evolution equations Eq (2.38) with the "+ prescription" (see Eq (2.24)) for a parton a:

$$\mu^2 \frac{\mathrm{d}f_a(x,\mu^2)}{\mathrm{d}\mu^2} = \frac{\alpha_S}{2\pi} \sum_b \int \frac{\mathrm{d}z}{z}\; P^R_{ab,+}(z)\; f_b(x/z, \mu^2)\,. \tag{4.6}$$

where the splitting functions in this equation are regularised by the + prescription. Inserting explicitly the expression for $P^R_{ab,+}$ it yields:

$$\mu^2 \frac{\mathrm{d}f_a(x,\mu^2)}{\mathrm{d}\mu^2} = \frac{\alpha_S}{2\pi} \sum_b \left(\int_0^1 \frac{\mathrm{d}z}{z}\; P^R_{ab}(z)\; f_b(x/z, \mu^2) - f_b(x,\mu^2) \int_0^1 \mathrm{d}z\; P^R_{ab}(z) \right)\,, \tag{4.7}$$

where we have used the definition of the + prescription:

$$\begin{aligned} \int_0^1 \mathrm{d}z \frac{f(z)}{z} P_+(z) &= \int_0^1 \mathrm{d}z \left(\frac{f(\frac{x}{z})}{z} - f(x) \right) P(z) \\ &= \int_0^1 \mathrm{d}z\; \frac{f(\frac{x}{z})}{z} P(z) - f(x) \int_0^1 \mathrm{d}z\; P(z)\,. \end{aligned}$$

For a parton species a (a quark of a given flavour or a gluon), one introduces the function

$$\begin{aligned}\Delta_a(\mu^2,\mu_0^2) \equiv \Delta_a(\mu^2) &= \exp\left(-\sum_b \int_{\mu_0^2}^{\mu^2} \frac{\mathrm{d}\mu'^2}{\mu'^2} \int_x^{z_M} \mathrm{d}z\ \frac{\alpha_S}{2\pi} P_{ba}^R(z)\right) \\ &= \exp\left(-\sum_b \int_{\ln\mu_0^2}^{\ln\mu^2} \mathrm{d}\ln\mu'^2 \int_x^{z_M} \mathrm{d}z\ \frac{\alpha_S}{2\pi}\ P_{ba}^R(z)\right)\end{aligned} \tag{4.8}$$

which is called the *Sudakov form factor* from an initial scale μ_0^2 to some evolved scale μ^2. We shall see shortly that this function has a simple physical interpretation. Note that the functions P_{ba}^R are the unregularised $a \to b$ LO splitting functions, with R standing for the *real* emissions (see section 2.3). We may use the unregularised splitting functions since we have introduced an explicit cut-off z_M.

In general, the divergence coming from soft real emission is cancelled by virtual contributions, it is thus possible to define a *resolvable* branching. It corresponds to a splitting of one into two partons, where at least in principle one can resolve the splitting. The *non-resolvable* branching consists of a contribution without branching and the virtual contributions. The upper integration limit z_M we introduced defines the boundary between resolvable and unresolvable branchings, it is an explicit infrared cut-off $z_M = 1 - \epsilon$ with ϵ a positive number very close to zero. Branchings with z above this range are classified as unresolvable, they involve the emission of undetectable soft parton.

Using

$$\frac{\partial e^{-\alpha(x)}}{\partial x} = -e^{-\alpha(x)} \frac{\partial \alpha(x)}{\partial x}\,,$$

one can differentiate Eq (4.8) in respect to $\ln\mu^2$ to get

$$\frac{\mathrm{d}\Delta_a(\mu^2)}{\mathrm{d}\ln\mu^2} = -\Delta_a(\mu^2)\frac{\alpha_S}{2\pi}\sum_b \int_x^{z_M} \mathrm{d}z\ P_{ba}^R(z)\,, \tag{4.9}$$

and inject this expression into Eq (4.7):

$$\mu^2 \frac{\mathrm{d}f_a(x,\mu^2)}{\mathrm{d}\mu^2} = \sum_b \int \frac{\mathrm{d}z}{z}\ \frac{\alpha_S}{2\pi} P_{ab}^R(z)\ f_b(x/z,\mu^2) + \frac{1}{\Delta_a(\mu^2)}\frac{\mathrm{d}\Delta_a(\mu^2)}{\mathrm{d}\ln\mu^2} f_a(x,\mu^2)\,. \tag{4.10}$$

Furthermore Eq (4.10) can be rewritten in a more compact way by multiplying with $1/\Delta$ and using $\frac{\partial}{\partial\mu^2}\frac{f}{\Delta} = \frac{1}{\Delta}\frac{\partial f}{\partial\mu^2} - \frac{f}{\Delta^2}\frac{\partial\Delta}{\partial\mu^2}$. Let us also proceed at a change of the name of the variables: $\mu \to \mu_1$ and $z \to z_1$, which gives:

$$\frac{\mathrm{d}}{\mathrm{d}\ln\mu_1^2}\left(\frac{f_a(x,\mu_1^2)}{\Delta_a(\mu_1^2)}\right) = \frac{1}{\Delta_a(\mu_1^2)}\sum_b \int_x^{z_M} \frac{\mathrm{d}z_1}{z_1}\ \frac{\alpha_S}{2\pi}\ P_{ab}^R(z_1)\ f_b(x/z_1,\mu_1^2)\,. \tag{4.11}$$

Notice that this is similar to the DGLAP evolution equation except that f has been replaced by f/Δ and that the regularised function $P_+^R(z)$ has been replaced by the unregularised one $P^R(z)$. This equation can be integrated over $\ln\mu^2$ to give an

integral equation for $f_a(x, \mu^2)$:

$$f_a(x,\mu^2) = f_a(x,\mu_0^2)\ \Delta_a(\mu^2) + \sum_b \int_{\ln\mu_0^2}^{\ln\mu^2} \mathrm{d}\ln\mu_1^2 \frac{\Delta_a(\mu^2)}{\Delta_a(\mu_1^2)} \int_x^{z_M} \frac{\mathrm{d}z_1}{z_1}\ \frac{\alpha_S}{2\pi}\ P_{ab}^R(z_1)\ f_b(x/z_1,\mu_1^2)\,, \tag{4.12}$$

where we have used $\Delta_a(\mu_0^2) = 1$. The same kind of solution can be written for $f_b(x/z_1, \mu_1^2)$:

$$f_b(x/z_1,\mu_1^2) = \Delta_b(\mu_1^2) f_b(x/z_1,\mu_0^2) + \sum_c \int_{\ln\mu_0^2}^{\ln\mu_1^2} \mathrm{d}\ln\mu_2^2 \frac{\Delta_b(\mu_1^2)}{\Delta_b(\mu_2^2)} \int_{\frac{x}{z_1}}^{z_M} \frac{\mathrm{d}z_2}{z_2}\ \frac{\alpha_S}{2\pi}\ P_{bc}^R(z_2)\ f_c(x/z_1z_2,\mu_2^2)\,, \tag{4.13}$$

which can be inserted into Eq (4.12). Clearly, the solution for $f_c(x/z_1z_2, \mu_2^2)$ may be written in the same way and inserted into Eq (4.13).

4.2.3 Interpretation in terms of Parton Branching

Looking at Eq (4.12), we can now give a simple and intuitive interpretation to the Sudakov form factor [46]. Assuming the parton a is a gluon at the scale μ^2 carrying

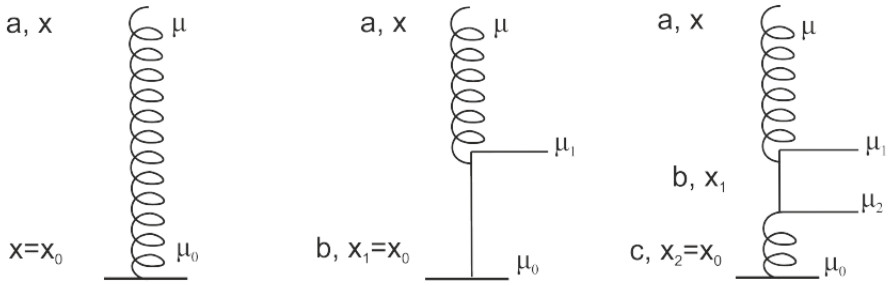

Figure 4.4: *Evolution by iteration* [46].

the proton's momentum fraction x, one wants to know where it comes from.

The first option is the simplest: there was no splitting between the initial scale μ_0^2 and μ^2. This is shown in the left-hand side of Fig (4.4) and is described by the first term of Eq (4.12). The Sudakov form factor $\Delta_a(\mu^2)$ is thus the probability for the parton a to evolve from μ_0^2 to μ^2 without *resolvable* branching. There was no branching so $x = x_0$. The fact that $\Delta_a(\mu_0^2) = 1$ is consistent with the above interpretation of $\Delta_a(\mu^2)$. Each parton species a has its own form factor $\Delta_a(\mu^2)$, which describes its probability of evolving between two scales without resolvable branching.

A second possibility is that the parton a was actually born during the splitting of another parton b at some scale μ_1^2. Parton b could be a quark splitting into a quark-gluon pair as illustrated by the middle diagram of Fig (4.4) or a gluon splitting into a gluon-gluon pair. This possibility is described by the second term of Eq (4.12). If the final parton a carries the fraction x of the proton's longitudinal momentum, then the parton b carried a fraction $x_1 = x/z_1$. Furthermore, assuming

parton b was the initial parton, then $x_0 = x_1 = x/z_1$, and this corresponds to the first term of Eq (4.13). The factor $\Delta_a(\mu^2)/\Delta_a(\mu_1^2)$ represents the probability for the parton a of evolving from μ_1^2 to μ^2 without resolvable branching, whereas $\Delta_b(\mu_1^2)$ is the probability for the parton b to evolve from μ_0^2 to μ_1^2 without *resolvable* branching.

However, parton b is not necessarily the initial parton, it could itself come from splitting of another parton c. Mathematically, this is described by the second term of Eq (4.13). Parton c then carried a momentum fraction $x_2 = x/(z_1 z_2$ and splitted into parton b at scale μ_2^2. Of course, parton c could be a quark or a gluon, the gluon case being illustrated in the right-hand side of Fig (4.4). If this time it was the initial parton then $x_0 = x_2$.

Of course, this process can be iterated to include more splittings. A single evolution chain from μ_0 to μ is called an *event*. For every event following one of the scenario discussed above x_0 can be different, first because the number of splitting is different but moreover, because z_1, z_2 etc. can be different in every event. Obtaining the solution of the DGLAP evolution equations requires taking into account all possible options, i.e. integrate over all possible x satisfying the energy-momentum conservation. Note that integrating over the momentum fraction x with a conservation rule (e.g. $\delta(z_1 x_1 - x)$) is the same as integrating over the splitting variable z, as we did in Eq (4.12).

The singularity at $z \to 1$ has been treated with the introduction of the $z_M = 1-\epsilon$ cut-off. The branchings with $z > z_M$ are classified as unresolved. The Sudakov form factor sums virtual and real contributions to all orders. Virtual corrections affect the no-branching probability and are included via unitarity: the resolvable branching probability tells us via unitarity the sum of virtual and unresolvable real contributions.

The formulation of parton branching in terms of the Sudakov form factor can be solved by iteration (see Eq (4.12)) and thus is well suited to computer implementation. It is the basis of the Parton Branching Monte Carlo techniques for simulating QCD jets.

4.2.4 Interpretation of the evolution scale

A priori, the DGLAP evolution scale μ has no physical meaning. In order to give the evolution scale a physical interpretation, one can associate the evolution scale to a given kinematic variable. This section follows the development of [46] and discusses possible associations and ordering conditions which arise as the consequence of these choices.

Virtuality and p_T-ordering

The four vector of the evolving partons in the splitting process have coordinates $k = (k_0, k_x, k_y, k_z) = (E_k, \vec{k}) = (E_k, k_T, k_z)$, with $k_T = (k_x, k_y)$. The kinematics of the process is shown in Fig (4.5), with μ' the scale of the branching. Using the light

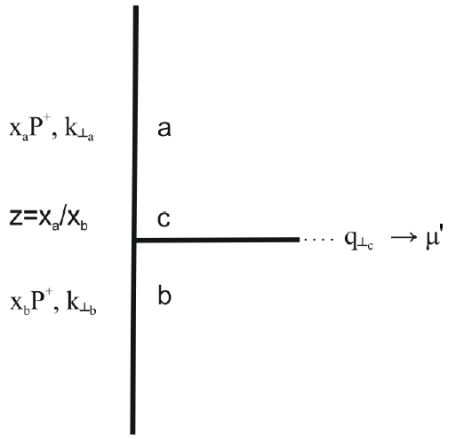

Figure 4.5: *The kinematics of the splitting process* [46].

cone variables $k = (k_+, k_-, k_T)$, where $k_\pm = \frac{1}{\sqrt{2}}(k_0 \pm k_z)$, the following relation holds:

$$\begin{aligned} k^2 &= 2k_+k_- - k_T^2 \\ \Leftrightarrow k_- &= \frac{k^2 + k_T^2}{2k_+}\,. \end{aligned} \tag{4.14}$$

One can write a momentum conservation condition from the kinematics of Fig (4.5):

$$k_b = k_a + q_c\,, \tag{4.15}$$

which can be rewritten in terms of the minus component conservation:

$$\frac{k_b^2 + k_{T,\,b}^2}{2k_{+,\,b}^2} = \frac{k_a^2 + k_{T,\,a}^2}{2k_{+,\,a}^2} + \frac{q_c^2 + q_{T,\,c}^2}{2q_{+,\,c}^2}\,. \tag{4.16}$$

One can assume that $k_{+,\,a} = zk_{+,\,b}$ and that $q_{+,\,c} = (1-z)k_{+,\,b}$. Furthermore, putting particles b and c on mass shell $k_b^2 = 0$, $q_c^2 = 0$, it yields:

$$k_{T,b}^2 = \frac{k_a^2 + k_{T,\,a}^2}{z} + \frac{q_{T,\,c}^2}{1-z}\,. \tag{4.17}$$

Working in the collinear approximation the strong ordering condition in the transverse momenta holds $k_{T,\,b}^2 \ll k_{T,\,a}^2$ and one can neglect $k_{T,\,b} = 0$ which gives us $k_{T,\,a} = -q_{T,\,c}$ by momentum conservation in the transverse plane. Eq (4.17) thus becomes

$$k_a^2(1-z) = -q_{T,\,c}^2\,. \tag{4.18}$$

The key of this development is now to associate the virtuality of the parton a with the DGLAP scale of the branching μ'^2. Making this association $\mu'^2 = -k_a^2$ we thus obtain:

$$\mu'^2(1-z) = q_{T,\,c}^2\,. \tag{4.19}$$

With this association the partons in the cascade are ordered in virtuality. Eq (4.19) is known as the *virtuality ordering* condition.

One can go a step further and work in the limit $z \to 0$, important for the high energy regime, then Eq (4.18) becomes

$$k_a^2 = -q_{T,\ c}^2 \,. \tag{4.20}$$

This time one can associate the DGLAP evolution scale with the transverse momentum to get:

$$\mu'^2 = q_{T,c}^2 \,. \tag{4.21}$$

This condition imposes the partons in the cascade to be ordered in p_T and Eq (4.21) condition is called the *p_T-ordering* condition.

Angular ordering

This section introduces the concept of colour coherence of QCD and the ordering condition which arises from it (for a more complete description see e.g. [2]). Coherence effects are common to all gauge theories. In electrodynamics for example it accounts for the suppression of soft bremsstrahlung from e^+e^- pairs, called the *Chudakov effect*. The Chudakov effect is shown in Fig (4.6). For simplicity, one

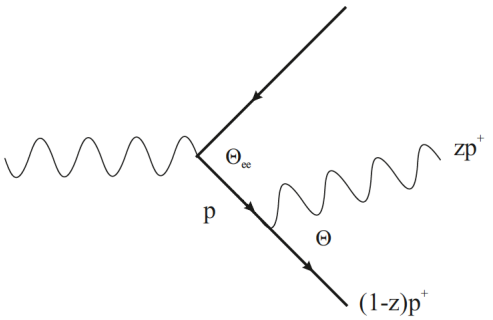

Figure 4.6: *Emission of a soft photon from the e^+e^- pair* [46].

shall assume the angles are small $\Theta_{ee}, \Theta \ll 1$ with the angle between the e^+e^- pair Θ_{ee} and the angle between the electron and the photon Θ. According to the uncertainty principle the time available for the photon emission is the inverse of the energy imbalance in the vertex $e^- \to \gamma e^-$, $\Delta t = 1/\Delta E$.

$$\Delta E = p - \sqrt{z^2p^2 + k_T^2} - \sqrt{(1-z)^2p^2 + k_T^2} \approx \frac{k_T^2}{2z(1-z)p} \,, \tag{4.22}$$

taking the limit $z \to 0$, we get

$$\Delta E \sim \frac{k_T^2}{2zp} \tag{4.23}$$

In the small angle approximation, the transverse momentum of the emitted photon is $k_T \approx zp\Theta$. From that we obtain

$$\Delta t \approx \frac{2}{zp\Theta^2} \sim \frac{1}{zp\Theta^2} \,. \tag{4.24}$$

In this time interval, the transverse separation of the pair will become $\Delta b \sim \Theta_{ee}\Delta t$. Only photon able to resolve the e^+e^- pair can be emitted. Otherwise, they cannot

resolve the individual charges of the electron (positron) and see only the net charge of the system, which is zero, implying no emission. In order to be able to resolve the transverse separation of the e^+e^- pair, the photon wavelength has to satisfy $\Delta b > \lambda/\Theta$, which yields $\Theta_{ee} > \Theta$.

A similar effect occurs in chromodynamics where this coherence effect reveals itself as an *angular ordering* of the soft gluons emissions [62]. The difference between the theories is that now one has to treat the colour charge of the gluon, which is a bit more complicated than the electric charge of the photon. The closest case to electrodynamics is two external lines, forming a colour singlet, like in $e^+e^- \to q\bar{q}$, where the gluon radiation from the $q\bar{q}$ pair outside the cone between $q\bar{q}$ is suppressed.

This coherent branching phenomena appears in the cascades of soft gluons emissions as illustrated in Fig(4.7). The transverse momentum of the i-th particle is

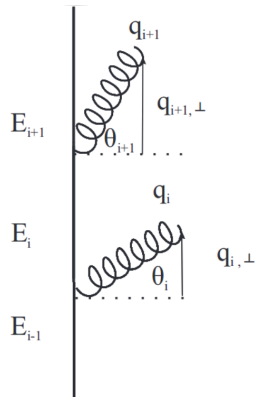

Figure 4.7: *Coherent branching in the cascade of soft gluons emissions* [46].

thus:

$$|q_{T,i}| = |\vec{q}_i| \sin\Theta_i = (1 - z_i)|\vec{k}_{i-1}| \sin\Theta_i \,, \tag{4.25}$$

and similarly, for the next emission:

$$|q_{T,i+1}| = |\vec{q}_{i+1}| \sin\Theta_{i+1} = z_i(1 - z_{i+1})|\vec{k}_{i-1}| \sin\Theta_{i+1} \,. \tag{4.26}$$

For the calculus of $q_{T,i}$, one assumes that $k_{T,i-1} = 0$ and the angle Θ_i is with respect to the beam axis. In the same way, to compute $q_{T,i+1}$, $k_{T,i}$ is neglected so the angle Θ_{i+1} is again with respect to the beam axis.

Defining the rescaled transverse momentum [40]

$$\frac{|q_{T,i}|}{1 - z_i} \equiv \bar{q}_{T,i} \,, \tag{4.27}$$

and dividing Eq (4.26) by Eq (4.25) one gets:

$$\frac{\bar{q}_{T,i+1}}{\bar{q}_{T,i}} = z_i \frac{\Theta_{i+1}}{\Theta_i} \,. \tag{4.28}$$

Making use of the angular ordering condition $\Theta_{i+1} > \Theta_i$ one obtains ordering condition for rescaled transverse momenta

$$\bar{q}_{T,i+1} > z_i \bar{q}_{T,i} \,. \tag{4.29}$$

For large z, this condition reduces to ordering in rescaled transverse momenta. For small z, in the limit $z \to 0$, the transverse momenta $\bar{q}_{T,i+1} > 0$ and can then perform a so-called *random walk* [63].

The rescaled transverse momenta can be associated with the DGLAP scale at which the branching happens, $\bar{q}_{T,i} = \mu'$, and rewrite Eq (4.27):

$$q_{T,i}^2 = (1 - z_i)^2 \mu'^2 \,, \tag{4.30}$$

which is known as the *angular ordering* condition.

4.2.5 The transverse momentum during the evolution

DGLAP equations are obtained in the collinear limit. However in the PB method one generates the splitting variable z, the branching scale μ' and transverse momentum is introduced for every branching. The kinematics of a branching is illustrated in Fig (4.8).

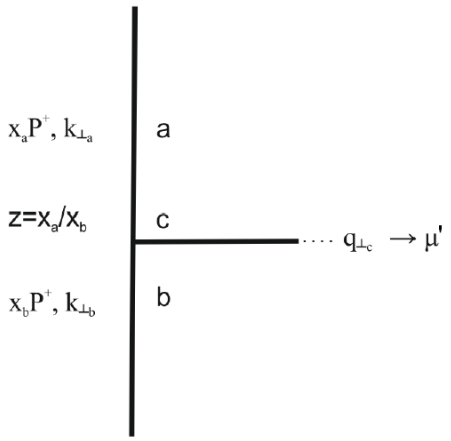

Figure 4.8: *The kinematics of the splitting process* [46].

The transverse momenta of the emitted and propagating partons can be obtained from p_T-, virtuality or angular ordering conditions discussed in the previous subsections, where the connection between the transverse momenta and the branching scale was introduced. Once the relation of q_T and μ' is chosen, one can calculate k_T of the propagating parton using the following formula:

$$\vec{k}_{T,a} = \vec{k}_{T,b} - \vec{q}_{T,c} \,. \tag{4.31}$$

This formula indicates that the k_T is accumulated during the evolution process. The transverse momentum in the parton branching method thus contains the whole history of the evolution [46].

Having k_T computed at each branching, one can construct the TMD parton density for every parton species $A_a(x, k_T, \mu^2)$. The following relation must be satisfied:

$$\int \mathrm{d}k_T^2 A_a((x, k_T, \mu^2)) = f_a(x, \mu^2) \,. \tag{4.32}$$

It means that the collinear PDF is the TMD PDF integrated over k_T^2. Using Eq (4.12) one can write an evolution equation for a TMD [54]:

$$\begin{aligned} A_a(x, k_T, \mu^2) = & A_a(x, k_T, \mu_0^2)\ \Delta_a(\mu^2) \\ & + \sum_b \int_{\ln \mu_0^2}^{\ln \mu^2} \frac{\mathrm{d} \ln \mu_1^2}{\pi} \frac{\Delta_a(\mu^2)}{\Delta_a(\mu_1^2)} \Theta(\mu^2 - \mu_1^2)\Theta(\mu_1^2 - \mu_0^2) \\ & \times \int_x^{z_M} \frac{\mathrm{d}z_1}{z_1}\ \frac{\alpha_S}{2\pi}\ P_{ab}^R(z_1)\ A_b\left(x/z_1, k_T + (1-z)^d \mu_1, \mu_1^2\right)\ , \end{aligned} \tag{4.33}$$

with d a power taking a different value which depends on the choice of ordering. The angular ordering condition corresponds to $d = 1$, the virtuality ordering to $d = 1/2$ and the p_T-ordering to $d = 0$. The transverse momentum thus accumulates at each branching depending on the scale, the splitting variable and the choice of ordering.

Note that the way of calculating k_T does not affect the collinear evolution. The variable μ^2 is generated according to the Sudakov form factor and the splitting variable z according to the collinear splitting functions. In both cases, there is no dependence on k_T or q_T. The details on the parton branching method we performed in this thesis will be discussed in next chapter.

Chapter 5

Analysis

This chapter contains my analysis on the solution of DGLAP evolution equation with the PB method using MC techniques. In the first section, a small summary of the probability theory we need in this thesis is presented. Then in the second section, details on the evolution are given. This leads us to the third section where the results are shown and discussed. Finally in the fourth section some results of a more advanced code (CASCADE) are presented.

5.1 Probability theory and Monte Carlo techniques

This section summarizes the elements of probability theory which are needed for this thesis. We follow the development of [61], further details can be found in text books (see e.g. [64]).

Monte Carlo method refers to any procedure which makes use of random number and uses probability statistics to solve a problem. It was invented in the 1930s by Fermi while studying the neutron diffusion. Nowadays, it is widely used in computations of complex processes for the simulation of natural phenomena, but also for designing detectors, understanding their behaviour and comparing experimental data to theory. Monte Carlo methods are a class of computational algorithms relying on repeated random samplings to compute the probabilities, to generate variables according to a given distribution, to solve numerically the integrals.

5.1.1 Random numbers and probability distributions

Monte Carlo methods require *random numbers* (RN). But how can we tell if a number is random? One needs a sequence of numbers, where each number is completely uncorrelated of the other numbers in the series. The RN considered in this thesis are always in the interval $[0, 1]$ and will be generated by the program RANLUX [65]. The RN generated on a computer are determined according to some algorithm, so they are never really random and are called *pseudo-random numbers*. A common RN generator is the *linear congruential random number generator* [64], which uses the recurrence

$$X_{n+1} = (aX_n + b) \bmod m \tag{5.1}$$

where X is the sequence of pseudo-random values. There are 4 integers that specify the generator: the modulus m, the multiplier a, the increment c and the seed or

initial value X_0.

Now consider an experiment where the outcome depends on a single variable x, one can ask what is the probability of observing values of x in the interval $[x, x+dx]$. This is given by $f(x)dx$ with $f(x)$ corresponding to the probability density function (*p.d.f.*), not to be confused with the PDF used for parton density function discussed before. The probability to find x in the interval $[a, b]$ is given by

$$P(a \leq x \leq b) = \int_a^b \mathrm{d}x \; f(x) \,. \tag{5.2}$$

The *p.d.f.* is normalized in the following way

$$\int_{-\infty}^{+\infty} \mathrm{d}x \; f(x) = 1 \,. \tag{5.3}$$

It means the probability of finding any value of x from the range of all the possible outcomes is equal to 1. In addition, it has to satisfy

$$f(\infty) = f(-\infty) = 0 \,. \tag{5.4}$$

With the knowledge of a *p.d.f.*, one can obtain the probability to obtain x smaller or equal than $t \in [a, b]$

$$P(x \leq t) = F(t) = \int_a^t \mathrm{d}x \; f(x) \,, \tag{5.5}$$

where $F(t)$ is called a *cumulative distribution* and it can be used to define the *p.d.f.*:

$$f(x) = \frac{\mathrm{d}F(x)}{\mathrm{d}x} \,. \tag{5.6}$$

One of the most important quantities in probability theory is the expectation value, for an arbitrary function $h(x)$. It is defined as:

$$E[h(x)] = \int_a^b \mathrm{d}x \; f(x) \; h(x) = \int \mathrm{d}F(x) \; h(x) = \frac{1}{b-a} \int \mathrm{d}x \; h(x) \,, \tag{5.7}$$

where we used the special case $\mathrm{d}F(x) = \mathrm{d}x/(b-a)$ for a uniform distribution in the range $[a, b]$. The expected value of a certain variable x is called the *mean value* and is defined

$$E(x) = \int_a^b \mathrm{d}x \; f(x) \; x = \langle x \rangle \,. \tag{5.8}$$

The spread of a distribution is measured by the *variance* σ^2

$$var(x) = \sigma^2 = E((x - \langle x \rangle)^2) \,, \tag{5.9}$$

which corresponds to the mean quadratic deviation from the mean value. The square-root of σ^2 is called the *standard deviation.*

Let us now discuss the distributions needed in this thesis. To begin with, a frequently encountered problem is, given a sequence of RN $(x_1, x_2, ...)$ distributed

according to a *p.d.f.* $f(x)$, to determine a sequence of RN $(u_1, u_2, ...)$ distributed according to another *p.d.f.* $g(u)$. The task is to find a suitable transformation $u(x)$ connecting distributions $f(x)$ and $g(u)$. One uses the equality between the probability to find $x' \leq x$ and the probability to find $u' \leq u(x)$ (with $u' = u(x')$):

$$\int_{-\infty}^{x} \mathrm{d}x' \; f(x') = \int_{-\infty}^{u(x)} \mathrm{d}u' \; g(u') \,, \tag{5.10}$$

then using Eq (5.5) it reads:

$$F(x) = G(u(x)) \,, \tag{5.11}$$

which can be inverted to obtain u distributed according to $g(u)$

$$u(x) = G^{-1}(F(x)) \,, \tag{5.12}$$

with G^{-1} the inverse of G. It seems simple but to solve the problem analytically, the inverse function G^{-1} has to exist and be analytically calculable. Also, the *p.d.f.* f and g must be integrable analytically. These conditions are rarely fulfilled all at once, so this problem will need another method. It can still be solved using another Monte Carlo technique: the *importance sampling* method. The random variables needed in the thesis are generated according to this importance sampling method which will be discussed in subsection 5.1.3.

Now let us discuss the properties of two basic distributions:

- **Uniform distribution** It is the simplest distribution, which will be used as a base for generating random variables following another distribution. The *p.d.f.* for a continuous uniform RN $x \in [x_{min}, x_{max}]$ is given by:

$$f(x) = \begin{cases} \frac{1}{x_{max} - x_{min}}, & x \in [x_{min}, x_{max}] \,, \\ 0 & \text{otherwise.} \end{cases} \tag{5.13}$$

  which means finding any value of x between x_{min} and x_{max} is equally probable. The mean value of x and the variance are:

$$E(x) = \frac{x_{min} + x_{max}}{2} \,, \tag{5.14}$$

$$\sigma^2 = \frac{(x_{max} - x_{min})^2}{12} \,. \tag{5.15}$$

  An important feature of uniform distribution is that from a uniformly distributed RN x in the range $[0, 1]$, one can easily obtain a RN u following another *p.d.f.* $g(u)$. Following Eq (5.10) we get:

$$u(x) = G^{-1}(x) \,, \tag{5.16}$$

  if $G^{-}1$ can be found.

- $f'(x) = \mathbf{1/x}$ **distribution** The normalised integral is:

$$\int_{x_{min}}^{x_{max}} \frac{1}{x'} \, \mathrm{d}x' = \log \frac{x_{max}}{x_{min}} \tag{5.17}$$

Since this $f'(x)$ function is not normalized to unity, one has to include the normalization factor, the distribution is then defined as follows:

$$f(x) = \frac{f'(x)}{\log \frac{x_{max}}{x_{min}}} = \frac{1}{\log \frac{x_{max}}{x_{min}}} \frac{1}{x}\,, \tag{5.18}$$

with $x \in [x_{min}, x_{max}]$.

Taking a random number R generated according to a uniform distribution in the range $R \in [0, 1]$, it is possible to obtain random variables which follow a $1/x$ law. To do so, one uses Eq (5.10), the primitive function $F(x)$ and Eq (5.18) to get:

$$\begin{aligned} F(x) &= \int_{x_{min}}^{x} f(x')\mathrm{d}x' \\ &= \frac{1}{\log \frac{x_{max}}{x_{min}}} \int_{x_{min}}^{x} \frac{1}{x'}\mathrm{d}x' = \frac{1}{\log \frac{x_{max}}{x_{min}}} \log \frac{x}{x_{min}} \\ R &= \frac{\log \frac{x}{x_{min}}}{\log \frac{x_{max}}{x_{min}}}\,. \end{aligned} \tag{5.19}$$

Solving this equation for x and iterating we get:

$$x_i = x_{min} \left(\frac{x_{max}}{x_{min}} \right)^{R_i}\,. \tag{5.20}$$

The values x_i can be generated from a uniform distribution of RN R_i.

5.1.2 Law of large numbers and Central limit theorem

The Monte Carlo (MC) methods are based on two essential laws: the *law of large numbers* and the *central limit theorem*.

By the law of large numbers, the average of the results obtained from numerous trials should be close to the expected value, and will tend to become closer as more trials are performed. Mathematically, let us generate N randomly distributed numbers x_i following uniform distribution in an interval from a to b. Let us then calculate the value of a function $u(x_i)$ for each of the generated x_i. The average of $u(x_i)$ converge to the expectation value of u when $N \to \infty$.

$$\frac{1}{N} \sum_{i=1}^{N} u(x_i) \to \frac{1}{b-a} \int_a^b u(x)\mathrm{d}x\,. \tag{5.21}$$

The quantity of the left-hand-side is a Monte Carlo estimate of the integral on the right-hand-side. The law of large numbers says that the MC estimate is consistent as the size of the random sample becomes large. At this stage, nothing is said about how large it has to be.

The law of large numbers tells that for infinitely large numbers the MC estimate of the integral converges to its true estimate. The second important law, the Central

Limit Theorem, states that when independent random variables are added, their properly normalized sum tends towards a normal distribution, even if the original variables themselves are not normally distributed. Central Limit Theorem tells us how the estimate of the integral from Eq (5.21) is distributed for large but finite N.

5.1.3 Monte Carlo integration

The MC methods can be used to solve integrals. Let us assume one wants to obtain a reliable estimate of the true value of an integral:

$$I = \int_{x_{min}}^{x_{max}} f(x)\mathrm{d}x\,, \tag{5.22}$$

To solve this integral, one may uses the law of large numbers. Generating N RN $x_i \in [x_{min}, x_{max}]$ from a uniform distribution $g(x)$, calculating $f(x_i)$ for every x_i and then averaging them, we obtain the expected value of $f(x)$:

$$E[f(x)] = \int_{x_{min}}^{x_{max}} f(x)g(x)\mathrm{d}x \approx \frac{1}{N}\sum_{i=1}^{N} f(x_i) = \bar{f}\,, \tag{5.23}$$

with $g = \frac{1}{x_{max}-x_{min}}$ we get:

$$E[f(x)] = \frac{1}{x_{max}-x_{min}} \int_{x_{min}}^{x_{max}} f(x)\mathrm{d}x\,. \tag{5.24}$$

The Monte Carlo estimate of the integral is then:

$$I \approx I_{MC} = \frac{x_{max}-x_{min}}{N}\sum_{i=1}^{N} f(x_i)\,. \tag{5.25}$$

Applying the definition of the variance Eq (5.9), we get:

$$V[I] = \frac{1}{N}(b-a)^2\left(\frac{1}{N}\sum f_i^2 - \left(\frac{\sum f_i}{N}\right)^2\right) \tag{5.26}$$

This formula allows us to estimate the uncertainty of a MC integration. However, it gives a probabilistic uncertainty band, which means we can only give a probability that the MC estimate lies within a certain range of the true values [66].

Importance sampling

An option to further improve the accuracy and efficiency of the MC integration is to use the *importance sampling* method and a normalized function $g(x)$, integrable in $[x_{min}, x_{max}]$, and which approximates $f(x)$:

$$\begin{aligned} I &= \int_{x_{min}}^{x_{max}} f(x)\mathrm{d}x = \int_{x_{min}}^{x_{max}} \frac{f(x)}{g(x)}\, g(x)\mathrm{d}x \\ &= \int_{x_{min}}^{x_{max}} h(x)g(x)\mathrm{d}x \\ &= E\left[h(x)\right]\,, \end{aligned} \tag{5.27}$$

with $h = f/g$. The integration thus reduces to calculating the expectation value $E[h(x)]$. Using the law of large numbers, one can generate N times x_i according to the *p.d.f.* $g(x)$, for every x_i calculate $h(x_i)$, and then average them to obtain the approximation of $E[h(x)]$:

$$I \approx I_{MC} = \frac{1}{N} \sum \frac{f(x_i)}{g(x_i)} \,. \tag{5.28}$$

For example, using $g(x) = (1/x)1/\log\left(\frac{x_{max}}{x_{min}}\right)$ (see Eq (5.18)), it yields:

$$I = \frac{\log\left(\frac{x_{max}}{x_{min}}\right)}{N} \sum \frac{f(x_i)}{\frac{1}{x_i}} \,. \tag{5.29}$$

The variance in this method is given by:

$$V\left[h(x)\right] = E\left[\left(h(x) - E[h(x)]\right)^2\right] \tag{5.30}$$

A disadvantage of importance sampling is that when $g(x)$ becomes zero, or approaches zero quickly, somewhere where $f(x)$ is not zero, $V[h(x)]$ may becomes infinite [66].

5.2 Parton Branching Method from scratch

This section provides a description of the Parton Branching method with Monte Carlo techniques. The goal is to solve the integral evolution equation Eq (4.12):

$$\begin{aligned} f_a(x,\mu^2) &= f_a(x,\mu_0^2)\ \Delta_a(\mu^2) \\ &+ \sum_b \int_{\ln\mu_0^2}^{\ln\mu^2} \mathrm{d}\ln\mu_1^2 \frac{\Delta_a(\mu^2)}{\Delta_a(\mu_1^2)} \int_x^{z_M} \frac{\mathrm{d}z_1}{z_1}\ \frac{\alpha_S}{2\pi}\ P_{ab}^R(z_1)\ f_b(x/z_1,\mu_1^2)\,, \end{aligned} \tag{5.31}$$

In the following, we will describe a forward evolution from a known initial parton

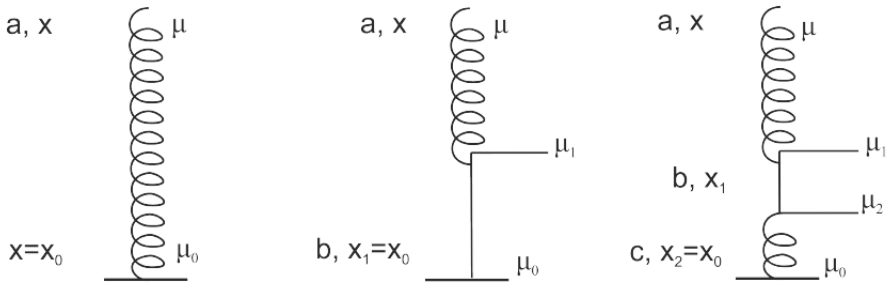

Figure 5.1: *Examples of 0-, 1-, 2-branchings* [46].

at a given scale μ_0^2 until a maximum scale μ^2. The number of branchings that will take place as well as the final parton at scale μ^2 are unknown and will be randomly generated. The scales μ_0^2 and μ^2 are kept fixed for all the discussed events.

This section is divided into 5 subsections. The next three subsections correspond to the left, middle and right-hand side of Fig (5.1) where 0-branching, 1-branching and 2-branchings events are shown respectively. These cases are only consider at LO. The notations in the subsections agree with the corresponding piece of Fig (5.1). In the fourth subsection, the choice made on the splitting functions will be discussed. The last subsection describes the application of this simplified PB method to the DY process.

5.2.1 0-branching event

We begin by considering an event with no branching, corresponding to the left-hand side of Fig (5.1). First, a word on the starting conditions of the evolution. It starts with a parton a at scale $\mu_0^2 = 1$ GeV. The choice for this value corresponds approximately to the mass of the proton. The parton a carries a fraction x of the momentum of the proton. x has to be randomly generated according to some starting parton density:

$$y(x, \mu_0^2) = 3\frac{(1-x)^5}{x}\,. \tag{5.32}$$

This parton density describes well the x dependence of the PDF shapes at small x, for gluons as for the sea quarks. To simplify the analysis, it will be used for every parton. We proceed with an importance sampling method with the approximate function $y' = \frac{1}{x}\frac{1}{\log\frac{x_{max}}{x_{min}}}$. It gives us a generated x and a weight w_x because we used this alternative method and not the true parton density. A complete example of the importance sampling method and how to compute the weight will be provided further for the generation of the splitting variable z.

In addition to this longitudinal fraction of momentum, we consider k_x, k_y, intrinsic transverse components for the parton. The intrinsic k_T is assumed to be a Gaussian $\exp -k_T^2/\sigma^2$ with $\sigma^2 = k_0^2/2$ where k_0 has a fixed value. By generating uniformly an angle $\theta \in [0, 2\pi]$, the generated k_T is can be separated into the k_x and k_y directions by projecting the transverse momentum to the two orthogonal directions.

The evolution starts thus with a parton a with (x, w_x, k_x, k_y) at scale μ_0^2. One has to generate the scale μ_1^2 at which the branching should happen. Let us recall the Sudakov form factor:

$$\begin{aligned} \Delta_a(\mu_1^2, \mu_0^2) &= \exp\left(-\sum_b \int_{\ln\mu_0^2}^{\ln\mu_1^2} \mathrm{d}\ln\mu'^2 \int_0^{z_M} \mathrm{d}z\ \frac{\alpha_S}{2\pi}\ P_{ba}^R(z)\right) \\ \Leftrightarrow \ln\Delta_a(\mu_1^2, \mu_0^2) &= -\int_{\ln\mu_0^2}^{\ln\mu_1^2} \mathrm{d}\ln\mu'^2\ \frac{\alpha_S}{2\pi}\ I_z\,, \end{aligned} \tag{5.33}$$

with I_z the result of the integral over z. The scale is now generated by using the probabilistic interpretation of the Sudakov form factor $\Delta_a(\mu_1^2, \mu_0^2) = R$ with

$R \in [0,1]$ a uniformly distributed RN. We have the following equation for μ_1^2:

$$\begin{aligned} & -\frac{\alpha_S}{2\pi}\, I_z \int_{\ln \mu_0^2}^{\ln \mu_1^2} \mathrm{d} \ln \mu'^2 = \ln R \\ \Leftrightarrow\ & \ln\left(\frac{\mu_1^2}{\mu_0^2}\right) = -\frac{2\pi}{\alpha_S\, I_z}\, \ln R \\ \Leftrightarrow\ & \mu_1^2 = \mu_0^2\, R^{-\frac{2\pi}{\alpha_S\, I_z}}\,. \end{aligned} \tag{5.34}$$

If the generated scale is above μ^2, it means there was no branching between μ_0^2 and μ^2. The information about a parton a at a scale μ^2 and x can be put in a histogram for $f_a(x,\mu^2)$ vs x. Events of this type correspond to this piece of the evolution equation Eq (4.12):

$$f_a^{(0)}(x,\mu^2) = f_a(x,\mu_0^2)\Delta_a(\mu^2,\mu_0^2) \tag{5.35}$$

Note that in this case, no transverse momentum was generated since there was no splitting.

5.2.2 1-branching event

The evolution starts this time with a parton b corresponding to the middle illustration of Fig (5.1). The initial momentum fraction x_1 and the weight w_x, as well as the intrinsic transverse momentum components k_{x_1}, k_{y_1} are generated as discussed previously. In the following, all the RN R_i are uniformly generated in the range $[0,1]$.

Next the scale μ_1^2 at which the first branching happens is generated according to the equation

$$\ln R_1 = -\frac{\alpha_S}{2\pi}\, I_z \int_{\ln \mu_0^2}^{\ln \mu_1^2} \mathrm{d} \ln \mu'^2 \tag{5.36}$$

Let us assume that this time the generated scale is lower than our final scale $\mu_1^2 < \mu^2$.

Since a branching is happening, one has to generate the splitting variable z_1. The splitting functions are complicated, we cannot perform the generation exactly according to the splitting function. Instead, we implement an importance sampling method and generate z_1 according to some easier function. A special weight w_z must then be applied to correct the generated distributions.

At LO, a quark can split and continue the evolution only as a gluon or as a quark of the same flavour and a gluon can split only to a gluon or a quark. In other words, one has to answer the question if b splits into a parton b (P_{bb}^R) or a different parton a (P_{ab}^R). This question can be answered using the probabilistic interpretation of the splitting functions [46], but to simplify the analysis, we only take into account splitting into the same parton species $a = b$. Note that it does not correspond to the example in the middle of Fig (5.1), where $a \neq b$. This choice is discussed in subsection (5.2.4).

The splitting variable z_1 will thus be generated according to the properly normalized splitting function $P_{bb}(z)$ with $b = q$ or g:

$$R_2 = \frac{\int_\epsilon^{z_1} \mathrm{d}z \; P_{bb}^R(z)}{\int_\epsilon^{1-\epsilon} \mathrm{d}z \; P_{bb}^R(z)} = \frac{\int_\epsilon^{z_1} \mathrm{d}z \; P_{bb}^R(z)}{N_P}\,, \tag{5.37}$$

with N_f the normalization factor. Since the splitting function in Eq (5.37) is complicated and it is not possible to find analytically the inverse of this function, the importance sampling method has to be used.

For example, if we consider quarks:

$$P_{bb}^R(z) = P_{qq}^R(z) = \frac{4}{3}\left[\frac{1+z^2}{1-z}\right]\,, \tag{5.38}$$

we choose an approximate function, $g(z) = \frac{1}{1-z}\frac{1}{N_g}$ normalized to unity with the factor $N_g = \int_\epsilon^{1-\epsilon} \mathrm{d}z \; \frac{1}{1-z}$. Now we solve the following equation for z_1:

$$\begin{aligned} R_2 &= \frac{\int_\epsilon^{z_1} \frac{1}{1-z'}\mathrm{d}z'}{\int_\epsilon^{1-\epsilon} \frac{1}{1-z'}\mathrm{d}z'} \\ \Leftrightarrow \; -\ln\left(\frac{1-z_1}{1-\epsilon}\right) &= -R_2 \ln\left(\frac{1-(1-\epsilon)}{1-\epsilon}\right) \\ \Leftrightarrow \frac{1-z_1}{1-\epsilon} &= \left(\frac{\epsilon}{1-\epsilon}\right)^{R_2} \\ \Leftrightarrow z_1 &= 1-(1-\epsilon)\left(\frac{\epsilon}{1-\epsilon}\right)^{R_2} \end{aligned} \tag{5.39}$$

This z comes with a certain weight w_z to compensate for generating it according to $g(z)$ and not from Eq (5.37):

$$\begin{aligned} w_{z_1} &= \frac{f(z_1)}{g(z_1)} = \frac{P_{qq}(z_1)}{N_P} \cdot \frac{1}{g(z_1)} = \frac{4}{3}\frac{1}{N_P}\frac{1+z_1^2}{1-z_1} \; \cdot \; \frac{1}{\frac{1}{1-z_1}\frac{1}{N_g}} \\ &= \frac{4}{3}(1+z_1^2)\;\frac{N_g}{N_P} \end{aligned} \tag{5.40}$$

Now that we have generate z_1, x can be calculated simply by applying the momentum conservation expressed by the delta function $\delta(z_1 x_1 - x)$:

$$x = z_1 x_1\,. \tag{5.41}$$

For the evolution of the transverse components, the procedure depends on the choice of ordering (see subsection 4.2.4). It is accumulated as follows:

$$\begin{aligned} k_x &= k_{x_1} + \sqrt{\mu_1^2}\cos(\phi_1)(1-z_1)^d\,, \\ k_y &= k_{y_1} + \sqrt{\mu_1^2}\sin(\phi_1)(1-z_1)^d\,, \end{aligned} \tag{5.42}$$

where $\phi_1 = 2\pi R_3$ is a random angle. The power d takes a different value depending on the choice of ordering. The angular ordering condition corresponds to $d = 1$, the

virtuality ordering to $d = 1/2$ and the p_T-ordering to $d = 0$.

Now that each of the variables has evolved, one can generate a scale for the next branching. Assuming this scale is bigger than the maximum evolution scale μ^2, the evolution is stopped.

The procedure is repeated many times ($\sim 10^7$ or more) and one has many 1-branching events generated. A histogram is filled with x and weight $w_x \cdot w_{z_1}$ for the scale μ^2 and parton a ($f_a(x, \mu^2)$). Another histogram takes $k_T = \sqrt{k_x^2 + k_y^2}$ and weight $w_x \cdot w_{z_1}$ for the scale μ^2 and parton a ($A_a(k_T, \mu^2)$). As we don't allow changing from species, we start either from a gluon which splits into two gluons and one of them continues the evolution, or from a quark which radiates a gluon and another quark of the same flavour continues the evolution. One can built the histograms for each of the species. Of course, $x_1, w_{x_1}, k_{x_1}, \mu_1^2, z_1, ...$ can have different values in every event.

The contribution to the histogram $f_a(x, \mu^2)$ vs x from the 1-branching events corresponds to the following piece of the evolution equation Eq (4.12):

$$f_a^{(1)}(x, \mu^2) = \int_{\ln \mu_0^2}^{\ln \mu^2} \mathrm{d} \ln \mu_1^2 \frac{\Delta_a(\mu^2)}{\Delta_a(\mu_1^2)} \int_x^{z_M} \frac{\mathrm{d}z_1}{z_1} \frac{\alpha_S}{2\pi} \sum_b P_{ab}^R(z_1)\ f_b(x/z_1, \mu_0^2)\ \Delta_a(\mu_1^2, \mu_0^2)\,. \tag{5.43}$$

5.2.3 2- and more branchings event

Now let us discuss an event with two branchings, corresponding to the right-hand side of Fig (5.1)). In the following, the RN R_i are uniformly distributed in the range $[0, 1]$. A parton c with initial momentum fraction x_2, weight w_x, transverse components k_{x_2} and k_{y_2} is generated.

The scale μ_2^2 at which the branching happens is generated according to the Sudakov form factor:

$$\ln R_1 = -\frac{\alpha_S}{2\pi}\ I_z \int_{\ln \mu_0^2}^{\ln \mu_2^2} \mathrm{d} \ln \mu'^2\,. \tag{5.44}$$

Let us assume that the generated scale is lower than our final scale $\mu_2^2 < \mu^2$.

We consider only the case where the parton c splits into a parton of the same species ($b = c$). Note that it does not correspond to the example in the right-hand side of Fig (5.1), where $b \neq c$. The splitting variable z_2 should be generated according to:

$$R_2 = \frac{\int_\epsilon^{z_2} \mathrm{d}z\ P_{cc}^R(z)}{\int_\epsilon^{1-\epsilon} \mathrm{d}z\ P_{cc}^R(z)}\,. \tag{5.45}$$

We proceed by using the importance sampling method described in the previous subsection. The weight w_{z_2} coming from the splitting variable z_2 must also be computed.

The evolution of the transverse momentum is generated as follows:

$$\begin{aligned} k_{x_1} &= k_{x_2} + \sqrt{\mu_2^2}\cos(\phi_2)(1-z_2)^d\,, \\ k_{y_1} &= k_{y_2} + \sqrt{\mu_2^2}\sin(\phi_2)(1-z_2)^d\,, \end{aligned} \tag{5.46}$$

where $\phi_2 = 2\pi R_3$ is a random angle. The scale μ_1 of the next branching is generated:

$$\ln R_4 = -\frac{\alpha_S}{2\pi}\ I_z \int_{\ln\mu_2^2}^{\ln\mu_1^2} \mathrm{d}\ln\mu'^2\,. \tag{5.47}$$

Assuming that $\mu_1^2 < \mu^2$ and considering only the case where the parton b splits into a parton of the same species ($a = b$). z_1 can be generated according to the splitting function:

$$R_5 = \frac{\int_\epsilon^{z_1} \mathrm{d}z\ P_{bb}^R(z)}{\int_\epsilon^{1-\epsilon} \mathrm{d}z\ P_{bb}^R(z)}\,, \tag{5.48}$$

with the method described above. The weight w_{z_1} coming from this generation has to be calculated.

The transverse momentum evolution is generated:

$$\begin{aligned} k_x &= k_{x_1} + \sqrt{\mu_1^2}\cos(\phi_1)(1-z_1)^d\,, \\ k_y &= k_{y_1} + \sqrt{\mu_1^2}\sin(\phi_1)(1-z_1)^d\,, \end{aligned} \tag{5.49}$$

where $\phi_1 = 2\pi R_6$ is a random angle.

Now assume one generates a scale which is finally higher than our maximum scale and the evolution is thus stopped after two branchings. The information about the parton a at scale μ^2, $x = z_1 z_2 x_2$ and weight $w_{z_1}\cdot w_{z_2}\cdot w_x$ fill the histogram $f_a(x,\mu^2)$ vs x.

Another histogram takes $k_T = \sqrt{k_x^2 + k_y^2}$ and weight $w_{z_1}\cdot w_{z_2}\cdot w_x$ for the scale μ^2 and parton a ($A_a(k_T,\mu^2)$). This procedure is repeated many times ($\sim 10^7$ or more) and one has many 2-branchings events generated. Remember that the partons are not allowed to change from species.

The 2-branchings contribution to the histogram $f_a(x,\mu^2)$ vs x comes from this piece of the evolution equation:

$$\begin{aligned} f_a^{(2)}(x,\mu^2) = \sum_b \int_{\ln\mu_0^2}^{\ln\mu^2} \mathrm{d}\ln\mu_1^2 \frac{\Delta_a(\mu^2)}{\Delta_a(\mu_1^2)} \int_x^{z_M} \frac{\mathrm{d}z_1}{z_1}\ \frac{\alpha_S}{2\pi}\ P_{ab}^R(z_1) \\ \times \left(\sum_c \int_{\ln\mu_0^2}^{\ln\mu_1^2} \mathrm{d}\ln\mu_2^2 \frac{\Delta_b(\mu_1^2)}{\Delta_b(\mu_2^2)} \int_{\frac{x}{z_1}}^{z_M} \frac{\mathrm{d}z_2}{z_2}\ \frac{\alpha_S}{2\pi}\ P_{bc}^R(z_2)\ f_b(\frac{x}{z_1 z_2}, \mu_2^2) \right)\,, \end{aligned} \tag{5.50}$$

where, in our case, $a = b = c$.

At last all the pieces from Eqs (5.35, 5.43, 5.50) can be combined to answer the question of what is the probability of finding a parton a at a scale μ^2 at a given x. Of

course the process could have more splittings if a 3rd, 4th, 5th,... scale was generated below the maximum scale bu we stopped our examples at 2 branchings to avoid redundancy. The steps described above are then iterated to find the contribution of each order of branching. They all sum up to give the solution of the evolution equation:

$$f_a(x,\mu^2) = f_a^{(0)}(x,\mu^2) + f_a^{(1)}(x,\mu^2) + f_a^{(2)}(x,\mu^2) + \dots . \tag{5.51}$$

5.2.4 Splitting functions as probability densities

We would like to generate the splitting variable z according to a probability density which consists of two parts (P_{bb}^R and P_{ab}^R). To choose from which part z is going to be generated, we can compute the integrals of the splitting functions and normalize the probabilities in the following way:

$$\begin{aligned} P_1 &= \frac{\int_\epsilon^{1-\epsilon} \mathrm{d}z\ P_{bb}^R(z)}{\sum_{c=a,b}\int_\epsilon^{1-\epsilon} \mathrm{d}z\ P_{cb}^R(z)}\,, \\ P_1 &= \frac{\int_\epsilon^{1-\epsilon} \mathrm{d}z\ P_{ab}^R(z)}{\sum_{c=a,b}\int_\epsilon^{1-\epsilon} \mathrm{d}z\ P_{cb}^R(z)}\,, \\ P &= P_1 + P_2 = 1\,, \end{aligned} \tag{5.52}$$

A uniformly distributed RN $R' \in [0,1]$ is generated and compared with P_1. If $R' < P_1$, z_1 is generated according to properly normalized $P_{bb}^R(z)$. Otherwise, if $R' > P_1$, z_1 is generated according to properly normalized P_{ab}^R.

This method was applied with numerical values, $\epsilon = 0.00001$ and the following splitting functions:

$$P_{qq}^R = \frac{4}{3}\left[\frac{1+z^2}{1-z}\right], \tag{5.53}$$

$$P_{gg}^{R,L} = 6\left[\frac{1}{z} + \frac{1}{1-z}\right], \tag{5.54}$$

$$P_{qg}^R = \frac{1}{2}[z^2 + (1-z)^2]\,, \tag{5.55}$$

$$P_{gq}^R = \frac{4}{3}\left[\frac{1+(1-z)^2}{z}\right], \tag{5.56}$$

where the L in P_{gg} stands for the leading contributions.

We found out that for a gluon, the probability to become a quark is approximately 1.7% meaning that in first approximation, when we have a gluon in the evolution, it splits and evolves only as a gluon. The choice to take into account only the P_{gg} splitting function for the gluon evolution is thus well motivated.

If instead the starting parton is a quark, the probability to stay a quark after a splitting is 50% because the splitting functions P_{qq} and P_{gq} are symmetric under $z \leftrightarrow (1-z)$. The choice to keep only P_{qq} must then be corrected by a factor $\frac{1}{2}$ at each splitting which corresponds to the possibility for the quark to become a gluon, and then to stay a gluon for the rest of the evolution as explained previously.

5.2.5 Application to the DY

In this subsection we discuss the application of this method to find the DY cross section differentiated with respect to the dilepton transverse impulsion p_T^{ll}. To simplify this analysis, we only consider the $u\bar{u}$ channel for the colliding partons.

Near the Z boson peak, the DY cross section corresponds to the term proportional to χ_2 in Eq (3.10), i.e. the term:

$$\hat{\sigma}_Z(\hat{s}) = \frac{4\pi\alpha^2}{3\hat{s}} \frac{1}{N_c} \frac{1}{\sin^4 2\theta_W} (A_l^2 + V_l^2)(A_{q_u}^2 + V_{q_u}^2) \frac{\hat{s}^2}{(\hat{s} - M_Z^2)^2 + M_Z^2 \Gamma_Z^2}, \tag{5.57}$$

with the fine-structure constant $\alpha = 1/137$, the number of active colours $N_c = 3$, the Z boson mass $M_Z = 91.1876$ GeV, and its decay width $\Gamma_Z = 2.4952$. The weak mixing angle θ_W is taken to be $\sin^2\theta_W = 0.23129$. A quick calculation gives the value of the parameter $\sin^4(2\theta_W)$. The parameters $V_l = -0.03783$ and $V_{q_u} = 0.268$ are the effective vector couplings of the Z to charged leptons and quark up respectively while $A_l = -0.50123$ and $A_{q_u} = 0.519$ are the effective axial-vector couplings. These numerical values were taken from the very complete review in [8].

In subsections 5.2.1-5.2.3, each event was composed of one "chain" of splittings. Now we want to make a hard interaction, we need thus to evolve *two* chains from the initial scale $\mu_0^2 = 1$ GeV^2 to collide them at the maximum scale $\mu^2 = M_Z^2$. We proceed at the evolution as previously, first we generate two quarks up: $a^{(i)}$ $(i = 1, 2)$ with momentum fraction $x^{(i)}$, weight $w_x^{(i)}$, and transverse components $k_{x_0}^{(i)}$ and $k_{y_0}^{(i)}$. Then we produce a branching scale $\mu_k^{2,(i)}$, a splitting variable $z_k^{(i)}$ with weight $w_{z_k}^{(i)}$. Next we evolve the transverse components and we generate the next scale $\mu_{k-1}^{2,(i)}$. The process is then iterated until the scale generated is higher than $\mu^2 = M_Z^2$. It means that there is no other constraint on the number of branchings which are counted by the index $k^{(i)}$.

Let us recall that the number of branchings k is not known before the end of the evolution, so k is counted in reverse, as follows: k for the first branching, $k-1$ for the second, $k-2$ for the third, ... decreasing until the last branching. When the evolution is stopped we know the number of splittings: the value of k. This value can of course change at each event and for both chain. This special counting is used in order to respect the formalism of subsections 5.2.1-5.2.3.

Now the different pieces that enter in the hadronic cross section are discussed. First, the partonic cross section defined in Eq (5.57) and depends on $\hat{s}$. The square center-of-mass energy of the parton-parton interaction yields (see Eq(3.3)):

$$\hat{s} = x_1 x_2 s \,. \tag{5.58}$$

with $\sqrt{s} = 13$ TeV because we want to simulate the LHC data.

We also need to take all the weights into account since we used importance sampling method:

$$w = \prod_{i=1,2} w_x^{(i)} \prod_{j=1}^{k^{(i)}} w_{z_j} \quad . \tag{5.59}$$

Also, as we discussed in subsection 5.2.4, one needs to apply a third weight to the cross section because of our choice to consider only the P_{qq} splitting function. This gluon weight is given by:

$$w_g = \left(\frac{1}{2}\right)^k , \tag{5.60}$$

with $k = k^{(1)} + k^{(2)}$.

The longitudinal momentum components $k_z^{(1)} = \frac{\sqrt{s}}{2}x_1$ and $k_z^{(2)} = -\frac{\sqrt{s}}{2}x_2$ can be combined to the evolved transverse components to form the four momentum of the partons. The transverse momentum and the mass of the dilepton system can then be extracted from the sum of these four momentum $p^\mu = k^{\mu,(1)} + k^{\mu,(2)}$.

The differential hadronic cross section is then given by:

$$\mathrm{d}\sigma_Z = \mathrm{d}\hat{\sigma}_Z(\hat{s}) \cdot w \cdot w_g \,. \tag{5.61}$$

This cross section fills a histogram σ_Z vs M_Z, the invariant mass of the Z boson generated. Finally, for the events which have their invariant mass near the Z mass peak 76 GeV $\leq M_Z \leq$ 106 GeV, we fill a histogram σ_Z vs $p_T(Z)$.

5.3 Results

This sections provides the results of the analysis. The simplified Parton Branching method, introduced in the previous section, is used to perform a forward evolution from a starting scale $\mu_0^2 = 1$ GeV^2 until $\mu^2 = M_Z^2$. The strong coupling variable is kept fixed $\alpha_S(M_Z) = 0.118$. The PDF initial parametrisations are given by:

$$f_a(x, \mu_0^2) = 3\frac{(1-x)^5}{x} , \tag{5.62}$$

for a quark or a gluon a.

The intrinsic k_T distribution is assumed to be a Gaussian $\exp(-k_T^2/\sigma^2)$ with $\sigma^2 = k_{T_0}^2/2$ and k_{T_0} a fixed value. The same form is again used for all partons.

In section 4.2.4, we introduced p_T -, virtuality and angular ordering conditions as different ways of associating the evolution scale with the given kinematics. We showed that from the association of the branching scale μ'^2 with a given kinematic variable, the evolution of the k_T follows. It was shown that depending on the ordering condition the transverse momentum of the propagating parton can be written as:

$$k_{x,i+1} = k_{x,i} + \sqrt{\mu_i^2}\cos(\phi_i)(1-z_i)^d \,, \tag{5.63}$$

$$k_{y,i+1} = k_{y,i} + \sqrt{\mu_i^2}\sin(\phi_i)(1-z_i)^d \,, \tag{5.64}$$

where i runs over the number of radiations and with the power d taking a different value which depends on the choice of ordering. The angular ordering condition

corresponds to $d = 1$, the virtuality ordering to $d = 1/2$ and the p_T-ordering to $d = 0$.

The first subsection is devoted to a comparison between the evolution for gluons and for quarks. Collinear and TMD PDFs from the simplified PB method are presented at the initial and final scales. In the second subsection, the transverse momentum of the DY Z boson obtained from our approach is considered. We discuss different values for the intrinsic transverse momenta of the partons, the choice of the parameter $z_M = 1 - \epsilon$ defining resolvable branching as well as the choice of ordering conditions.

5.3.1 Evolution with P_{qq} vs P_{gg}

The knowledge of how the real parts of the splitting functions behave is crucial for the solution of the DGLAP evolution equations by the Parton Branching method. The splitting functions considered are:

$$P_{qq}^R = \frac{4}{3}\frac{1+z^2}{1-z}\,, \tag{5.65}$$

$$P_{gg}^{R,L} = 6\left(\frac{1}{z} + \frac{1}{1-z}\right)\,, \tag{5.66}$$

where the L stands for leading contributions. The splitting functions depend only on z. Since P_{qg} and P_{gq} are not investigated, the partons are not allowed to change of species, which means that during a branching, a quark will evolve as a quark of the same flavour while a gluon can only evolve into another gluon.

In this section, the results are shown using $k_{T_0} = 0.7$ GeV, $\epsilon = 10^{-5}$, and the angular ordering ($d = 1$) in Eq (5.64).

The Fig (5.2)-(5.3) are composed of 6 and 5 histograms:

1. The initial collinear PDF vs x_0 at fixed $\mu_0^2 = 1$ GeV^2 and integrated over k_T,
2. The evolved collinear PDF vs x at fixed $\mu^2 = M_Z^2$ and integrated over k_T,
3. The initial TMD PDF vs k_{T_0} at fixed $\mu_0^2 = 1$ GeV^2 and integrated over x,
4. The evolved TMD PDF vs k_T at fixed $\mu^2 = M_Z^2$ and integrated over x,
5. The number of radiation during the evolution,
6. The k_T distribution accumulated after the first radiation (shown only in P_{qq} case).

The initial collinear and TMD PDFs are generated in the same way for both the gluon and quark, it follows that Figs (5.2)(1) and (3) are identical to Figs (5.3)(1) and (3).

Let us discuss the number of radiation in case of quarks (Fig (5.2)(5)) and gluons (Fig (5.3)(5)). As one can see we have much more radiations in gluon evolution than in quark one. It can be understood as follows. The integral of the $P_{gg}^{R,L}$ is always

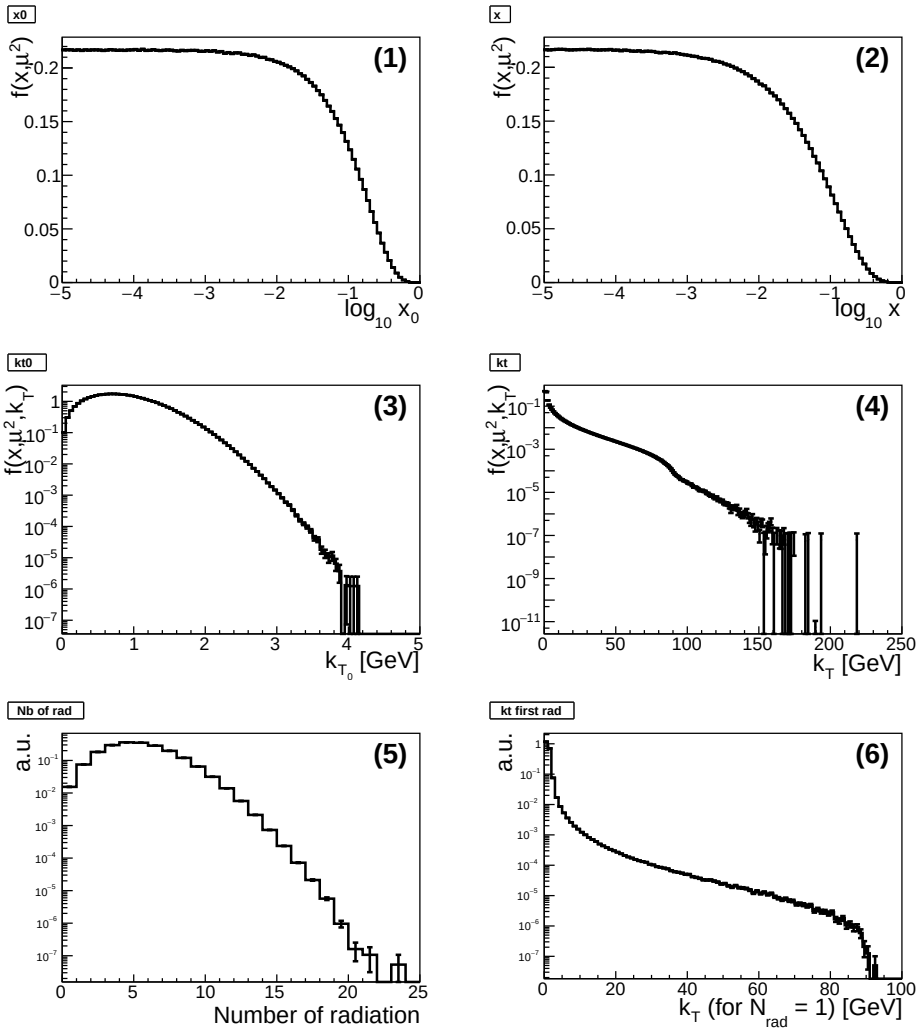

Figure 5.2: *Evolution of the collinear (1) and (2), and of the TMD PDFs (3) and (4) for a quark with the splitting function P_{qq}^R. The graph (5) is the number of radiations during the evolution. The graph (6) illustrates k_T after the first radiation.*

bigger than P_{qq}^R integral regardless of the value of z_M. As the Sudakow form factor decreases with an increasing splitting function integral, it follows that the Sudakov is smaller for the gluon than for the quark. Recalling the definition of the Sudakov as being the probability to evolve without any resolvable branching, it should lead to more radiations for the gluon than for the quark.
As a consequence we see that evolved k_T is harder in case of gluons (Fig (5.3)(4)) than in case of quarks (Fig (5.2)(4)) since k_T will accumulated to higher values with large number of radiations. Also, since there are more radiations in the gluon evolution, the gluon loses more energy than the quark. Therefore the collinear PDF for the gluon should migrate more to the small x region than the quark collinear PDF. The behaviours of the collinear (2) and TMD (4) PDFs confirm our prediction.

In Fig (5.2) (6) the k_T distribution accumulated after the first radiation is shown. This can give an idea about the step which Sudakov form factor can make, i.e at which scale the first branching will occur.

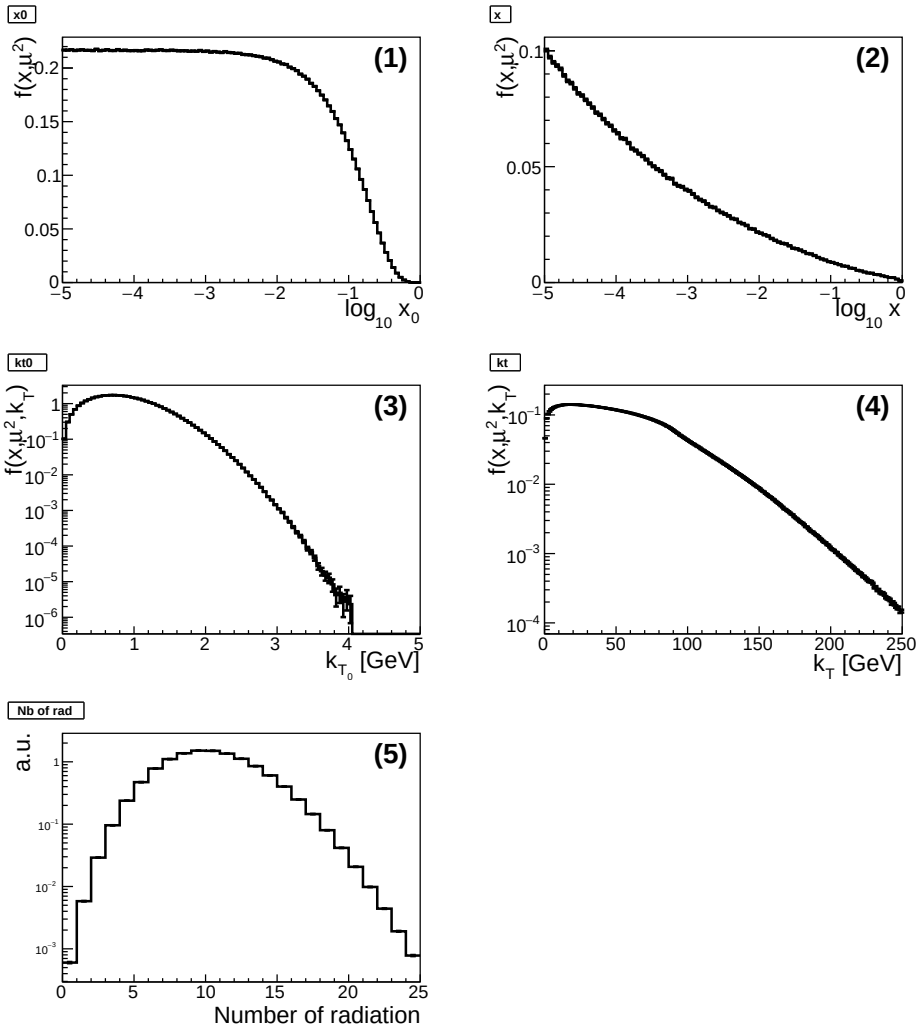

Figure 5.3: *Evolution of the collinear (1) and (2), and of the TMD PDFs (3) and (4) for a gluon with the splitting function $P_{gg}^{R,L}$. The graph (5) is the number of radiations during the evolution.*

5.3.2 Transverse momentum of the Z boson

In this subsection, we test the idea of applying TMD instead of collinear PDFs to obtain prediction for the Z boson p_T spectrum. We perform the simplified PB method, then the DY cross section at the mass peak of the Z is used. The centre-of-mass energy is $\sqrt{s} = 13$ TeV and we analyze the transverse momentum of the events in the range $76 < M_Z < 106$ GeV. We assume that we generate only quarks and anti-quarks up, thus the only splitting function used is $P_{qq} = P_{uu}$.

We shall see how changing parameters affects the distribution. First we will discuss different values for the intrinsic transverse momenta of the starting quarks, then the choice of the parameter z_M and finally the ordering condition.

In Fig (5.4) the results for the $p_T(Z)$ spectrum with angular ordering and $z_M = 1 - 10^{-5}$ are presented for three different values of the parameter $k_{T_0} = 0.2$ GeV, $k_{T_0} = 0.7$ GeV, $k_{T_0} = 1.2$ GeV.

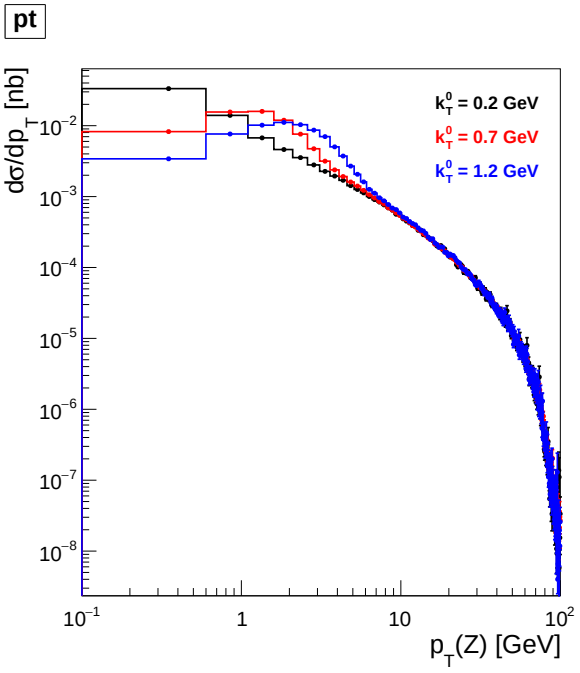

Figure 5.4: $p_T(Z)$ *with different* k_{T_0}.

Changing this initial partons transverse momentum width should not affect the high-p_T region, where a lot of radiations leading to the generation of transverse momentum should have smoothed the initial disparity away. Indeed, the results show that the influence of changing this initial partons transverse momentum width is only visible for the low-p_T region. Looking at the shape of the distribution we see that for the default value of $k_{T_0} = 0.7$ the simulated spectrum peaks at about 2 GeV. In inclusive DY measurement the peak of the $p_T(Z)$ distribution is approximately at 5 GeV. Discussion on that matter can be found in the end of this subsection.

Let me comment on the normalisation for the figures I show in this section. As elaborated in subsection (5.2.5) the event weights are propagated into the code with an additional care. Although several simplifications of the method as discussed later do not allow to bring the final normalisation to the reasonable value. It is worth mentioning that for the current analysis the normalisation is not important and the discussion on the shape is present.

Now, the results shown in Fig (5.5) correspond to an evolution with angular ordering and $k_{T_0} = 0.7$ GeV but for different values of the parameter $z_M = 1 - 10^{-3}$, $z_M = 1 - 10^{-4}$, $z_M = 1 - 10^{-5}$.

One can see that all these values of z_M lead to the same shape for the spectrum of $p_T(Z)$ but lead to different yields, so there are less Z bosons when increasing z_M. It can be understood as following. When z_{max} is increased, the Sudakov form factor decreases hence the number of radiation grows. As discussed in the end of subsection 5.2.4 each splitting is corrected by a factor 1/2 due to the possibility for the quark to become a gluon. In other words, the gluon weight introduced in

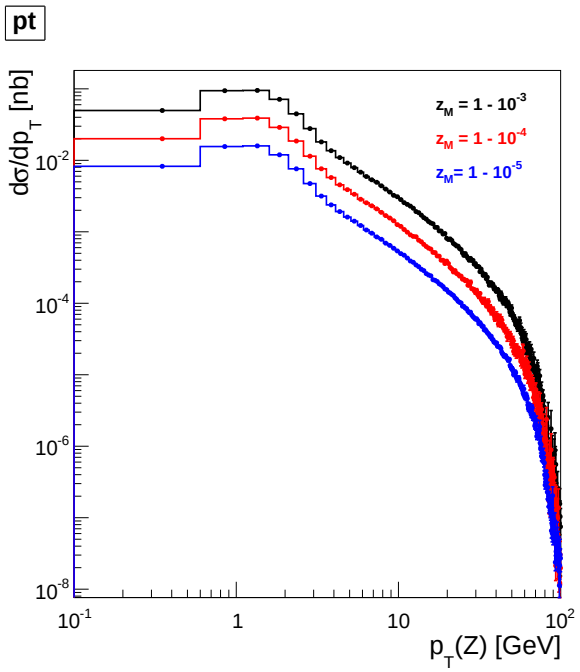

Figure 5.5: $p_T(Z)$ *with different* z_M.

subsection 5.2.5 is enhanced:

$$w_g = \left(\frac{1}{2}\right)^k , \tag{5.67}$$

with k being the number of radiations. Thus having more radiations will increase the probability of getting gluon during the evolution and thus will reduce the Z boson production what is observed in Fig (5.5).

In Fig (5.6), the results for the $p_T(Z)$ distribution with $k_{T_0} = 0.7$ GeV and $z_M = 1 - 10^{-5}$ are presented for the three ordering conditions: angular, virtuality and p_T-ordering.

We can see that the three predictions differ a lot from each other, especially the one obtained with the p_T-ordering. From the plot one cannot conclude which is the best since no comparison with data is shown. As mentioned earlier the approach elaborated in the thesis uses several approximations which lead to the simulation being not compatible with the data: fixed α_s scale, non-dynamic z_M, only P_{qq} in the evolution. The last approximation is especially important. In case of Z production at 13 TeV energy, the gluon PDF is much higher than quark PDF and thus gluons cannot be completely neglected, because there are much more gluons and that compensates lower splitting probability for g $\to q\bar{q}$. As we saw in the previous subsections gluons change a lot the kinematics during the evolution compared to the quarks.

In [46] it was shown that angular ordering provides the best description on the measured $p_T(Z)$ spectra by LHC and it was shown that p_T-ordering does not give the stable results for the TMDs, whereas virtuality and angular ordering do.

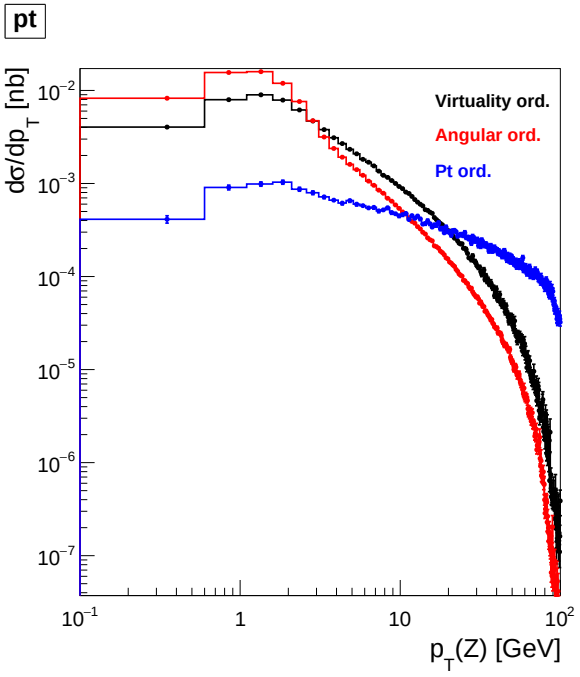

Figure 5.6: $p_T(Z)$ *with different ordering.*

5.4 CASCADE

I explored a tool which allows to use TMDs from the PB method (or other TMDs) to the LHC measurements, particularly the DY analyse from ATLAS experiments. The tool is called CASCADE [57, 67].

It works as follows: one takes the LO or NLO matrix element for the Z boson production generated by another Monte Carlo. The matrix element does not generate any p_T at LO and generate large p_T at NLO. Small transverse momenta of the incoming quark-antiquark pair can be generated according to the TMDs, which is an input of CASCADE. Thus the small p_T dependence (or $p_T < 20$ GeV) comes directly from the PB method. There is no tuning of free parameters. With a help of the RIVET interface [68] [1] I made a comparison of the latest PB TMD set, PB-NLO-HERAI+II-2018-set2 [60], with the DY measurements from ATLAS at 8 TeV [29]. In Fig (5.7) the measured transverse momentum of the Z boson is shown in three invariant mass ranges: $46 < M < 66$ GeV, $66 < M < 116$ GeV, $116 < M < 150$ GeV. The normalised distributions are in a good agreement with the TMDs.

[1] RIVET is a generator-independent program, where truth events can be processed to show the truth-level distributions resulting from measurements and compared to the reference data. In this way, new generator predictions may be run through an RIVET analysis plugin and the result may be compared to the experimental data directly (assuming that the data are corrected for detector effects).

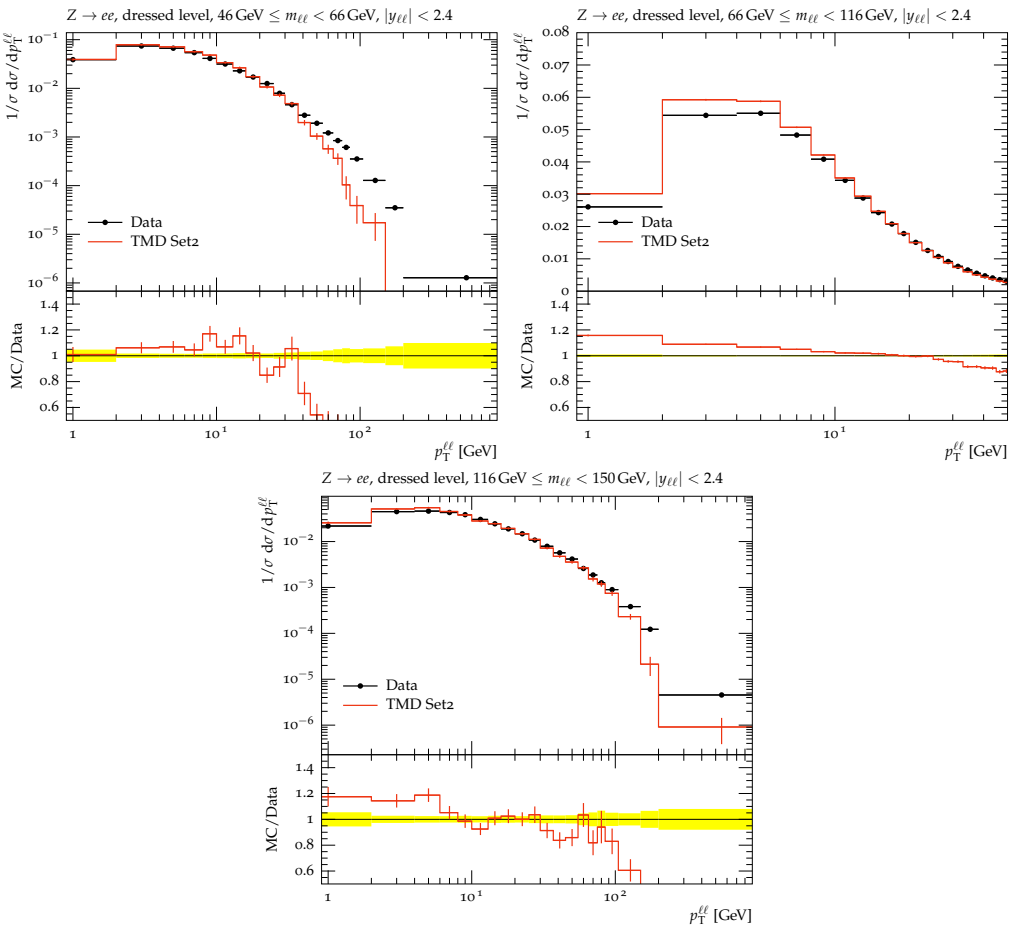

Figure 5.7: *The measured normalised distributions of the transverse momentum of the Z boson are shown in three invariant mass ranges: 46 < M < 66 GeV, 66 < M < 116 GeV, 116 < M < 150 GeV. The date are compared to the TMD prediction* [29].

Chapter 6

Conclusions and Prospects

In this thesis a new approach to solve the DGLAP evolution equation is discussed. From the solution with the Parton Branching (PB) method one can obtain, in addition to the standard collinear Parton Distribution Functions (PDFs), also the Transverse Momentum Dependent PDFs (TMDs). The PB method allows a determination of kinematic variables at every branching and a construction of the TMDs in a large range in longitudinal momentum fraction x and evolution scale.

During this thesis I learned the Monte Carlo techniques used in the LHC event simulation tools and wrote a code based on the simplified parton branching method and obtained the Z boson p_T-spectrum for LHC collisions at 13 TeV.

I studied independently different elements of ordering condition: the connection between the evolution scale and a kinematic variable and the soft gluons resolution scale parameter, z_M. I also investigated the effect of the intrinsic transverse momentum distribution on the Z boson transverse momentum. The code uses several simplification to obtain the results within the master thesis: scale of α_S is fixed, only quark to quark splitting is considered during the evolution. If these steps were completed I expect that simulated $p_T(Z)$ distribution would be closer to the LHC measurements. I also explored a tool which allows to use TMDs from the PB method to the LHC measurements, particularly the DY analyses from ATLAS experiments. The tool is called CASCADE. I made a comparison of the latest PB TMD set with the DY measurements from ATLAS at 8 TeV. The results show good agreement with the measurements.

The PB TMD approach is a part of a broader program which aims in precision predictions for observables at high energy collisions. Although in my master thesis only the DY process is discussed, the method can be, nonetheless, applied to any QCD process, like jet production, Higgs production etc.. One could especially study the low energy DY data which might be sensitive to the intrinsic momenta. This also opens new perspectives for a better precision for the calculations of higher order corrections to the physical observables, not only for LHC measurements, but also in the context of the new colliders.

TMDs are today a reliable alternative to the present approach based on the collinear factorisation and parton showers. Work is still needed to improve its deep

understanding, to control well related uncertainties and to develop tools to make it more easily available for the full LHC community. The ultimate goal being to make TMDs adopted by the community as the default approach for hadron distributions, being better fundamentally founded and providing higher precision.

Bibliography

[1] C. Burgard. *Standard Model of physics*. visited on 2019-05-03. URL: http://www.texample.net/tikz/examples/model-physics/.

[2] B. R. Webber R. K. Ellis W. J. Stirling. *QCD and Collider Physics*. Cambridge University Press, 1996.

[3] H. D. Politzer. In: *Phys. Rev. Lett.* (1973), p. 1346.

[4] D. J. Gross and F. Wilczek. In: *Phys. Rev. Lett.* **30** (1973), p. 1343.

[5] W. E. Caswell. In: *Phys. Rev. Lett.* **33** (1974), p. 244.

[6] L.V. Avdeev, O.V. Tarasov, and A.A. Vladimirov. In: *Physics Letters* **B96** (1980), p. 94. DOI: https://doi.org/10.1016/0370-2693(80)90219-1.

[7] A. Warburton and ATLAS Collaboration. In: 2015. eprint: 1509.04380.

[8] M. et al. Tanabashi. In: *Phys. Rev.* **D 98** (2018). DOI: 10.1103/PhysRevD.98.030001.

[9] F. Halzen and Alan D. Martin. *Quarks and Leptons: an introductory course in modern particle physics*. 1984.

[10] Laurent Favart. *Physique auprès des collisionneurs*. Lectures at ULB. 2018.

[11] E. D. Bloom et al. In: *Phys. Rev. Lett.* **23** (1969), p. 930.

[12] M. Breidenbach et al. In: *Phys. Rev. Lett.* **23** (16 1969), p. 935.

[13] C. G. Callan and David J. Gross. In: *Phys. Rev. Lett.* **22** (1969), p. 156. DOI: 10.1103/PhysRevLett.22.156.

[14] F. D. Aaron et al. In: *JHEP* **01** (2010), p. 109. eprint: 0911.0884.

[15] A.C. Benvenuti et al. In: *Physics Letters* **B 223** (1989), p. 485. DOI: https://doi.org/10.1016/0370-2693(89)91637-7.

[16] M. Arneodo et al. New Muon Collaboration. In: *Nucl. Phys.* **B 483** (1997), p. 3. eprint: hep-ph/9610231.

[17] Y. V. Kovchegov and E. Levin. *Quantum Chromodynamics at High Energy*. Cambridge University Press, 2012. DOI: 10.1017/CBO9781139022187.

[18] G. Altarelli and G. Parisi. In: *Nucl. Phys.* **B 126** (1977), p. 298. DOI: 10.1016/0550-3213(77)90384-4.

[19] V. S. Fadin, E. A. Kuraev, and L. N. Lipatov. In: *Phys. Lett.* **60 B** (1975), p. 50.

[20] Durham University. *Online PDF plotting and calculation*. visited on 2019-05-06. URL: http://www.texample.net/tikz/examples/model-physics/.

[21] S. D. Drell and Tung-Mow Yan. In: *Phys. Rev. Lett.* **25** (1970). [Erratum: Phys. Rev. Lett.25,902(1970)], p. 316.

[22] Samantha Katherine Dooling. "Differential Cross Section Measurement of Drell-Yan Production and Associated Jets with the CMS Experiment at the LHC". PhD thesis. Hamburg University, 2015.

[23] W. J. Stirling and M. R. Whalley. In: *Journal of Physics G: Nuclear and Particle Physics* **D 19** (1993), p. D1.

[24] R. D. Field. *Applications of Perturbative QCD*. Vol. **77**. 1989, p. 1.

[25] G. Altarelli, R.K. Ellis, and G. Martinelli. In: *Nuclear Physics* **B 143** (1978), p. 521. ; ibid. **B 146** (1978) p. 544 (erratum).

[26] J. Kubar-Andre and F. E. Paige. In: *Phys. Rev.* **D 19** (1979). DOI: 10.1103/PhysRevD.19.221.

[27] Kyoko Yamamoto. "Measurement of the Drell-Yan differential cross-section d(sigma)/d(pT) at high dilepton mass inproton-proton collisions at sqrt(s) = 7 TeV with the ATLAS detector". PhD thesis. Iowa State University, 2012.

[28] A. S. et al. Ito. In: *Phys. Rev.* **D 23** (1981), p. 604. DOI: 10.1103/PhysRevD.23.604.

[29] G. Aad et al. In: *Eur. Phys. J.* **C 76**.5 (2016), p. 291. eprint: 1512.02192.

[30] P. B. Arnold and M. H. Reno. In: *Nuclear Physics* **B 319**.1 (1989), p. 37. DOI: https://doi.org/10.1016/0550-3213(89)90600-7.

[31] T. Sjostrand, S. Mrenna, and P. Z. Skands. In: *Comput. Phys. Commun.* **178** (2008), p. 852. eprint: 0710.3820.

[32] G. Parisi and R. Petronzio. In: *Nuclear Physics* **B 154**.3 (1979), p. 427.

[33] J. C. Collins, D. E. Soper, and G. F. Sterman. In: *Nucl. Phys.* **B 250** (1985), p. 199. DOI: 10.1016/0550-3213(85)90479-1.

[34] V. Khachatryan et al. In: *JHEP* **02** (2017), p. 96. eprint: 1606.05864.

[35] J. Collins and H. Jung. In: *HERA and the LHC: A Workshop on the implications of HERA for LHC physics. Proceedings, Part B*. 2005. eprint: hep-ph/0508280.

[36] J. Collins. *Foundations of Perturbative QCD*. Cambridge University Press, 2011. DOI: 10.1017/CBO9780511975592.

[37] S. Catani, M. Ciafaloni, and F. Hautmann. In: *Nucl. Phys.* **B 366** (1991), p. 135. DOI: 10.1016/0550-3213(91)90055-3.

[38] J. Collins and R.K. Ellis. In: *Nuclear Physics* **B 360** (1991), p. 3. DOI: 10.1016/0550-3213(91)90288-9.

[39] I. I. Balitsky and L. N. Lipatov. In: *Sov. J. Nucl. Phys.* **28** (1978), p. 822.

[40] G. Marchesini. In: *Nucl. Phys.* **B445** (1995), p. 49. eprint: hep-ph/9412327.

[41] F. Hautmann. In: *Phys. Lett.* **B 535** (2002), p. 159. eprint: hep-ph/0203140.

[42] F. Hautmann et al. URL: TMDlib.tmdlib.hepforge.org.

[43] F. Hautmann et al. URL: TMDplotter.tmdplotter.desy.de.

[44] F. Hautmann et al. In: *Eur. Phys. J.* **C 74** (2014), p. 3220. eprint: 1408.3015.

[45] A. Buckley et al. "Les Houches 2013: Physics at TeV Colliders:Standard Model Working Group Report". In: (2014).

[46] Aleksandra Lelek. "Determination of TMD parton densities from HERA data and application to pp processes". PhD thesis. Universität Hamburg, 2018.

[47] R. Angeles-Martinez et al. In: *Acta Phys. Polon.* **B 46**.12 (2015), p. 2501. eprint: 1507.05267.

[48] T. Becher, M. Neubert, and D. Wilhelm. In: *JHEP* **05** (2013), p. 110. eprint: 1212.2621.

[49] M. G. Echevarria et al. In: *JHEP* **07** (2015). [Erratum: JHEP **05**,073(2017)], p. 158. eprint: 1502.05354.

[50] N. A. Abdulov, A. V. Lipatov, and M. A. Malyshev. In: *Phys. Rev.* **D 97**.5 (2018), p. 054017. eprint: 1708.04057.

[51] F. Hautmann, M. Hentschinski, and H. Jung. In: (2012). eprint: 1205.6358.

[52] M. Diehl and J. R. Gaunt. In: *Adv. Ser. Direct. High Energy Phys.* **29** (2018), p. 7. eprint: 1710.04408.

[53] F. Hautmann et al. In: *Physics Letters* **B 772** (2017), p. 446. DOI: https://doi.org/10.1016/j.physletb.2017.07.005.

[54] F. Hautmann et al. In: *JHEP* **01** (2018), p. 70. eprint: 1708.03279.

[55] S. Dooling et al. In: *Phys. Rev.* **D 87**.9 (2013), p. 094009. eprint: 1212.6164.

[56] C. Oleari. "The POWHEG-BOX". In: *Nucl. Phys. Proc. Suppl.* **205-206** (2010), p. 36. eprint: 1007.3893.

[57] H. Jung and G. P. Salam. In: *Eur. Phys. J.* **C 19** (2001), p. 351. eprint: hep-ph/0012143.

[58] *xFitter*. URL: https://www.xfitter.org/xFitter/.

[59] F. Hautmann et al. In: *Phys. Lett.* **B 772** (2017), p. 446. eprint: 1704.01757.

[60] A. Bermudez Martinez et al. In: *Phys. Rev.* **D 99**.7 (2019), p. 074008. eprint: 1804.11152.

[61] H. Jung. "QCD and Monte Carlo method". Writeup for Tutorials at Terascale MC school 2018, DESY. 2018.

[62] S. Catani, B. R. Webber, and G. Marchesini. In: *Nucl. Phys.* **B 349** (1991), p. 635. DOI: 10.1016/0550-3213(91)90390-J.

[63] B. Andersson and others Small x Collaboration. In: *Eur. Phys. J.* **C25** (2002), p. 77. eprint: hep-ph/0204115.

[64] G. Cowan. *Statistical Data Analysis*. Oxford Science Publications, 1998.

[65] M. Luscher. In: *Comput. Phys. Commun.* **79** (1994), p. 100. eprint: hep-lat/9309020.

[66] S. Weinzierl. In: (2000). eprint: hep-ph/0006269.

[67] H. Jung. In: *Comput. Phys. Commun.* **143** (2002), p. 100. eprint: hep-ph/0109102.

[68] A. Buckley et al. In: *Comput. Phys. Commun.* **184** (2013), p. 2803. eprint: 1003.0694.